Roles of phosphatidylinositol 3-kinases and 3-phosphatases in Schwann cell myelination

By

Anne Marie Logan

A dissertation

Presented to the Neuroscience Graduate Program
and the Oregon Health & Science University
School of Medicine
in partial fulfillment of
the requirements for the degree of

Doctor of Philosophy

March 2015

School of Medicine
Oregon Health & Science University

CERTIFICATE OF APPROVAL

This is to certify that the Ph.D. dissertation of
ANNE LOGAN
has been approved on March 18, 2015

Advisor, Fred Robinson, Ph.D.

Member and Chair, Magdalena Petryniak, M.D.

Member, Ben Emery, Ph.D.

Member, Peter Mayinger, Ph.D.

Member, Philip Stork, M.D.

Member, Gary Westbrook, M.D.

TABLE OF CONTENTS

Chapter 5

List of Figures and Tables

List of Abbreviations

MTMR	myotubularin-related
PI	phosphoinositide
PI3P	phosphatidylinositol 3-phosphate
$PI(3,5)P_2$	phosphatidylinositol 3,5-diphosphate
CMT	Charcot-Marie-Tooth
CNS	central nervous system
PNS	peripheral nervous system
AP	action potential
E	embryonic day
SCP	Schwann cell precursors
AP2α	activator protein 2α
IGF2	insulin-like growth factor 2
NT3	neurtrophin 3
NRG1	neuregulin-1
TGF-β	transforming growth factor-beta
NGF	nerve growth factor
NRG1-III	neuregulin-1 type III
P0	myelin protein 0
MBP	myelin basic protein
PMP22	peripheral myelin protein 22
MAG	myelin-associated glycoprotein
MAPK	mitogen-activated protein kinase
PI3K	phosphoinositide 3-kinase / PI 3-kinase
SLI	Schmidt-Lanterman incisures
PLP1	proteolipid protein 1
TAG-1	transient axonal glycoprotein-1
Necl	Nectin-like
ALS	amyotophic lateral sclerosis
MS	multiple sclerosis
CIDP	chronic inflammatory demyelinating polyneuropathy
EMG	electromyography
MNCV	motor nerve conduction velocity
GJB1	gap junction beta-1
MFN2	mitofusin 2
AR-CMT	autosomal recessive CMT
PtdIns	phosphatidylinositol
PI4P	phosphatidylinositol 4-phosphate
PI5P	phosphatidylinositol 5-phosphate
$PI(3,4)P_2$	phosphatidylinositol 3,4-diphosphate
$PI(4,5)P_2$	phosphatidylinositol 4,5-diphosphate
$PI(3,4,5)P_3$	phosphatidylinositol 3,4,5-triphosphate
PLC	phospholipase C
PH	pleckstrin homology
MVB	multivesicular bodies
EGF-R	epidermal growth factor receptor
Atg14	Autophagy related protein 14
WIPI1	WD repeat domain phosphoinositide-interacting protein 1

DFCP1	double FYVE containing protein 1
MTM1	myotubularin 1
PH-GRAM	Pleckstrin homology-glucosyltransferases, rab-like GTPase activators and myotubularins
CC	coiled coil
Dlg1/SAP97	discs large 1/synapse associated 97
PIP3	$PI(3,4,5)P_3$ / phosphatidylinositol 3,4,5-triphosphate
MEF	mouse embryonic fibroblast
JPN	juxtaparanode
PDK	PI-dependent kinase
PTP	phosphatase
NCV	nerve conduction velocity
CMAP	compound muscle action potentials
NF-L	neurofilament light chain
Erk1/2	extracellular signal related kinase 1/2
EM	electron microscopy
Snx1/2	sorting nexins 1 and 2
CI-MPR	cation-independent mannose 6-phosphate receptor
FBS	fetal bovine serum
PFA	paraformaldehyde
NGS	normal goat serum
TFA	transverse fascicular area
p62/SQSTM1	p62/sequestosome 1
EEA1	early endosome antigen 1
LAMP1	lysosomal-associated membrane protein1
PBS	phosphate buffered saline
PB	phosphate buffer
DAPI	4',6-diamidino-2-phenylindole
DRG	dorsal root ganglion
NF-H	neurofilament heavy chain
LVPG	lentiviral plasmid

Acknowledgments

This work would not have been possible without the excellent guidance of my mentor, Dr. Fred Robinson. I want to thank him for his dedication to our research, his support, and the countless hours he has spent editing my grants, papers, and dissertation. He has been a role model for me during my training as a graduate student. I would also like to express my gratitude to the Robinson lab members, both past and present, for their help and contributions to my research work. I would like to especially thank a former technician in the lab, Aubree Ng. We worked together on the experiments studying Mtmr2 and Mtmr13 localization and the myelinating co-cultures. Much of the work presented here would not have been possible without her help and expertise. I would also like to thank the other labs on our floor including the members of the Logan Lab, Unni Lab, and Banker Lab for sharing reagents and providing assistance in troubleshooting experiments.

I would like to thank my fellow graduate students in the Robinson lab, Danielle Robinson and Anna Mammel, who spent countless hours editing drafts of this dissertation. I am incredibly grateful for their critical reading and valuable feedback, I could not have done it without them!

Melissa Williams in the Electron Microscopy core was invaluable in the preparation and processing of sciatic nerves for EM, and in the acquisition of images. She spent many, many hours with me on the electron microscope imaging and analyzing the state of myelination and the health of Schwann cells and axons. I would like to thank Stefanie Kaech Petrie and Aurelie Snyder in The Advanced Light Microscopy Core at the Jungers Center. Both spent countless hours working with me, assisting in imaging and analysis of nerve morphology. This work could not have been done without them. I would also like to thank the administrative director of the Neuroscience Graduate Program, Liz Lawson-Weber, for her answers to my endless questions, helping keep me

on track, and for keeping a watchful eye on my horse Eddie while I was too busy with school to make it out to the barn.

I would also like to express my gratitude to the members of my thesis committee, Magda Petryniak, Gary Westbrook, Peter Mayinger, and Phil Stork, for helping steer and focus my research over the years.

Lastly, I am incredibly grateful to my family, friends, and fellow classmates for their support and encouragement. I would not have survived the first year of graduate school without my study partner and good friend Jeannie Hunnicutt. And to my family and friends, thank you for being there for me and motivating me to reach my goals and follow my passion.

Abstract

The myotubularin (MTMR) family of phosphoinositide (PI) 3-phosphatases specifically catalyze the dephosphorylation of phosphatidylinositol 3-phosphate (PI3P) and 3,5-disphosphate ($PI(3,5)P_2$), two lipids that regulate membrane traffic within the endosomal-lysosomal pathway. A number of studies have shown that phosphoinositide regulation in endosomal-lysosomal pathways is critical for functional myelination. This is highlighted by seven disease-causing mutations in human endosomal-related genes (FIG4, MTMR2, MTMR5, MTMR13, FRABIN/FGD4, SH3TC2 and SIMPLE/LITAF) that cause demyelinating forms of Charcot-Marie-Tooth (CMT) peripheral neuropathy. In humans, loss of MTMR2, MTMR5, or MTMR13 causes CMT type 4B1, 2, or 3, respectively. CMT peripheral neuropathies are challenging to treat clinically because the molecular pathogenesis behind known inherited gene mutations remains unclear. By studying demyelinating CMT genes and their function in Schwann cells, we hope to elucidate the molecular mechanisms that lead to demyelination and secondary axonal degeneration. To do this, we use a CMT4B mouse model (*Mtmr13*$^{-/-}$) to investigate resulting changes in cellular signaling pathways, endo-lysosomal membranes, and PI levels that might contribute to myelin dysregulation. The research performed in this dissertation further characterizes our CMT4B mouse model and describes the localization of endogenous mouse Mtmr2 and Mtmr13 proteins in Schwann cells. We also use this mouse model to attempt to rescue *Mtmr13*$^{-/-}$-related myelin outfoldings by PI 3-kinase knockouts. We take a novel approach to studying PIs in Schwann cells by exploring the role PI 3-kinases play in myelination, something that had never been done previously. Together, the data presented here advances the understanding of the molecular and PI changes that result from *MTMR13* mutations and how these changes contribute to disease pathogenesis and progression.

Chapter 1

Introduction

1. The Nervous System: CNS and PNS

The nervous system is divided into two major divisions: the central nervous system (CNS), comprised of the brain and spinal cord, and the peripheral nervous system (PNS). The CNS and PNS function together to control voluntary and involuntary actions coordinating the thought and movement required to complete complex tasks unique to *Homo sapiens*.

The PNS consists of sensory and motor nerves and ganglia that house neuronal cell bodies. The PNS serves to connect the CNS to the organs, limbs, and skin of the periphery to allow for complex movement, sensation, and behavior[1]. The PNS is further divided into the somatic and autonomic systems, associated with the voluntary control of body movements and the involuntary control of internal organs, respectively. Sensory neurons relay information such as mechanical signals, temperature, and pain from internal organs and external stimuli to the CNS. Motor neurons carry signals from the CNS to muscles, organs, and glands, and respond to incoming sensory signals to adjust for environmental changes or bodily needs. Sensory and motor neurons of the PNS are divided into fiber categories based on diameter and conduction velocity, and these fibers may be myelinated or unmyelinated[2]. Most large caliber axons are myelinated, while smaller caliber neurons bundle together and remain unmyelinated[2]. Peripheral axons are myelinated by Schwann cells, whereas oligodendrocytes myelinate CNS axons[3].

2. Schwann cell Development and Myelination in the PNS

Schwann cells wrap their cell membranes around axons to form a multi-layered membrane sheet that acts as an electrical insulator and forms points of contact with the axon to provide trophic support[4]. The myelin sheath allows for electrical signals in

axons (action potentials, APs), to travel rapidly down the axon to the axon terminal[3]. At the terminal, the action potential-induced depolarization leads to the release of neurotransmitter on the target muscle, organ, or gland[3], inducing muscle contractions and altering organ and glandular function.

The coordination of Schwann cell migration and initiation of myelination requires a complex pattern of transcription factor expression and developmental cues[5]. Schwann cells are neural crest derived, instructed to migrate out to the periphery and myelinate nerve axons through a network of transcription factors and extracellular signals[5]. As the neural plate folds to form the neural tube during development, neural crest cells are derived from the dorsalmost tips of the tube[5]. Neural crest cells migrate to various locations in the embryo where they differentiate into smooth muscle cells, adipocytes, melanocytes, neurons, and Schwann cells, as well as other cell types[4]. Neural crest cells that will differentiate into Schwann cells go through multiple developmental stages before becoming mature, myelinating glial cells[6]. Schwann cell differentiation from neural crest begins around embryonic day (E) 12-13 in the mouse, giving rise to Schwann cell precursor (SCP) cells[7]. SCPs express Cadherin-19 and activator protein 2α (AP2α)[4], which are not expressed in progenitor neural crest cell lineage. SCPs provide trophic support to developing sensory and motor neurons during migration, and the targeted knockout of SCP cells leads to extensive neuronal death in transgenic mouse models[7]. Although essential for neuronal survival, SCPs also rely on paracrine signaling from axons for their own survival. This mechanism matches the number of axons with the correct number of SCPs in developing nerves[4,5], highlighting the interdependence of neurons and glia for survival during early nerve development.

At mouse E13-15, SCPs become immature Schwann cells through a coordinated change in molecular expression[5], although relatively little is known about the transcription factors that control this switch. The role of one transcription factor, Sox10,

has been studied in depth, and its expression is required for SCPs to mature into immature Schwann cells[8,9,10]. The switch from SCP to immature Schwann cell occurs at the same time as a change in the origin of trophic/survival support: SCP trophic support comes from an external source, whereas immature Schwann cells receive trophic support in an autocrine manner[4]. Immature Schwann cells secrete autocrine factors such as insulin-like growth factor 2 (IGF2) and neurtrophin 3 (NT3) that promote survival[4,5].

Schwann cell proliferation is highest in the immature stage around E15[5]. Axons in developing nerves stimulate Schwann cell proliferation to control and refine Schwann cell number as necessary. For example, in newborn mice Schwann cell proliferation decreases when Schwann cells lose contact with axons in a transected nerve[11]. Additionally, neuregulin-1 (NRG1) on the axon stimulates Schwann cell division[12] in co-cultures of neurons and Schwann cells, however this has not yet been proven *in vivo*. In addition to axonal NRG1, transforming growth factor-beta (TGF-β) and laminins (the major component of the basal lamina that surrounds Schwann cells) control Schwann cell proliferation and division[13]. The balance of Schwann cell number is also regulated by cell death signals. During normal development apoptosis is tightly controlled in immature Schwann cells by nerve growth factor (NGF) acting through the p75 neurotrophin receptor expressed on Schwann cells[5,14].

Immature Schwann cells undergo phenotypic changes as they differentiate into mature myelinating and non-myelinating Schwann cells. At E18 developing nerves consist of axon-Schwann cell bundles surrounded by connective tissue, fibroblasts, and blood vessels[5]. Just before birth, Schwann cells send cytoplasmic processes into bundles of axons and sort axons based on size, determined by the amount of NRG1 type III (NRG1-III) expressed on the axon surface[12]. This process, known as radial sorting, continues postnatally until all Schwann cells have formed a 1:1 relationship with

large caliber axons destined for myelination[15]. Small diameter axons known as C-fibers (less than about 1 μm) remain unmyelinated and are surrounded by non-myelinating Schwann cells to form Remak bundles[15]. Disruption of formation of Remak bundles in transgenic mice causes progressive degeneration of C-fibers and sensory neuropathy, suggesting that non-myelinating Schwann cells provide support to C-fibers and are required for maintenance of axonal integrity[3]. The exact molecular mechanisms that control radial sorting and Remak bundle formation remain to be determined, but radial sorting relies on laminins, beta-1 integrin, and the rho family GTPase Rac1[15,16].

The final transition from immature Schwann cell to myelinating Schwann cell requires many molecular changes, including downregulation of factors associated with the immature Schwann cell state and increased expression of genes required for myelination. The transcription factor Krox20/Egr2 is a critical regulator of myelin gene expression. Krox20 null mice have decreased expression of several major myelin genes, including myelin protein zero (P0), myelin basic protein (MBP), peripheral myelin protein 22 (PMP22), Connexin 32, and myelin-associated glycoprotein (MAG)[5,17]. Along with induction of myelin gene expression, mature Schwann cells undergo a high level of lipid synthesis in order to produce the multiple layered myelin membrane sheath[3].

NRG1 is a critical regulator of developmental myelination, as well as remyelination in response to nerve injury[13,18]. It is expressed on the axon, where it signals through the heterodimeric tyrosine kinase receptors ErbB2 and ErbB3 (ErbB2/B3) expressed on the Schwann cell surface[19]. Axonal NRG1-III binds to ErbB2/B3, activating several downstream secondary messenger cascades in the Schwann cell, including increased intracellular calcium, activation of mitogen-activated protein kinase (MAPK), and phosphoinositide 3-kinase (PI 3-kinase/PI3K) pathways[19,20]. It is well established that the thickness of the myelin sheath is related

to the size of the axon[12]. NRG1 signaling is responsible for myelin sheath thickness as demonstrated in mice with the Schwann cell *ErbB2* gene disrupted[19]. *ErbB2* mutant mice have markedly hypomyelinated peripheral nerves, suggesting that NRG1 signaling through ErbB2/B3 is required for proper myelin thickness[19]. The discovery that mice with axonal NRG1-III mutations also had thinner myelin sheaths, and that overexpression of NRG1-III leads to hypermyelination, further supports the hypothesis that NGR1 signaling controls the thickness of the myelin sheath[13,21]. These studies suggest a model in which Schwann cells determine axon caliber and myelin sheath thickness. According to this model, the amount of axonal NRG1-III expression, which increases with increasing axon caliber, determines the thickness of the myelin sheath by signaling to the Schwann cell through the ErbB2/B3 tyrosine kinase receptors[13]. Interestingly, the importance of NRG1 in the CNS remains less clear and somewhat controversial[22].

Myelination occurs by the spiral extension of glial membranes around an axon[23], which then becomes compacted to form compact myelin. In the PNS, Schmidt-Lanterman incisures (SLIs), cytosolic compartments that run radially through compact myelin, connect the noncompact myelin layers called the adaxonal (the innermost) layer with the abaxonal (outermost) layer[24]. These cytosolic channels allow for communication and intracellular trafficking between different regions of the Schwann cell. As myelin is produced developmentally, compact myelin is made both radially (leading to increased thickness) and longitudinally (leading to increased length of internode) at about the same time, with new membrane continuously being added to the growing tip and expanding both radially and laterally[2]. Mature compact myelin in the PNS consists of up to 160 membrane layers with internodes that extend to up to 2 mm in length[2]. Therefore, the leading edge of the growing myelin sheath is far from the Schwann cell body. To support the leading edge, Schwann cells must tightly regulate

membrane trafficking from the abaxonal area, which contains the nucleus and the major cytoplasmic region, to the adaxonal region, where the myelin is being deposited. This issue highlights the importance of intracellular trafficking in Schwann cells, something that will be discussed in later chapters of this dissertation.

The mechanism by which myelin becomes compacted requires the expression of the adhesive proteins MBP and the basic intracellular domain of P0, which are attracted to the positively charged phospholipids of the myelin membranes and neutralize the repulsive charges of adjacent myelin membranes[2]. This charge neutralization allows for the bilayers of myelin to be pulled tightly together in a zipper-like mechanism, forming compact myelin[2]. In the PNS, myelin compaction can occur even in the absence of MBP, most likely by compensation by P0 and PMP22[2,25]. In the CNS, however, loss of MBP leads to a complete loss of compact myelin[2].

3. CNS Myelination

Myelin first emerged in cartilaginous fish over 500 million years ago, and has since enabled greatly increased propagation of nerve impulses along axons in vertebrates[26]. Myelin remains a defining characteristic of vertebrates and has arisen by parallel evolution in some invertebrates[26]. Vertebrate nervous systems have established two distinct cell types that myelinate nerve axons: Schwann cells and oligodendrocytes. There are similarities and differences between these cell types, including origin, myelin composition and structure, and the mechanisms through which they control myelination[2]. Some of these differences are briefly highlighted here, as the focus of this thesis is Schwann cells and PNS myelination.

Oligodendrocytes myelinate large caliber axons in the CNS, but have many distinct features from Schwann cells. Unlike Schwann cells, oligodendrocytes are not

neural crest derived; instead they originate in the subventricular zone of the developing brain[27]. Another major difference between the two myelinating glial cell types is that a single Schwann cell myelinates a single internode on one axon. Oligodendrocytes have multiple processes and a single cell can myelinate up to 60 different axonal segments[27]. Additionally, the cytoplasmic channels through compact myelin in adult peripheral nerves called SLIs remain open throughout life in the PNS[2]. Early in CNS developmental myelination, similar radial channels are open to provide membrane trafficking routes to the myelin sheath growth area, but they are mostly closed in adult myelin sheaths[2]. Instead, mature oligodendrocytes have tight junctions that allow for passing of intracellular molecules through compact myelin in the adult CNS[2].

Another striking difference between myelin of the CNS and PNS is the relative abundance of myelin proteins[3]. For example, P0 is the most abundant protein in PNS myelin, accounting for about 21% of total myelin proteins, but is undetectable in CNS myelin[2]. Proteolipid protein 1 (PLP1) is the most abundant protein in CNS myelin (17%), but comprises only 0.2% of peripheral myelin proteins[3].

4. Myelin Function

Myelination is required for rapid nerve conduction velocity in mammals. The subdomains and machinery in myelinated axons that enable rapid nerve conduction include: the node of Ranvier, the paranode, the juxtaparanode, and the internode[28]. In this section, I discuss how these domains are formed and regulated by SCs, and the resulting functionality of myelinated axons.

Nodes of Ranvier are the gaps between myelinating Schwann cells along the length of the axon and are typically 1 μm in length[29]. The node of Ranvier and its flanking domains contain the critical machinery that enables saltatory conduction[24].

Saltatory originates from the latin word *saltare* meaning to leap or hop and refers to the propagation of APs down the axon by hopping from one node to the next. This mechanism leads to increased conduction velocity of APs, allowing for rapid signaling and reduced energy expenditure. APs are generated at the axon initial segment where the axon connects to the neuronal cell body[28]. With the myelin sheath acting as an insulator to the axon, APs are able to jump from one node, where ion channels are clustered to regenerate the AP, to the next as they travel down the axon to the axon terminal.

The unmyelinated node of Ranvier is the region of the axon exposed to the extracellular environment[28]. Nodes are highly enriched in axonal voltage-gated sodium and potassium channels. For example, the expression of nodal sodium channel $Na_V1.6$ is 25-fold higher than along the internode, and is one of the key channels responsible for regenerating the AP during saltatory conduction[28]. At the node, both the axon and the Schwann cell express cell adhesion molecules involved in node formation, clustering of scaffold proteins such as ankyrinG, and clustering nodal ion channels[29].

The node is flanked by paranodes on either side consisting of paranodal loops, regions of the Schwann cell where compact myelin membrane has opened up to form cytoplasm-filled loops of the Schwann cell that wind around the axon[28]. These paranodal loops attach the Schwann cell and its corresponding compact myelin sheath to the axon by cell adhesion molecules expressed on both the axon (Caspr and contactin) and the Schwann cell (neurofascin 155)[24]. Intact paranode structure is required for localization of ion channels at the node and AP propagation down the axon[24].

Juxtaparanodes found next to the paranodes are enriched in cell adhesion molecules expressed on the Schwann cell and the axon, including Caspr2 on the axon and transient axonal glycoprotein-1 (TAG-1) on the Schwann cell[24]. Caspr2 anchors

Shaker-type potassium channels at the juxtaparanode region, which are required for maintaining the internodal resting potential, preventing re-entrant excitation, and also have a role in mediating axoglial communication[24].

The internode is the portion of the axon directly under the compact myelin sheath. This domain contains a distinct set of Schwann cell and axonal surface proteins that mediate Schwann cell-axon interactions. MAG is an adhesion molecule expressed by the Schwann cell during myelination[24]. Interestingly, MAG knockout mice are able to myelinate normally, suggesting that other molecules also mediate axoglial adhesion along the internode[24]. Nectin-like (Necl) proteins are expressed by both the axon and the Schwann cell, and are necessary for axoglial interactions and adhesion along the internode[24,30]. Axons express high levels of Necl-1 and -2, whereas Schwann cells express high amounts of Necl-4 and very low amounts of Necl-2[30].

The four subdomains described above are characteristic of all myelinated fibers. Understanding the roles of individual molecules within each domain is critical to our overall understanding of how nodes of Ranvier and paranodal junctions participate in bi-directional signaling between neurons and glia. The development and maintenance of these subdomains is critical for APs to reach target muscles or organs. Without myelinated fibers, we would lack rapid conduction of nerve impulses that facilitate the integration of sensory and motor information.

5. Peripheral Nerve Injury

Damage to peripheral nerves can cause a host of pathological conditions and diseases in humans. Injury to peripheral nerves can occur from a variety of causes including laceration, compression, viral infection, or inflammatory autoimmune reaction[31]. Nerve injuries can also be toxin-mediated[31]. For example, certain

chemotherapeutic drugs, including Cisplatin and Vincristine, can cause acute peripheral nerve damage[31]. Additionally, nerve tumors that form in the PNS can affect nerve function causing clinical disability and pain[31]. Hereditary neuropathies, like Charcot-Marie-Tooth (CMT), also cause PNS nerve damage through genetic mutations that cause either axon or Schwann cell dysfunction.

Depending on the peripheral nerves affected, clinical outcome from nerve damage manifests differently[31]. Motor neuron damage or dysfunction results in muscle weakness or paralysis, whereas sensory neuron dysfunction results in altered or lost sensation[32]. Therapy for patients with motor nerve injury involves patient education and use of devices (such as leg or arm braces) which protect joints and surrounding tendons and ligaments from further stress or damage[32]. Peripheral nerve injury can also manifest as neuropathic pain requiring topical and oral medication to control the pain[31]. Research strategies commonly focus on trying to understand the origins of peripheral nerve dysfunction or attempt to initiate PNS remyelination. However, most PNS conditions are poorly understood and currently no therapies exist that successfully expedite nerve regeneration and/or remyelination.

The PNS has the unique ability to regenerate after *acute* nerve injury, unlike the CNS where nerve regeneration is sparse and normal function is rarely restored[11,33]. Following acute peripheral nerve injury, neurons and Schwann cells repair the injury site by regenerating new axons and initiating remyelination[33]. After injury, the neuronal cell body of an injured neuron usually shows increased neural activity, which opens calcium channels and initiates Jun-kinase signaling cascades[33]. Both neurons and Schwann cells in the injury region activate various signaling pathways, including the MAPK/ERK pathway and Notch signaling, to initiate nerve regeneration and myelin repair[33]. A few hours post-injury, the axon and myelin sheath begin to degenerate in a process known as Wallerian degeneration. Macrophages migrate to the site of injury and infiltrate the

site to clear debris. Schwann cells respond to the injury event by pulling away from the degenerating axon, dedifferentiating, then proliferating[33]. Proliferative Schwann cells cease expression of Krox20, a transcription factor that is expressed specifically in myelinating Schwann cells[33]. Reduction in Krox20 expression leads to decreased expression of pro-myelin and myelin-specific genes. Simultaneously, Schwann cells upregulate expression of transcription factors such as Sox10 and Oct6, which are associated with immature non-myelinating Schwann cells[33]. Dedifferentiated Schwann cells form Bands of Bunger, columnar structures along which regenerating axons grow[33]. Once the axon is successful regenerated, Schwann cells regain contact and trigger differentiation of the myelinating Schwann cell lineage by expressing myelin genes, then remyelinate the newly regenerated axon[33]. In addition to mechanical damage, injured nerves also lose neurotrophic support from their targets, which can contribute to neuronal cell death by apoptosis[33]. The neuroprotective role of neurotrophic support is currently under investigation as an avenue for treating peripheral nerve injuries and diseases[13].

Despite the ability of the PNS to regenerate after injury, remyelinated axons have significantly thinner myelin sheaths than those formed during developmental myelination[33]. This might be due to a decrease in Schwann cell responsiveness to axonal NRG1-III, which during developmental myelination is critical for myelin sheath thickness, as discussed previously[13]. NRG1-I and -III are critical during both developmental myelination and remyelination after injury; future studies will clarify the role of each isoform in these two distinct types of myelination[13].

The PNS has a remarkable capacity to regenerate and remyelinate nerves. A better understanding of the signaling events behind regeneration and remyelination will aid in the development of novel therapies to treat peripheral nerve injury and increase the clinical outcome of nerve injury and peripheral nerve disease.

6. Demyelinating Diseases

In contrast to Wallerian degeneration after nerve injury, demyelinating diseases primarily affect the function of the myelinating glial cell leading to secondary axonal degeneration and clinical disability in patients. Demyelination is a hallmark neuropathology of many neurological diseases of the CNS and PNS, including multiple sclerosis (MS), chronic inflammatory demyelinating polyneuropathy (CIDP), Guillain-Barre Syndrome, and CMT. MS is a chronic autoimmune disease in which the immune system attacks myelin and myelin-making cells (oligodendrocytes) of the CNS, leading to demyelination and secondary neurodegeneration, resulting in severe clinical disability[34]. In patients with CMT, demyelination results from an inherited genetic mutation in myelin genes or genes that are necessary for myelination[35,36]. Wallerian degeneration occurs as response to acute injury, whereas chronic injury caused by demyelinating diseases such as MS, CIDP, and CMT have little nerve regeneration[32].

7. Charcot-Marie-Tooth Disease

CMT is an inherited peripheral neuropathy that affects about one in 2500 people worldwide, and is the most common degenerative disorder of the PNS[37]. Inherited peripheral neuropathies have been challenging to treat, and there is no effective therapy to alleviate symptoms in these patients. In recent years, increased access to and better tools for genomic sequencing has revolutionized the molecular genetics of inherited neuropathies[38]. Over 40 CMT-causing genes have been identified containing various types of mutations, including duplications, point mutations, and truncations[39]. CMT is divided into two major subtypes: CMT1, which is a demyelinating form of the disease, and CMT2, an axonal form[38]. In demyelinating CMT, the Schwann cell or myelin is the

primary target of the disease, resulting in demyelination[38]. A subset of axons can sometimes be remyelinated, which is distinguished histologically by the presence of a thinner myelin sheath and onion bulb structures[38]; the remainder of axons largely fail to become remyelinated leading to secondary axonal degeneration and disability in CMT1 patients[40]. CMT2 gene mutations cause a defect in the axon, leading to axon atrophy, shrinkage, and degeneration[40]. This causes loss of nerve innervation at peripheral targets, again leading to disability.

Diagnosis of CMT1 or CMT2 is made clinically by electromyography (EMG) and by nerve biopsy studies. With EMG testing, demyelinating CMT (CMT1) is characterized by motor nerve conduction velocity (MNCV) less than 38 meter/second (m/s) in upper motor nerves, whereas axonal CMT (CMT2) is characterized by normal or slight reduction in MNCVs (usually greater than 45 m/s) with a decrease in compound motor and sensory action potential amplitude[38].

7.1 Clinical Presentation

CMT is a slowly progressive disorder, most often presenting in the second decade of life[41]. Common phenotypes include distal motor and sensory deficits, foot deformities, gait abnormalities, and atrophy of distal muscles of the lower legs and calves[41]. As the disease progresses, atrophy and sensory deficits of the hands are common, resulting in disfigured fingers causing loss of fine motor control and severe disability[37]. Foot drop also common in CMT patients, which occurs from deinnervation of distal foot muscles causing difficulty dorsiflexing the foot when walking[37]. Motor symptoms are more common than sensory symptoms in CMT patients, and most patients require assistance to ambulate through the use of leg braces that aid in walking and prevent foot drop[41]. Depending on the progression of CMT and the extent of

axonal degeneration, patients may become wheelchair-bound and become severely and permanently disabled. Clinical care of CMT patients involves the coordination of various specialists, including podiatrists for foot problems and care, physical therapists to help strengthen and conserve muscle tone, orthopedic surgeons for procedures to straighten hammer toes and lower arches, and a neurologist for making the initial diagnosis, overseeing care, and prescribing medication for neuropathic pain, when necessary[37].

7.2 Inheritance

Both CMT1 and CMT2 are most commonly inherited in an autosomal dominant manner[37]. Autosomal recessive and X-linked inheritance also occurs and is classified as CMT4 and CMTX, respectively[37]. Autosomal recessive forms of CMT are rare in Western countries, but are more common in countries with a high prevalence of consanguineous marriages[40]. Mutations in four genes account for over 90% of all CMT cases: PMP22, P0, gap junction beta-1 (GJB1), and mitofusin 2 (MFN2)[38]. The remaining 10% of CMT results from mutations in various other CMT-causing genes[38], including the myotubularin-related phospholipid phosphatases (MTMR) 2, 5 and 13, which are the focus of this thesis.

7.3 *MTMR2*, *MTMR5*, and *MTMR13* CMT4B-causing mutations

Autosomal recessive CMT (AR-CMT) is characterized by early onset and rapid clinical progression[38]. AR-CMT appears around age two or three, and results in severe polyneuropathy with marked distal limb and spinal deformities[38]. MTMR gene mutations lead to severe forms of demyelinating AR-CMT, collectively designated CMT4B[40]. Mutations in *MTMR2* cause CMT4B1, mutations in *MTMR13* cause CMT4B2, and mutations in *MTMR5* cause CMT4B3[38,40,42]. Sural nerve biopsies from

all three types show severe loss of myelinated fibers and the hallmark of CMT4B: myelin outfoldings and infoldings[38,42]. Myelin outfoldings and infoldings are excess loops of compact myelin formed outside and around the layer of myelin that surrounds the primary axon[43]. These aberrant myelin structures are most commonly found at paranodes and SLIs, regions of the Schwann cell that contain cytoplasm[43]. Paranodes and SLIs contain intracellular organelles such as endosomes and lysosomes, and are thought to be the regions of the Schwann cell where addition and turnover of myelin membrane takes place[43]. Exactly how mutations in either *MTMR2*, *5*, or *13* lead to myelin outfoldings remains unclear; however, based on the known role of MTMR proteins in regulating vesicular trafficking[44], it is hypothesized that loss of function may disrupt membrane trafficking in the Schwann cell critical for proper myelination.

MTMR2 mutations were first reported in a large Italian family with ten affected family members[45]. Affected individuals had severe motor and sensory neuropathy and focally folded myelin sheaths (myelin outfoldings/infoldings)[40]. The disease causing mutation was mapped to a substitution at the 1276 cysteine in exon 11[45]. A second, inbred family in Saudi Arabia was described a few years later, with compound heterozygous mutations causing MTMR2 gene disruption[45].

Multiple disease-causing mutations in *MTMR13*, the focus of this thesis, have been described[46,47]. CMT4B2 was first discovered in a Turkish family with four affected individuals with disease onset around age five[47]. The mutation was mapped to a homozygous in-frame deletion of exons 11 and 12[47]. In two other consanguineous families, from Tunisia and Morocco, affected family members have homozygous nonsense mutations in the *MTMR13* gene[46]. In these families, affected individuals presented with demyelinating sensory and motor neuropathy, as well as early-onset glaucoma causing severe visual impairment or complete loss of vision[46].

CMT4B3, caused by *MTMR5* mutations, was first described in 2013 in a Korean family with compound heterozygous mutations in *MTMR5[42]*. CMT4B3 appears less severe than 4B1 and 4B2, and the Korean patients described had no early motor deficits or developmental delay, but experienced progressive weakening of the legs and difficulty walking later in life[42]. By age 43, two of the three patients described were wheelchair-bound and the third patient was able to walk with crutches[42]. The function of MTMR5 in the Schwann cell is largely unknown, but it is structurally similar to MTMR13 and has been shown to interact with both MTMR2 and MTMR13[48].

Although the myotubularin disease-causing mutations have been mapped, relatively little is known about the normal function of these proteins in Schwann cells and their role in myelination. Understanding the molecular pathogenesis of the disease will require an initial understanding of the role of myotubularin proteins in Schwann cells and myelination. The next section will further describe the myotubularin proteins that cause CMT, and outline their known cellular functions.

8. Phosphoinsitides and Metabolizing Enzymes

Phosphoinositides (PIs) are essential lipids in eukaryotic cell membranes, responsible for regulating fundamental cellular processes[49]. PIs can be phosphorylated at three sites on the inositol ring to make seven distinct isoforms[49]. A large network of PI kinases and phosphatases tightly control the amount of each PI isoform[50]. The MTMR family of proteins are PI 3-phosphatases (or pseudophosphatases), with specificity to catalyze removal of phosphate groups on the third position[51]. Here I describe the role of PIs in the cell, discuss the MTMR family of proteins, and describe the known cellular functions of the myotubularins studied in this thesis work: MTMR2 and MTMR13.

8.1 Phosphoinositides

PIs arise from the phosphorylation of phosphatidylinositol (PtdIns) on the inositol ring of the phospholipid[52]. Although PIs make up only a minor portion of cellular membrane lipids, less than 1%, they are critical in nearly all aspects of cellular physiology, including endocytosis, exocytosis, proliferation, cell mobility and survival, the control of endosomal dynamics, and the regulation of virtually all membrane trafficking within the cell[53].

PtdIns is synthesized through the conversion of phosphatidic acid into PtdIns at the endoplasmic reticulum, then delivered to cellular membranes where it is reversibly phosphorylated to generate one of the seven distinct PI species: PI3P, PI4P, PI5P (the monophosphorylated derivatives of PtdIns), $PI(3,4)P_2$, $PI(3,5)P_2$, $PI(4,5)P_2$ (the bisphosphorylated), and $PI(3,4,5)P_3$ (the single triphosphorylated isoform)[50]. The phosphorylation reactions occurs at free –OH groups on the inositol ring[54]. The abundance of each PI species in the cell has been estimated, with some variations reported[50]. $PI(4,5)P_2$ and PI4P are thought to be the most abundant PIs in mammalian cells, followed by PI3P, $PI(3,5)P_2$, PI5P, and $PI(3,4)P_2$[55]. Production of $PI(3,4,5)P_3$ is induced upon cell stimulation, therefore levels of $PI(3,4,5)P_3$ are low in a resting cell and significantly higher when the cell becomes activated[49].

PI kinases and phosphatases are responsible for the metabolism and rapid turnover of membrane-bound PIs[54]. The seven PIs are enriched on specific intracellular membranes or the plasma membrane. For example, $PI(4,5)P_2$ is highly enriched on the plasma membrane and is involved in nearly all signal transduction events at the cell surface[49]. The classical downstream signaling pathway begins with cleavage of newly produced $PI(4,5)P_2$ by phospholipase C (PLC), giving rise to the

metabolites PI_3 and DAG, which propagate and amplify the plasma membrane signal[49]. To terminate $PI(4,5)P_2$ signaling at the plasma membrane and the activated downstream pathways, cellular 5-phosphatases remove the 5 phosphate group from $PI(4,5)P_2$, re-establishing the pool of plasma membrane PI4P and turning off signaling[49].

Aside from signal transduction at the plasma membrane, PIs are also critical in controlling cell signaling and trafficking within the cell[52]. For example, PI3P is highly enriched on early endosomes[50], but as endosomes mature, the lipid content is modified to higher amounts of $PI(3,5)P_2$ through further phosphorylation at the 5 position by Fab1/PIKfyve[50]. These two endosomal PIs control trafficking by modulating dynamics in the early/late endosome and lysosome[49].

The phosphorylated headgroup on intracellular PIs bind critical effector proteins, leading to recruitment of specific proteins to PI-enriched regions of the cell [49]. The phosphate(s) on the PI gives the lipid a negative charge, enabling cytosolic proteins to bind PIs through electrostatic interactions[54]. Specific protein sequences and domains known to bind PI headgroups are rapidly increasing as the study and understanding of PIs expands. One example of a known protein domain that binds PI headgroups is the pleckstrin homology (PH) domain, which binds electrostatically to the negatively charged PI through a cluster of basic (positive) residues within an unstructured region of the domain[54].

Interactions between PIs and PI-binding effector proteins are usually low affinity, transient interactions[54]. More stable, and more specific, interactions can be achieved when PIs cooperate with other binding sites on nearby membrane proteins. This cooperation is known as “coincidence detection” and is a powerful way to regulate membrane-cytosol interactions with high specificity[50]. A classic example of how PIs function as coincidence detectors is the clathrin adapter protein AP-2. AP-2 is selectively

recruited to the plasma membrane through binding to the negatively charged headgroup of $PI(4,5)P_{2[49]}$. Initial contact with $PI(4,5)P_2$ leads to a conformational change in one of the AP-2 protein subunits, leading to exposure of an additional binding site for $PI(4,5)P_2$ and a binding site for a membrane protein co-receptor[49]. These multiple interactions stabilize AP-2 association with the plasma membrane, increasing binding affinity and specificity[49]. Coincidence detection allows the cell to independently regulate each component of effector protein recruitment and binding by regulating the abundance and localization of PIs, as well as regulation of the protein co-receptor through phosphorylation or other modifications.

The localization and steady-state level of PIs is tightly controlled by the expression and enzymatic action of PI kinases and phosphatases, which is critical for intracellular membrane trafficking[56]. For example, intracellular vesicles must have a specific PI lipid composition to recruit the appropriate effector proteins enabling fusion of the vesicle with its destination membrane. The PI content of vesicles acts as an identity code to direct vesicular trafficking in the cell. The strategic localization of kinases and phosphatases assures that vesicles can rapidly change their PI membrane identity code when docked at the acceptor membranes. Additionally, the PI content of intracellular membranes enables recruitment of appropriate proteins to endosomes or lysosomes, for example, where their action is needed.

8.2 Endosomal PIs

PI3P and $PI(3,5)P_2$ are enriched on endo-lysosomal membranes and are key regulators of endo-lysosomal trafficking[57]. Endosomes are small intracellular membrane compartments that receive cargo from the plasma membrane and aid in cargo delivery to other compartments. The early endosome acts as a sorting station,

where small vesicles containing endocytosed cargo arrive and may be recycled back to the plasma membrane (via recycling endosomes) or targeted for degradation in the lysosome[58].

PI3P is highly enriched on early endosomal membranes and to a lesser extent on late endosomes, and controls several aspects of biology at the endosome[57]. Through the recruitment of specific PI-binding effector proteins, PI3P is required for the tethering and fusion of vesicles to the early endosome membrane[57]. It regulates sorting of endocytosed cargo destined either for recycling or degradation[57]. Additionally, PI3P controls the retrieval of proteins from the lysosome back to the endosome[58]. For each of these different processes, a unique set of effector proteins are recruited and bind to the PI3P headgroup on PI3P-rich endocytic membranes.

Protein binding domains containing FYVE and PX domains specifically bind PI3P[49]. The FYVE domain is between 60-70 amino acids in length and has a basic motif that creates a positively charged pocket for PI3P binding[59]. PX domains are 130 amino acid regions containing an N-terminal beta-sheet and a helical subdomain, which form a pocket in which PI3P binds[60]. Many PI3P binding proteins also bind Rab5, an early endosome-associated GTPase[59]. Together, PI3P and Rab5 act as a coincidence detection mechanism to control endocytic vesicle fusion and recruit specific proteins to endosomal membranes[59]. Aside from the function of PI3P at the endosome, it also plays a critical role in autophagy, which will be discussed in more detail later.

Once PI3P is on an endosomal membrane, it may either undergo dephosphorylation at the endosomal surface by 3-phosphatases, be degraded in the lumen of a multivesicular body when the endosome is internalized, or be further phosphorylated by Fab1/PIKfyve to make $PI(3,5)P_2$[57]. $PI(3,5)P_2$, which becomes enriched as the endosome matures into a late endosome, is thought to trigger membrane recycling through late endosome vesicle budding, thus controlling the size of

lysosomes[57]. PI(3,5)P_2 on late endosomes is also involved in the inward invagination of intraluminal vesicles into multivesicular bodies (MVB), which facilitates sequestration of cargo such as epidermal growth factor receptor (EGF-R)[57]. It is hypothesized that altering the expression of PI kinases and phosphatases disrupts the balance of PI3P and PI(3,5)P_2 on endosomes, which disrupts sorting and inhibits degradation plasma membrane receptors. Thus, PI3P and PI(3,5)P_2 are important regulators of intracellular membrane trafficking through the endosomal system[57].

8.3 PIs in Autophagy

The role of PIs in autophagy was first discovered in yeast when a screen for vacuolar sorting defects pulled out the protein Vps34, a PI 3-kinase[50] [61]. Pharmacologically inhibiting Vps34 using wortmannin or 3-methyladenin blocks functional autophagy, suggesting that Vps34 is critical in autophagy[62]. Additionally, increasing PI3P in mammalian cells stimulates autophagy, suggesting that PI3P produced by Vps34 is critical for autophagy[62].

Autophagy is the process by which cells degrade cytoplasmic proteins and organelles in response to starvation[63]. Autophagy is distinct from other endocytosis-mediated lysosomal degradation pathways, which degrade extracellular and plasma membrane proteins, and the ubiquitin-proteasome system[63]. There are three types of autophagy: macroautophagy, microautophagy, and chaperone-mediated autophagy[63]. The term “autophagy” generally refers to macroautophagy, or the bulk degradation of cytoplasmic proteins and organelles. The initiation of autophagy begins with formation of a membranous omegasome that is connected to the ER, but may also contain Golgi and mitochondrial membrane[63]. Autophagy related protein 14 (Atg14) at the omegasome recruits Vps34 to catalyze local PI3P production[63]. PI3P at the omegasome is

recognized by FYVE domain-containing proteins, including WIPI1 (WD repeat domain phosphoinositide-interacting protein 1) and DFCP1 (double FYVE containing protein 1)[64]. The omegasome membrane continues to grow and mature while other signaling proteins are recruited[64]. A PI3P rich, mature omegasome gives rise to the isolation membrane[64]. The isolation membrane in turn matures to become an immature autophagosome, and eventually the two ends of the membrane fuse to form a mature, double membraned autophagosome[64].

The sequenced recruitment of autophagy-related proteins is critical for initiation and progression of autophagy. Various proteins are responsible for controlling aspects of the autophagic process, but Vps34 appears to be a key regulator of autophagy initiation and progression, and can form various distinct autophagy-related complexes. One such complex is Vps34-Vps15-Atg14-Beclin1, which is critical for functional autophagy in mammalian cells[65]. This complex controls Vps34 kinase activity during autophagosome biogenesis and maturation[65]. Once the autophagosome matures it fuses with a lysosome, forming an autolysosome. At this point, internalized macromolecules are degraded by acidic lysosomal hydrolases and the monomeric units, amino acids, are exported back to the cytosol for reuse[63].

8.4 Summary of PIs in the cell

PI membrane lipids are central in cell signaling and regulation, and are involved in many aspects of cell life and death. They regulate intracellular trafficking, ion channel physiology, pumps and transporters, endocytic and exocytic processes, and autophagy. An emerging area of PI research is role of nuclear PIs and their soluble analogs in nuclear processes such as DNA repair, transcription regulation, and RNA dynamics[49]. Additionally, the study of PI metabolizing enzymes, such as PI-kinases and

phosphatases, remains a key component of PI signaling requiring further study in light of the numerous human diseases linked to mutations in PI metabolizing enzymes[64,66].

8.5 PI metabolizing enzymes: Myotubularin phosphatases

The myotubularins are a large, highly conserved family of proteins found in eukaryotic cells[51]. Humans express fourteen different myotubularin proteins: myotubularin 1 (MTM1) and myotubularin-related (MTMR) proteins 1-13[56]. Eight of the members of the myotubularin family are catalytically active phosphatases and six are catalytically inactive[48]. The catalytically active myotubularin proteins include: MTM1, MTMR1, MTMR2, MTMR3, MTMR4, MTMR6, MTMR7, and MTMR8[48]. These are PI 3-phosphatases that dephosphorylate PI3P and PI(3,5)P_2 and are responsible for controlling their abundance and turnover[48], as well as production of PI5P.

Catalytically inactive myotubularins do not have the canonical $C(X)_5R$ catalytic motif[56]. The proteins in this group include: MTMR5, MTMR9, MTMR10, MTMR11, MTMR12, and MTMR13[56]. These proteins do not act as active phosphatases or substrate-traps, but contain various domains with known functions that lend clues to their roles in the cell.

Aside from the catalytically active or inactive phosphatase motif, there are domains common to all MTMR proteins, as well as domains shared only by subsets of myotubularins. The common domains include: a PH-GRAM (Pleckstrin homology-glucosyltransferases, rab-like GTPase activators and myotubularins) domain, which binds PIs, a PDZ-binding domain, which mediates protein-protein interactions, and a coiled-coil (CC) domain critical for homo- and heterodimerization of myotubularins[56]. Additionally, a subset of myotubularins (MTMR3, 4, 5, and 13) also contain DENN domains, an intriguing domain because of its GTPase activity[56]. Colleagues in the lab

are currently studying the DENN domain of MTMR13 to understand Rab regulation in Schwann cells.

An interesting property of MTMR proteins is the ability to homo- and heterodimerize through CC domains[48]. The catalytically inactive pseudophosphatases heterodimerize with active myotubularins. Indeed, our group has shown that MTMR2 (active) and MTMR13 (inactive) form a complex and stabilize one another in the sciatic nerve[67]. Mutation of either *MTMR2* or *13* cause similar CMT4B phenotypes, as discussed above, suggesting that the two proteins function as a complex in Schwann cells. Aside from protein stabilization, heterodimerization may also increase the enzymatic activity of the catalytically active protein in the complex. Additionally, heterodimerization may play a role in localization and targeting to specific subcellular domains, or may be involved in PI substrate preference of the active myotubularin. For example, the MTMR8/9 complex exhibits preference for dephosphorylating PI3P, compared to the MTMR6/9 complex, which shows preference for $PI(3,5)P_{2[48]}$.

8.6 MTMR2 and MTMR13

Our lab is primarily focused on understanding the role of MTMR13 in Schwann cells and in the process of myelination. Because MTMR2 and MTMR13 heterodimerize, we also are interested in the role of MTMR2 in coordination with MTMR13. Both MTMR2 and MTMR13 are ubiquitously expressed[43]. MTMR2 has been studied in depth by Alessandra Bolino and colleagues, who made and characterized an *Mtmr2* knockout mouse model of CMT4B1[68,69]. This mouse model has greatly enriched our understanding of CMT peripheral neuropathies. These mice are viable, myelin compaction and ultrastructure is normal, and myelin outfoldings are observed at paranodal regions and SLIs. The myelin outfoldings are strikingly similar to those

observed in CMT4B1 patients, although the mouse phenotype appears somewhat less severe[68].

Because MTMR2 is ubiquitously expressed, cell type-specific *Mtmr2* knockout mice were also characterized. These mice demonstrated that loss of function of *Mtmr2* in Schwann cells alone, and not motor neurons, is sufficient to cause CMT-related myelin outfoldings[68]. These CMT mouse models also revealed that the scaffold protein discs large 1(Dlg1)/synapse associated 97 (SAP97) interacts with MTMR2 in Schwann cells, and that expression of Dlg1/SAP97 is almost entirely lost, with remaining protein mislocalized in *Mtmr2*$^{-/-}$ mice[68]. Dlg1/SAP97 is involved in polarized membrane trafficking, and MTMR2 regulates PIs critical for endo-lysosomal membrane trafficking, therefore it was hypothesized that MTMR2/Dlg1 may together regulate myelin membrane formation and homeostasis in Schwann cells. In nerves where MTMR2 is absent and the MTMR2/Dlg1 interaction is lost, excess myelin membrane is formed, which leads to formation of myelin outfoldings in regions of the myelin sheath closely associated with Schwann cell cytoplasmic regions where trafficking occurs[68].

A role for MTMR2 in axons was subsequently uncovered by investigating *Fig4/Mtmr2* double-knockout mice. Loss of *Mtmr2* in *Fig4*-null mice exacerbated neurodegeneration and reduced neuronal viability[70]. FIG4 is a PI 5-phosphatase required for both the generation and turnover of PI(3,5)P_2 through its phosphatase activity and its role in activation of the 5-kinase PIKfyve/Fab1 that generates PI(3,5)P_2 from PI3P. Mice with heterozygous deletion of *Fig4* (one wild type allele, one deletion allele) also showed a decrease in myelin outfoldings compared to *Mtmr2* only knockout mice[70], suggesting that an imbalance of PI(3,5)P_2 contributes to altered myelin growth and myelin outfoldings in *Mtmr2*$^{-/-}$ mice and CMT4B1 patients.

Less is known about MTMR13 in Schwann cells. *MTMR2* and *MTMR13* are genetically linked to CMT type 4 and mutations in either gene cause CMT4B. Early

studies of MTMR2 and MTMR13 showed that these proteins form a complex that fractionates in the light membrane fraction from mammalian cells[71]. As a result, it was hypothesized that the two proteins colocalize on early endosomes and control endo-lysosomal traffic. Our lab made and characterized *Mtmr13*$^{-/-}$ mice, which faithfully model CMT4B2 and contain the hallmark myelin outfoldings[72]. These outfoldings worsen as the mice age, and secondary axonal degeneration occurs in peripheral nerves[72]. Using this mouse model, we furthered our understanding of the role of MTMR13 in Schwann cells, which will be discussed in chapter 2.

An interesting domain on the MTMR13 protein, and perhaps a clue to its function, is the DENN domain, which MTMR2 lacks. MTMR13 may regulate Rab activation in Schwann cells through its DENN domain[48]. DENN domains are evolutionarily conserved protein modules that interact directly with members of the Rab family of small GTPases[48]. They function as guanine nucleotide exchange factors to activate Rabs by loading GTP. The role of Rab proteins in Schwann cells is relatively unknown, and the Robinson lab is poised to ask interesting questions about how Rabs might contribute to myelin membrane trafficking and maintenance.

8.7 PI metabolizing enzymes: PI 3-kinases

PI 3-kinases (PI3Ks), discovered in the mid-1980s, phosphorylate the 3 position on PIs[64]. Since their discovery, PI3Ks have been found in all eurkaryotic cells and play incredibly diverse roles. The large group of structurally-related PI3Ks are divided into three families: class I, class II, and class III[64].

The class I PI3Ks can phosphorylate PI to PI3P, PI4P to $PI(3,4)P_2$ and $PI(4,5)P_2$ to $PI(3,4,5)P_3$ ("PIP3"), with substrate preference for $PI(4,5)P_{2[64]}$. There are four class I PI3Ks in humans and mice, which are largely cytosolic in resting cells[64]. Upon

stimulation, they are recruited primarily to the plasma membrane where their substrates reside. Akt signaling at the plasma membrane is the canonical signaling pathway controlled by class I PI3Ks. PI(4,5)P_2 is phosphorylated by class I PI3Ks at the plasma membrane to make PIP3, which in turn recruits Akt through a PIP3-specific PH domain interaction[64]. Akt at the plasma membrane is phosphorylated and activates various downstream signaling pathways.

Class II PI3Ks are the least well-understood class of PI3Ks. Mammals have three class II PI3Ks: alpha, beta, and gamma[64]. These kinases are most commonly associated with membrane structures and are less cytoplasmic than the class I kinases. Various extracellular signals can stimulate class II kinase activity, but no clear mechanism of activation has been described[64]. *In vitro*, class II PI3Ks can phosphorylate PI4P but not PI(4,5)$P_{2[64]}$. A recent study showed that class II PI3Ks can also phosphorylate PI to produce a pool of PI3P involved in the initiation of autophagy in mouse embryonic fibroblast (MEF) cells[73].

There is a single class III PI3K in mammalian cells, Vps34, discussed in earlier sections. Vps34 has a single substrate, PI, distinguishing it from the other two classes of PI3Ks[62]. The primary role of Vps34 in endocytic sorting has been studied extensively in yeast; however, in mammalian cells Vps34 appears to also contribute to phagocytosis, autophagy, and possibly nutrient sensing through the activation of the mTOR pathways[62].

PI3K signaling is shut off by the degradation of PI isoforms by the MTMR family of 3-phosphatases discussed above. The tight regulation of PIs by kinase and phosphatase expression is critical for cell function, highlighted by mutations in both PI kinases and phosphatases that lead to human disease.

8.8 PIs in human disease

A number of mutations in both PI phosphatases and kinases cause human genetic disease, including CMT. For example, mutations in *MTM1* cause congenital myopathy X-linked centronuclear or myotubular myopathy, and *MTMR14* mutations cause an autosomal form of myotubular myopathy[66]. Mutations in the 5-phosphatase *FIG4* cause CMT4J in human patients and CNS neurodegeneration in mouse models[66]. Finally, mutations in *Fab1/PIKfyve* in mice lead to severe neurodegeneration[74]. These disease causing mutations in PI metabolizing enzymes highlight the importance of PIs.

Most genes involved in PI-related human diseases are ubiquitously expressed, but the resulting human diseases appear to manifest only in specific cell types. For example, in CMT Schwann cells are disproportionately affected by loss of function of a PI 3-phosphatase. In *MTM1* myopathies, muscle cells are primarily affected[66]. In both of these examples, the mutated protein is expressed in every cell in the body, but only one cell type is affected. The cell type-specific manifestation of disease suggests that such proteins are responsible for specific and critical cellular functions that remain poorly understood, and in our studies of CMT we hope to understand why loss of myotubularin protein function is specifically detrimental to Schwann cells.

Additionally, endosomal PIs, the focus of the research in our lab, appear to be especially sensitive to dysregulation. Aside from the CMT-causing MTMR proteins involved in endosomal trafficking, loss of function of three other proteins (LITAF, FRABIN, SH3CT2) known to control traffic through or at the early endosome cause CMT, further highlighting the importance of endosomal trafficking in neurons and glia[58,66]. By studying the basic biology of endosomal trafficking, we hope to gain an understanding of the mechanisms behind these diseases and uncover potential therapeutic targets.

The collection of mutations in PI kinases and phosphatases that cause human disease suggests that PI regulation in mammalian cells is critical, and that loss of PI regulation is detrimental. When phosphatase function is lost, the resulting phenotype could be due to an imbalance in both the substrates and products of that enzyme[75]. The *Fig4/Mtmr2* double-knockout mouse was used to demonstrate that renormalizing substrate PI levels through kinase knockdown in a phosphatase-deficient system is a viable method for altering a phenotype[70]. We further address the hypothesis that manipulating levels of PIs in a phosphatase deficient system may be of therapeutic benefit through the rebalancing of PI levels in mammalian cells. The work described in the following chapters will investigate this issue in further detail.

Figures and Legends

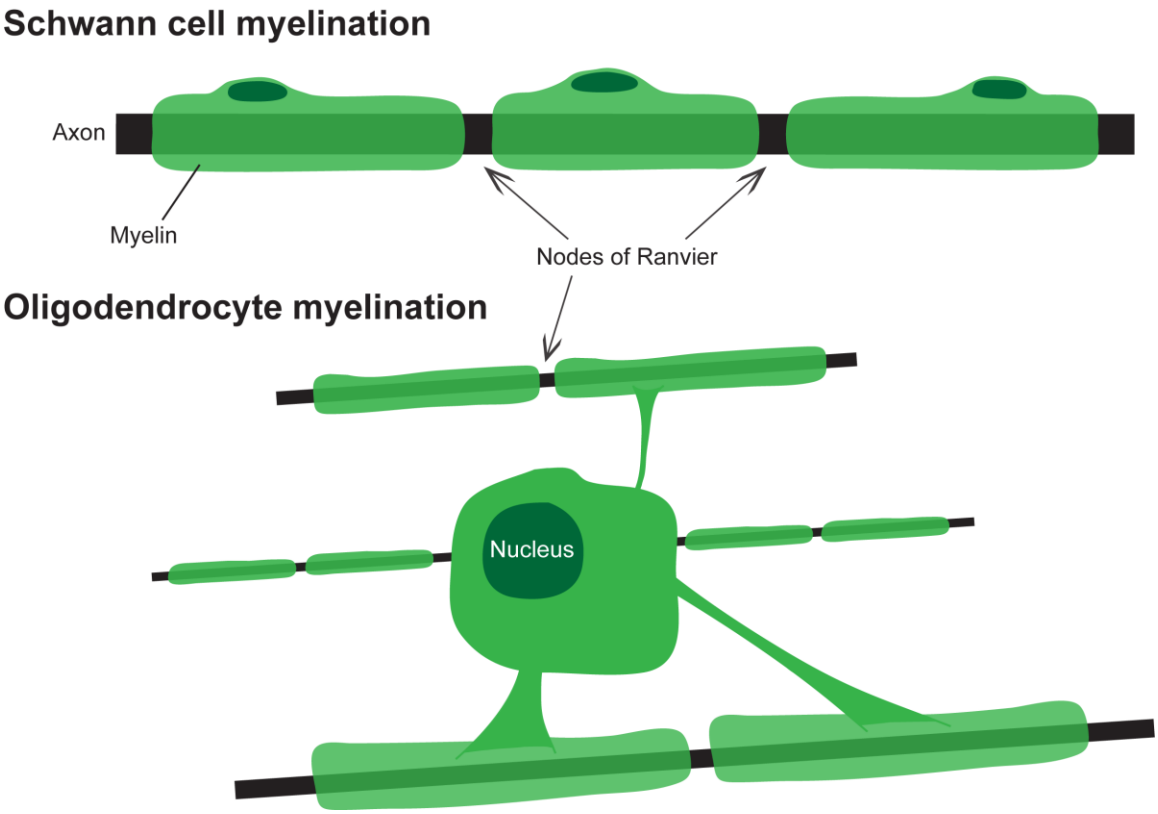

Figure 1.1: Schwann cell versus oligodendrocyte myelination. Compact myelin covers the internode regions of an axon leaving an unmyelinated gap called the node of Ranvier. A single Schwann cell myelinates a single internode, whereas a single oligodendrocyte can myelinate many internodes on the same or multiple axons.

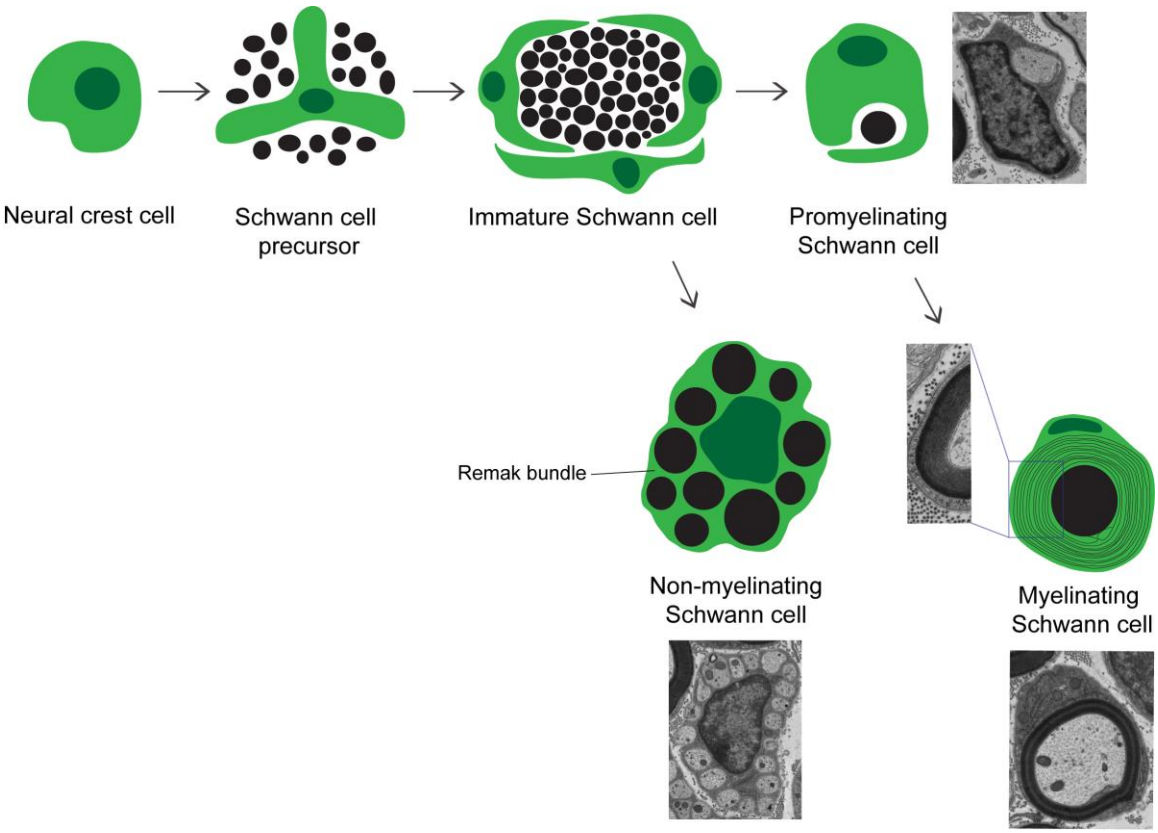

Figure 1.2: Schwann cell development. Neural crest cells differentiate into Schwann cell precursors through coordinated changes in molecular expression. Schwann cell precursors further develop into immature Schwann cells, which become either myelinating or non-myelinating Schwann cells. Immature Schwann cells that contact large caliber axons become promyelinating Schwann cells, which further mature into myelinating Schwann cells. Those that contact smaller fibers become mature, non-myelinating Schwann cells. This schematic shows the progression of Schwann cell development and maturation, as well as electron micrographs of particular phases during Schwann cell development. Also shown is an EM image of compact myelin, where individual wraps of compact myelin are visible.

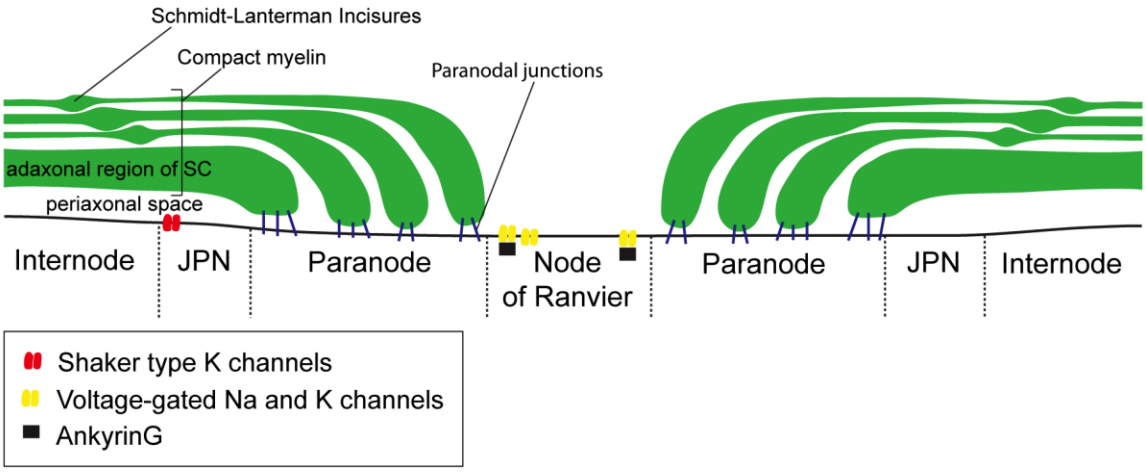

Figure 1.3: Regions of the Schwann cell and myelinated segment. Schematic longitudinal view of the node of Ranvier and surrounding regions. The node of Ranvier is flanked by paranodes, followed by the juxtaparanodal (JPN) region, then the internode region covered by compact myelin. The node of Ranvier is enriched in ion channels, which are anchored at the node by ankyrinG, and is responsible for regeneration of the AP in signal propagation. At the paranode, the compact myelin opens up to form paranodal loops filled with SC cytoplasm. The paranodal loops form paranodal, septate-like junctions with the axon for axo-glia communication. The JPN lies under compact myelin and is enriched in Shaker-type potassium channels that are required for maintaining the resting membrane potential and preventing re-entrant excitation. The internode region of the axon lies under the compact myelin sheath. Schmidt-Lanterman incisures are small regions of cytoplasm that run radially through the compact myelin sheath to provide a communication pathway between the axon and SC cell body.

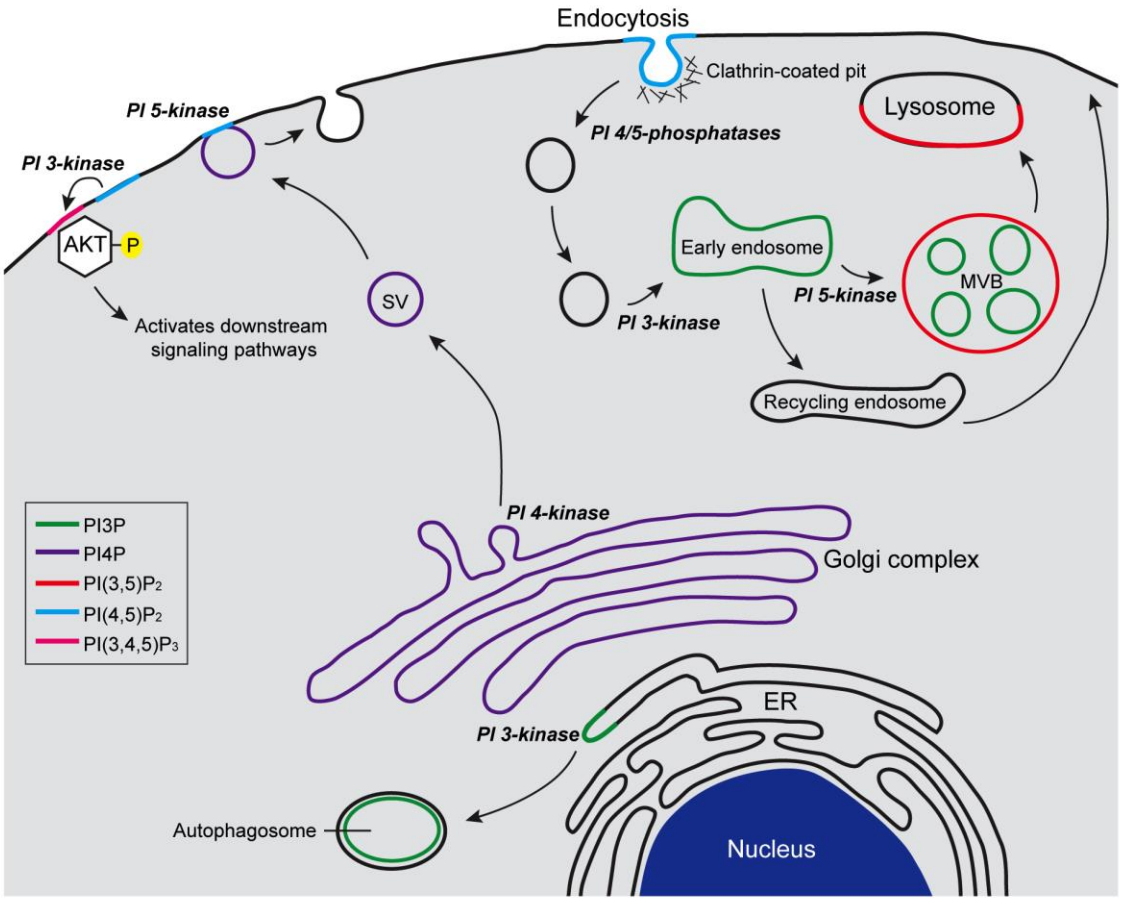

Figure 1.4: Phosphoinositides and their metabolizing enzymes. PIs are enriched on stereotyped intracellular membranes. The kinases and phosphatases required for changing the PI membrane identity code are also shown. Activation of the AKT signaling pathway occurs at the plasma membrane through PI 3-kinase mediated phosphorylation of plasma membrane PI(4,5)P_2 to PI(3,4,5)P_3 ("PIP3"), which then recruits PI-dependent kinase (PDK) to phosphorylate and activate AKT. *SV = secretory vesicle.*

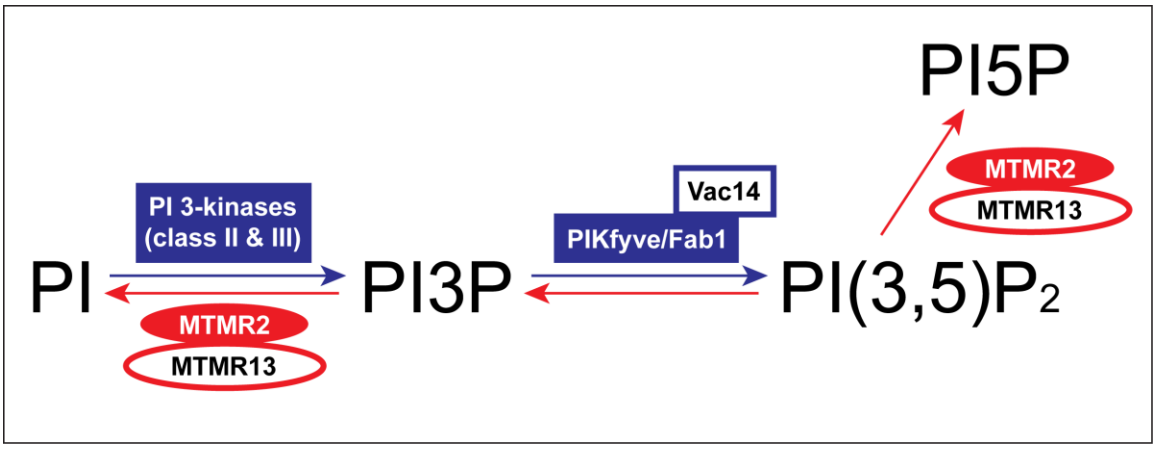

Figure 1.5: Endosomal phosphoinositides regulated by the MTMR2/MTMR13 complex. Dysregulation of PI3P and PI(3,5)P_2 in Schwann cells likely contributes to myelin abnormalities in *MTMR2* and *MTMR13* knockout mice and humans with CMT. The phosphatases MTMR2 and MTMR13 form a complex in Schwann cells and dephosphorylate PIs, depicted by red arrows in this schematic. The corresponding kinases that produce PI3P and PI(3,5)P_2 are shown in blue. We hypothesize that maintaining the critical balance of PIs in Schwann cells is required for wild type myelination, and that loss of MTMR2 or MTMR13 leads to altered PI levels and abnormal myelin.

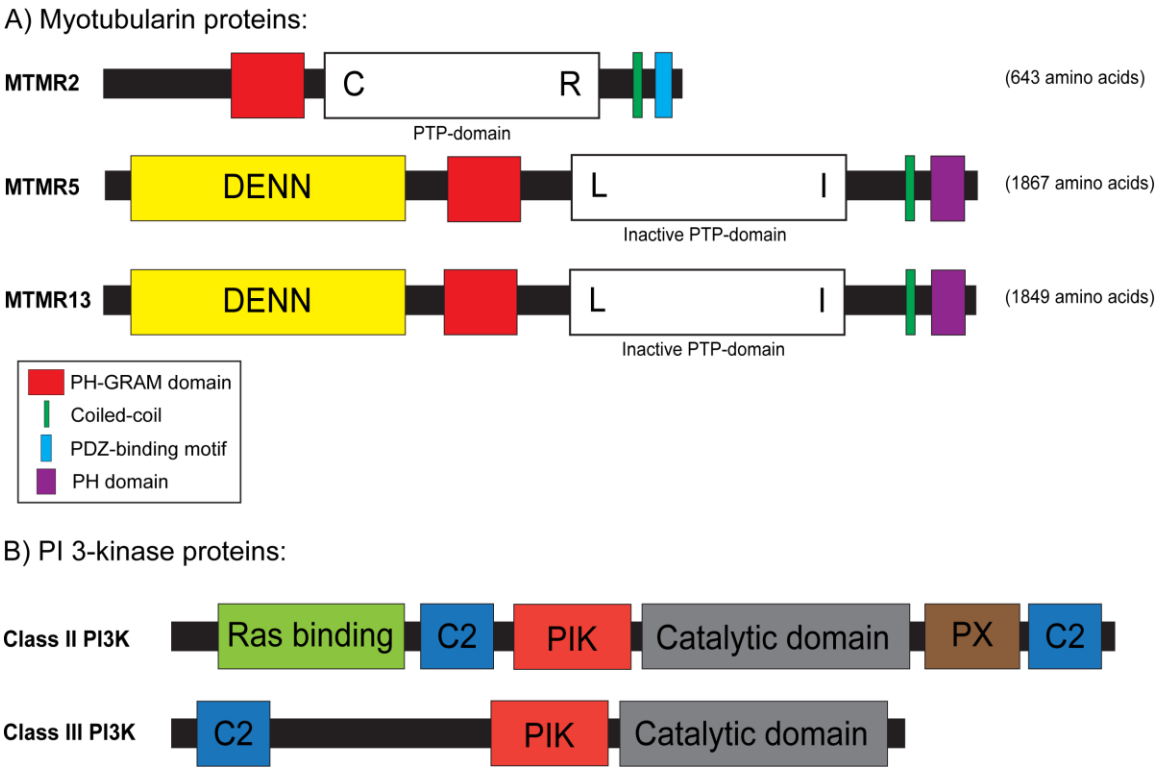

Figure 1.6: Domain compositions of the myotubularin proteins MTMR2, MTMR5, and MTMR13 and class II and III PI 3-kinases. (**A**) MTMR2 contains a PH-GRAM domain followed by an active phosphatase (PTP) domain with the catalytic residues cysteine and arginine, a coiled-coil domain, and a PDZ-binding motif. MTMR5 and 13 have similar protein structures, and include the following domains: DENN, PH-GRAM, inactive PTP, coiled-coil, and PH. MTMR2, MTMR5, and MTMR13 are 643, 1867, and 1849 amino acids in length, respectively. (**B**) shows schematic representations of the class II and III PI 3-kinases. Domains on class II PI 3-kinases include: a Ras binding domain, which mediates activation of the small GTPas Ras, C2 domains, a phosphatidylinositol kinase homology (PIK) domain, a C-terminal catalytic domain, and a PX domain. Class III PI 3-kinases contain a C2 domain, PIK domain, and C-terminal catalytic domain.

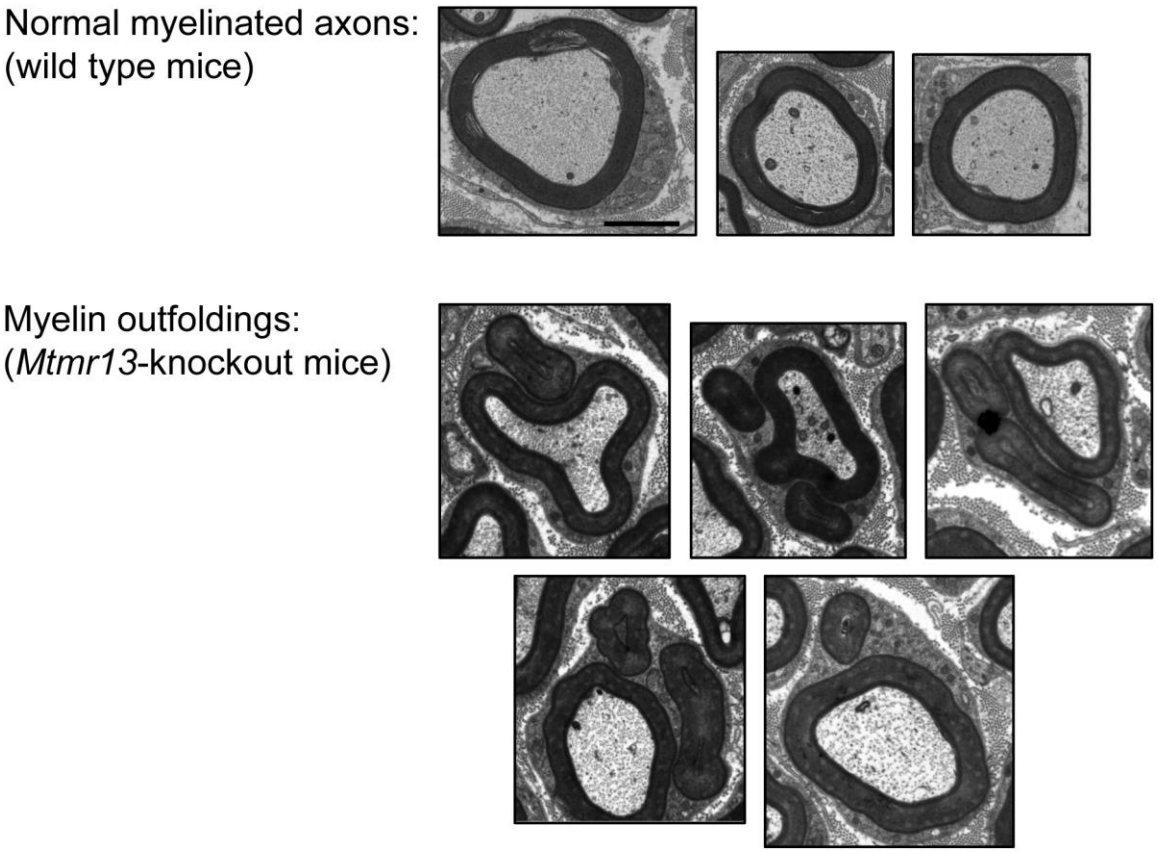

Figure 1.7: Normal myelinated peripheral nerve axons and myelin outfoldings. Representative EM images of wild type mouse mid-sciatic nerve with normal, uniform compact myelin sheaths. Myelin outfoldings are common in *Mtmr13* knockout sciatic nerves and are strikingly similar to the outfoldings observed in nerve biopsies from human CMT4B2 patients (*images of human nerve biopsy not shown*). Scale bar: 2 µm.

PI3K Class	***Yeast***	***Drosophila***	**Human**	**Mouse**	***In vivo* substrate and product**
Class I	-	*Pi3K92E*	*p110α, p110β, p110γ, p110δ*	*p110α, p110β, p110γ, p110δ*	PI(4,5)P_2 → PI(3,4,5)P_3
Class II	-	*Pi3K68D*	*PIK3C2α, PIK3C2β, PIK3C2γ*	*Pik3c2α, Pik3c2β, Pik3c2γ*	PI → PI3P PI4P → PI(3,4)P_2
Class III	*Vps34*	*Vps34*	*VPS34 (PIK3C3)*	*Vps34 (Pik3c3)*	PI → PI3P

Table 1.1: PI 3-kinases in Yeast, *Drosophila*, Human, and Mouse, and their *in vivo* substrates and products. This table lists the three classes of PI3Ks and their corresponding members in yeast, *Drosophila,* humans, and mice. Class I PI3Ks have been shown to be capable of phosphorylating PI, PI4P, and PI(4,5)P_2, but exhibit substrate preference for PI(4,5)P_2 *in vivo*. The class III PI3K has a single substrate, PI.

Chapter 2

The CMT4B disease-causing phosphatases Mtmr2 and Mtmr13 localize to the Schwann cell cytoplasm and endomembrane compartments, where they depend upon each other to achieve wild type levels of protein expression

Aubree A. Ng[1,*], **Anne M. Logan[1,2,*]**, Eric J. Schmidt[1] and Fred L. Robinson[1,†]. *Human Molecular Genetics* 22 (8): 1493-1506 (2013).

*The authors wish it to be known that, in their opinion, the first two authors should be regarded as joint first authors.

[1]The Jungers Center for Neurosciences Research, Department of Neurology, Oregon Health & Science University, 3181 SW Sam Jackson Park Road, Portland, OR 97239, USA.

[2]Neuroscience Graduate Program, Oregon Health & Science University.

†Corresponding Author: The Jungers Center for Neurosciences Research, Department of Neurology, Oregon Health & Science University, Mail Code L623, 3181 SW Sam Jackson Park Road, Portland, OR 97239, USA. Tel 503-494-8783; Fax 503-494-9161; Email: robinsof@ohsu.edu

Preface

The work is published in *Human Molecular Genetics.*

Anne Logan and Aubree Ng, co first-authors, designed and performed the majority of the experiments and data analysis in the manuscript, with the following exceptions: Eric Schmidt gathered and analyzed the *Mtmr13*$^{-/-}$ mice morphology data, and Fred Robinson performed the fractionation experiments and the lysosome size quantification. Anne Logan and Aubree Ng also contributed to writing sections of the manuscript, editing, and critical reading of the manuscript.

Fred Robinson contributed to the conception of the project, the experimental design, and wrote the manuscript.

The contents of chapter two are published in modified form:
Aubree A. Ng*, Anne M. Logan*, Eric J. Schmidt and Fred L. Robinson. *Human Molecular Genetics* 22 (8): 1493-1506 (2013).

Abstract

The demyelinating peripheral neuropathy Charcot-Marie-Tooth type 4B (CMT4B) is characterized by axonal degeneration and myelin outfoldings. CMT4B results from mutations in either myotubularin-related protein 2 (*MTMR2;* CMT4B1) or *MTMR13* (CMT4B2), phosphoinositide (PI) 3-phosphatases that dephosphorylate phosphatidylinositol 3-phosphate (PI3P) and PI(3,5)P_2, lipids which regulate endo-lysosomal membrane traffic. The catalytically active MTMR2 and catalytically inactive MTMR13 physically associate, although the significance of this association is not well understood. Here we show that Mtmr13 loss leads to axonal degeneration in sciatic nerves of older mice. In addition, CMT4B2-like myelin outfoldings are present in *Mtmr13*$^{-/-}$ nerves at postnatal day 3. Thus, *Mtmr13*$^{-/-}$ mice show both the initial dysmyelination and later degenerative pathology of CMT4B2. Given the key role of PI 3-kinase-Akt signaling in myelination, we investigated the state of the pathway in nerves of CMT4B models. We found that Akt activation is unaltered in *Mtmr13*$^{-/-}$ and *Mtmr2*$^{-/-}$ mice. Mtmr2 and Mtmr13 are found within the Schwann cell cytoplasm, where the proteins are partially localized to punctate compartments, suggesting that Mtmr2-Mtmr13 may dephosphorylate their substrates on specific intracellular compartments. Mtmr2-Mtmr13 substrates play essential roles in endo-lysosomal membrane traffic. However, endosomes and lysosomes of *Mtmr13*$^{-/-}$ and *Mtmr2*$^{-/-}$ Schwann cells are morphologically indistinguishable from those of controls, indicating that loss of these proteins does not cause wholesale dysregulation of the endo-lysosomal system. Notably, Mtmr2 and Mtmr13 depend upon each other to achieve wild type levels of protein expression. Mtmr2 stabilizes Mtmr13 on membranes, indicating that the Mtmr13 pseudophosphatase is regulated by its catalytically active binding partner.

Introduction

Phosphoinositides (PIs), phosphorylated derivatives of phosphatidylinositol, are found in all eukaryotic organisms [49,76]. As membrane-tethered signaling molecules, PIs regulate many processes, including cell division, cell growth and survival, intracellular membrane trafficking, actin dynamics and signaling [49,64]. PI kinases, phosphatases, and phospholipases collectively regulate PI abundance, turnover and localization, and the importance of this regulation is highlighted by numerous human disease-causing mutations that have been identified in PI kinases and phosphatases [77]. However, the cellular mechanisms by which the dysregulation of PIs lead to disease have largely remained unclear.

Mutations in genes encoding proteins involved in PI signaling cause certain forms of Charcot-Marie-Tooth disease (CMT), one of the most common inherited neurological disorders [78]. CMT is a heterogeneous collection of peripheral neuropathies that lead to progressive degeneration of the muscles of the extremities and loss of sensory function. Although CMT-causing mutations have been identified in over 40 human genes, the mechanisms by which these mutations lead to disease are generally poorly understood [79,80,81]. CMT type 4B (CMT4B) is a severe, autosomal-recessive form of demyelinating CMT. Nerves from CMT4B patients show severe axonal loss and focally folded myelin sheaths, the latter of which are considered the hallmark of the condition [82]. Mutations in myotubularin-related protein 2 (*MTMR2*) and *MTMR13* cause CMT4B1 and CMT4B2, respectively [46,47,83]. MTMR2 and MTMR13 are two members of a large family of PI 3-phosphatases that are key regulators of PIs in eukaryotes [84,85,86,87]. MTMR2 specifically dephosphorylates phosphatidylinositol 3-phosphate (PI3P) and phosphatidylinositol 3,5-bisphosphate ($PI(3,5)P_2$), two lipids that regulate membrane traffic within the endo-lysosomal pathway [76,88,89,90,91,92,93]. Therefore, it is theorized that CMT4B arises from defects in membrane transport in

Schwann cells. Notably, MTMR13 is a catalytically inactive “pseudophosphatase” that likely functions as a scaffold, binding to MTMR2 and other proteins [94,95,96].

Mouse models of CMT4B1 and CMT4B2, generated by disrupting *Mtmr2* and *Mtmr13,* recapitulate several key aspects of CMT4B, most notably the striking myelin outfolding [72,97,98,99]. In addition, Schwann cell-specific deletion of *Mtmr2* is sufficient to cause myelin outfoldings, strongly suggesting that this may be the initially affected cell type in CMT4B1 [100]. However, a recent study of *Mtmr2/Fig4* double-knockout mice has uncovered a role for Mtmr2 in neurons as well [70]. In this study, we assess whether the axonal degeneration observed in CMT4B2 patients is found in *Mtmr13*$^{-/-}$ mice. Mouse models are proving highly useful for studying the underlying cellular causes of CMT4B. Work with *Mtmr2*$^{-/-}$ mice has led to the proposal of a plausible model in which Mtmr2 functions as part of a regulatory network that titrates membrane addition during myelination [101]. However, the specific roles of Mtmr2 and Mtmr13 in the regulation of PI3P, PI(3,5)P_2 and endo-lysosomal traffic in Schwann cells remain unclear. Given the enrichment of PI3P and PI(3,5)P_2 on endo-lysosomal membranes, the Mtmr2-Mtmr13 complex might be expected to localize to these substrate rich compartments, but the localization of Mtmr2 and Mtmr13 is unclear.

Here, we have focused on several important questions regarding the cellular etiology of CMT4B. First, where are Mtmr2 and Mtmr13 localized in myelinating Schwann cells? Second, how is the Schwann cell endo-lysosomal pathway impacted of by the loss of Mtmr2 or Mtmr13? Third, is the PI 3-kinase-Akt signaling pathway, which is known to promote myelination, dysregulated in mouse models of CMT4B? Finally, we explore the relationship between MTMR2 and MTMR13, focusing on how the two proteins reciprocally regulate protein stability and membrane localization.

Results

Axonal degeneration in the absence of Mtmr13

Symptoms of CMT4B usually appear between the ages of 2 and 13, with muscle atrophy apparent in the distal portions of upper and lower limbs [82]. Neurophysiologically, CMT4B is characterized by marked reductions in nerve conduction velocity (NCV), affecting both motor and sensory nerves [82]. Nerve biopsies from CMT4B patients show severe axonal loss, with surviving fibers either hypomyelinated or demyelinated. The pathological hallmark of CMT4B is the presence of distinctive myelin outfoldings and infoldings [102,103].

Two mouse models of CMT4B2 have been described, both of which utilize animals with similar gene trap mutations in *Mtmr13* [72,99]. *Mtmr13*$^{-/-}$ mice recapitulate several key aspects of human CMT4B2, namely reduced NCV and compound muscle action potential (CMAP) amplitude, as well as myelin outfolding and infolding [72,99]. A key component of CMT4B2 is axonal degeneration, which leads to disability in patients [82]. However, the extent to which this feature of the condition is recapitulated in *Mtmr13*$^{-/-}$ mice is unclear [72,99]. To address this issue, we examined peripheral nerve pathology in 28-month-old *Mtmr13*$^{-/-}$ mice, an advanced age at which we reasoned axonal degeneration might be pronounced. Sciatic nerve cross-sections from *Mtmr13*$^{-/-}$ mice showed a notable decrease in toluidine blue staining, suggesting demyelination or loss of myelinated axons, which was discerned even at low magnification (Fig. 2.1A,B). Higher magnification microscopy revealed significant axon loss, evidenced by a statistically significant decrease of nearly 60% in the density of myelinated axons (Fig. 2.1C-F,G). In *Mtmr13*$^{-/-}$ nerves, numerous degenerated axon-Schwann cell units were observed, consisting of remnants of Schwann cell membranes and cytoplasm, as well as redundant basal lamina detached from Schwann cells (Fig. 2.1F). At 28 months, most

intact *Mtmr13*$^{-/-}$ axons possessed abnormally folded myelin sheaths (Fig. 2.1D,F). Consistent with demyelination and axon loss, we observed reductions in the levels of neurofilament light chain (NF-L) and myelin basic protein (MBP) in aged *Mtmr13*$^{-/-}$ mice (Supplemental Fig. 2.7).

We also assessed whether older *Mtmr13*$^{-/-}$ mice show hypomyelination, a feature of CMT4B2 that likely reflects suboptimal remyelination following demyelination [82]. At 28 months, the surviving *Mtmr13*$^{-/-}$ axons are significantly hypomyelinated, as indicated by a statistically significant increase in the average *g* ratio, a metric of myelin thickness obtained by dividing the axonal perimeter by the myelin perimeter (Fig. 2.1H-I). We observed further evidence of segmental demyelination-remyelination in *Mtmr13*$^{-/-}$ nerves in the presence of "onion bulb" structures, remnants of Schwann cell membrane and cytoplasm, as well as unattached basal lamina (Fig. 2.1F,J,K). In summary, peripheral nerves from aged *Mtmr13*$^{-/-}$ mice show clear evidence of axonal degeneration, hypomyelination and segmental demyelination-remyelination, all of which are prominent pathological features of human CMT4B2.

Initial myelination is abnormal in *Mtmr13*$^{-/-}$ mice

In hopes of providing insight into the development of CMT4B2, we sought to determine when myelination first goes awry in the postnatal development of *Mtmr13*$^{-/-}$ mice. To address this issue, we examined *Mtmr13*$^{-/-}$ sciatic nerves at postnatal day three (P3), an early stage of myelination when most large axons (>1 μm) are in a 1:1 relationship with Schwann cells and most have acquired a thin myelin sheath. Notably, we found that outfoldings are present to a significant degree in P3 nerves from *Mtmr13*$^{-/-}$ animals, where these structures are about seven times more prevalent than in wild type nerves (Fig. 2.1L,M). This finding suggests that initial myelination may be abnormal in

CMT4B2. The data we present here indicate that loss of *Mtmr13* in mice recapitulates both the late degenerative pathology and the likely initial myelination abnormalities of CMT4B2, highlighting the utility of this model for the study of the underlying cellular causes of this condition.

Akt activation is unaltered in mouse models of CMT4B

Despite the availability of authentic mouse models of CMT4B, the underlying cellular causes of the condition remain unclear. Although the process of membrane trafficking is implicated, abnormalities in Schwann cell signaling pathways could also cause CMT4B. To address this issue, we investigated the activation of the PI 3-kinase-Akt and extracellular signal regulated kinase 1/2 (Erk1/2) pathways in sciatic nerves from CMT4B model mice. In addition, we examined the status of Discs-large homolog 1 (Dlg1), a PDZ domain scaffold protein that associates with Mtmr2 [97].

The PI 3-kinase-Akt signaling pathway is a key regulator of cell growth, metabolism and survival, and plays a critical role in myelination. Binding of axonal Nrg1 type III to glial ErbB2/3 receptor tyrosine kinases leads to activation of Class I PI 3-kinases, which generate $PI(3,4,5)P_3$ [64]. In Schwann cells and oligodendrocytes, elevated $PI(3,4,5)P_3$ leads to activation of the Akt kinase pathway, and subsequently mTOR, thus representing a strong pro-myelination signal [21,104,105,106,107]. In addition, there is evidence for decreased Akt signaling and/or increased apoptosis in cell culture models where myotubularins have been depleted [86,108,109,110]. Given the potential relevance of Akt signaling to the myotubularin phosphatases and to CMT4B, we examined Akt kinase activation in sciatic nerves of adult *Mtmr13*$^{-/-}$ and *Mtmr2*$^{-/-}$ mice. By monitoring phosphorylation of serine 473, we found that Akt activation was not significantly altered in the absence of Mtmr13 or Mtmr2 (Fig. 2.2A-C). We also

considered the possibility that Akt signaling might be dysregulated during initial myelination in CMT4B model mice but normal in adults. To address this, we examined Akt activation in sciatic nerves from P4 mice. Akt activation was not significantly altered in sciatic nerve extracts from P4 *Mtmr13*$^{-/-}$ or *Mtmr2*$^{-/-}$ mice (Fig. 2.2F,G).

The Dlg1 scaffold protein regulates polarized membrane addition in *Drosophila* [111,112]. Dlg1 binds to Mtmr2, and the localization of Dlg1 to paranodes of Schwann cells is largely eliminated in *Mtmr2*$^{-/-}$ nerves [100]. A plausible model has been proposed in which the loss of Dlg1/Mtmr2-mediated control of membrane addition leads to the excessive local myelin deposition observed in CMT4B1 [101]. Dlg1 has also been implicated as a negative regulator of Schwann cell myelin thickness via the protein's inhibitory effect on Akt signaling [113]. To explore whether Dlg1 function might be altered in *Mtmr13*$^{-/-}$ Schwann cells, we examined the levels of the protein in sciatic nerves. Dlg1 protein levels were not significantly altered in *Mtmr13*$^{-/-}$ sciatic nerves, but were slightly suppressed in *Mtmr2*$^{-/-}$ nerves (Fig. 2.2A).

Erk1/2 signaling plays an important role in Schwann cell and oligodendrocyte myelination [114,115]. Moreover, alterations in PI3P levels and endocytosis might be expected to influence growth factor signaling in Schwann cells by controlling the recycling or degradation of activated receptor tyrosine kinases. Accordingly, we examined Erk1/2 activation in peripheral nerves of *Mtmr13*$^{-/-}$ and *Mtmr2*$^{-/-}$ mice. A trend toward higher Erk1/2 activity in the knockout nerves was not statistically significant, suggesting that kinase activation is unaltered in nerves from adult CMT4B model mice (Fig. 2.2A,D,E). In summary, our investigation of Akt and Erk1/2 activation suggests that alterations in these signaling pathways are not a feature of CMT4B.

Cellular localization of Mtmr2 and Mtmr13 in Schwann cells

A clear understanding of the localization of Mtmr2-Mtmr13 in myelinating Schwann cells will likely be key to determining how membrane traffic and/or signaling are disturbed in CMT4B. However, the subcellular localization of Mtmr2 and Mtmr13, particularly in Schwann cells, is unclear at present. The PI 3-phosphatase complex might be expected to localize to specific endo-lysosomal compartments rich in PI3P and/or $PI(3,5)P_2$, in order to act upon its substrates. Alternatively, Mtmr2-Mtmr13 might be found on membrane compartments lacking PI3P and $PI(3,5)P_2$, thereby acting to prevent the aberrant accumulation of substrates at these locations. In accord with both of these proposals, we and others have used fractionation to demonstrate that significant portions of the endogenous proteins are associated with membranes [94,116].

To investigate the localization of Mtmr2 and Mtmr13, we began by generating affinity-purified rabbit antibodies to both proteins [94]. We assessed the specificity of these antibodies by performing immunofluorescence on sciatic nerves from wild type and mutant mice. Mtmr13 and Mtmr2 immunofluorescence were greatly reduced in *Mtmr13*$^{-/-}$ and *Mtmr2*$^{-/-}$ nerve sections, respectively (Fig. 2.3A-D), indicating that the antibodies used here are specific for Mtmr13 and Mtmr2. When examined in nerve cross sections, we observed that both Mtmr13 and Mtmr2 were localized to the Schwann cell and the axoplasm (Fig. 2.3E,G). Both phosphatases were excluded from the nucleus and from compact myelin (Fig. 2.3E,G). Within the Schwann cell cytoplasm, both phosphatases were partially localized to punctate structures (Fig. 2.3E,G). Mtmr13 immunofluorescence was punctate to a greater degree than was Mtmr2 immunofluorescence (Fig. 2.3E,G). These data strongly suggest that Mtmr13 and Mtmr2 are partially localized to endomembrane compartments in Schwann cells.

Impact of loss of Mtmr2 or Mtmr13 on the Schwann cell endo-lysosomal pathway

There are a number of examples where the loss of the PI kinases or phosphatases that regulate PI3P and PI(3,5)P_2 leads to dramatically abnormal endo-lysosomal membranes, usually the swelling or expansion of these compartments [117,118,119,120,121,122]. We therefore evaluated the impact of loss of Mtmr2 or Mtmr13 on the Schwann cell endo-lysosomal pathway. EEA1-positive early endosomes and Lamp1-positive late endosomes/lysosomes in *Mtmr2*$^{-/-}$ and *Mtmr13*$^{-/-}$ myelinating Schwann cells were indistinguishable from those of wild type controls (Fig. 2.4A-D). Consistently, endo-lysosomal morphology appeared normal in primary *Mtmr2*$^{-/-}$ and *Mtmr13*$^{-/-}$ Schwann cells (Fig. 2.4E-H) and in mouse embryo fibroblasts (MEFs) derived from mutant embryos (Supplemental Fig. 2.8). We also examined lysosome morphology in Schwann cells using high magnification EM. Lysosome size was not significantly altered in myelinating Schwann cells of *Mtmr13*$^{-/-}$ nerves (Supplemental Fig. 2.10). In accord with our morphological findings, Lamp1 protein levels were unaltered in sciatic nerve, brain and MEF cells from *Mtmr13*$^{-/-}$ and *Mtmr2*$^{-/-}$ mice (Fig. 4.4I,J; Supplemental Fig. 2.8). During our ultrastructural (EM) analysis of lysosomes (Supplemental Fig. 2.10), abnormalities were not apparent in other organelles or vesicular populations (*data not shown*). Clathrin-coated pits were identified in both wild type and *Mtmr13*$^{-/-}$ Schwann cells, although a quantitative evaluation of the prevalence of these structures was not possible.

To investigate a potentially relevant effector of PI3P, we sought to evaluate the function of the retromer complex in Schwann cells of CMT4B model mice. The retromer complex, composed of sorting nexins 1 and 2 (Snx1/2), Vps26, Vps29 and Vps35, acts to recycle the cation-independent mannose 6-phosphate receptor (CI-MPR) from late endosomes to the trans-Golgi network in a PI3P-dependent manner. Consistently, perturbations affecting PI3P levels have been shown to alter the localization and/or

abundance of Snx1/2, Vps26, and CI-MPR or its yeast homolog Vps10p [123,124]. Although we were unable to identify antibodies suitable for assessing the localization or abundance of CI-MPR in Schwann cells, we examined the levels of several components of retromer in sciatic nerve or brain extracts. We found that the levels of Snx1 and Vps26 in *Mtmr13*$^{-/-}$ and *Mtmr2*$^{-/-}$ nerves were similar to controls (Fig. 2.4I,K,L). Likewise, Vps26 and Vps35 levels were normal in brain extracts from mutant mice (Supplemental Fig. 2.8F,H,I). A definitive assessment of retromer function in mouse models of CMT4B will require further studies focused on the status the retromer cargo CI-MPR.

Mtmr2 and Mtmr13 depend upon each other to achieve wild type levels of protein expression in peripheral nerve

We have demonstrated that Mtmr2 and Mtmr13 physically interact [94], a finding subsequently supported by others [95]. However, the biological function of Mtmr2-Mtmr13 association remains enigmatic. To further explore the relationship between the proteins, we examined the levels of each in sciatic nerves of mutant mice. We consistently observed a 50% reduction in Mtmr2 protein levels in *Mtmr13*$^{-/-}$ nerves (Fig. 2.5A,B). Likewise, Mtmr13 protein levels were reduced by about 70% in *Mtmr2*$^{-/-}$ nerves (Fig. 2.5A,C). To investigate whether Mtmr2 and Mtmr13 enhance each protein's abundance in other tissues and in primary fibroblasts, we evaluated the levels of the two proteins in brain extracts and MEFs. Loss of Mtmr2 or Mtmr13 does not alter the levels of the binding partner in brain extracts or MEF cells (Fig. 2.5D,E). Thus, in a CMT4B-relevant tissue, loss of either Mtmr2 or Mtmr13 lowers the abundance of the other protein by 50% or 70%, respectively.

To further explore what appears to be a novel, stabilizing effect of Mtmr2 upon Mtmr13, we investigated the membrane association of the two proteins. MTMR2 and

MTMR13 were expressed in HEK293 cells and membrane and cytosolic fractions were isolated (Fig. 2.6). MTMR2 was present in both membrane and cytosolic fractions; MTMR13 was predominantly found in the membrane fraction, and was not detected in the cytosol (Fig. 2.6B). Notably, the co-expression of MTMR2 substantially enhanced the abundance of MTMR13 in the membrane fraction (Fig. 2.6B).

To assess whether the stabilizing effect of MTMR2 on membrane-associated MTMR13 requires direct association, we tested whether deletion of coiled-coil sequences would decrease the abundance of MTMR13. Indeed, a mutant form of MTMR2 lacking the coiled-coil sequence (MTMR2-ΔCC) failed to enhance MTMR13 levels in the membrane fraction (Fig. 2.6B). Consistently, the abundance of MTMR13-ΔCC, which is incapable of association with MTMR2, was not enhanced by the expression of MTMR2 (Fig. 2.6B). The abundance of another mutant, MTMR13-ΔPH, which lacks the C-terminal PH domain and the PDZ domain-binding motif, but retains the coiled-coil motif, was enhanced by the co-expression of MTMR2 (Fig. 2.6B). In summary, the enhanced abundance of membrane-associated MTMR13 requires direct association with MTMR2.

Discussion

Mtmr13-deficient mice model both the initial dysmyelination and advanced degenerative pathology of CMT4B2

Mtmr13$^{-/-}$ mice show myelin outfoldings and deficits in electrophysiology, both consistent with CMT4B2 [72,99]. However, the clinically critical aspect of CMT4B2 is axonal loss, as the degree of axonal degeneration is considered the best correlate of clinical deterioration in patients with demyelinating CMT [125]. Although examples of axonal degeneration were reported in *Mtmr13*$^{-/-}$ mice at about 14 months of age, the

dramatic fiber loss observed in CMT4B2 patients was not evident, and a quantitative assessment of axonal degeneration in these mice is lacking [72,99]. To address this issue, we examined the mid-sciatic nerves of mice at 28 months, when we reasoned axonal degeneration might be more pronounced. In these older animals, we found significant axon loss, with the density of myelinated axons reduced by nearly 60%. The axon density we report for nerves of 28-month-old *Mtmr13*$^{-/-}$ mice (6402 myelinated axons/mm^2) is broadly similar to that reported for sural nerves of 2- and 3-year-old CMT4B patients (8400 myelinated axons/mm^2) [103].

In a second aspect of this study, we determined that CMT4B2-like myelin outfoldings arise during initial myelination, as these features are present in the sciatic nerves of P3 *Mtmr13*$^{-/-}$ mice. Thus, loss of Mtmr13 may cause a defect in initial myelination rather than, or in addition to, abnormalities in myelin remodeling or sheet homeostasis, as suggested for Mtmr2 [70,97]. We conclude that *Mtmr13*$^{-/-}$ mice are an effective model of both the likely initial dysmyelination and the advanced axonal pathology of CMT4B2, highlighting the strength of this model for investigation of the underlying cellular causes of CMT4B2.

Akt activation is unaltered in mouse models of CMT4B1 and CMT4B2

The PI 3-kinase/Akt signaling pathway plays a critical role in promoting myelination [21,104,105,106,107]. Given the potential relevance of Akt signaling to the pathology of CMT4B, we examined activation of the kinase in sciatic nerves of *Mtmr2*$^{-/-}$ and *Mtmr13*$^{-/-}$ mice, both during initial myelination (day 4) and in adults (3-4 months). We found no significant change in the degree of Akt activation in these models of CMT4B.

A recent study demonstrated that the loss of Pten in Schwann cells causes myelin outfoldings similar to those observed in CMT4B [126]. Myelin outfoldings and tomacula in *Pten*$^{-/-}$ nerves very likely result from elevated PI(3,4,5)P_3 levels and elevated Akt signaling. The authors suggest that myelin outfoldings and tomacula may represent a "final common pathway" or phenotype, which can be triggered by mutations in a number of proteins with very different functions [126], although involvement in PI signaling appears to be a recurring theme [3,81]. Our data on Akt activation in CMT4B model nerves are consistent with this model, as while the authors observed a dramatic enhancement of Akt phosphorylation in *Pten*$^{-/-}$ nerves, we report here that Akt phosphorylation in *Mtmr2*$^{-/-}$ and *Mtmr13*$^{-/-}$ nerves is normal [126]. Thus, in the models of CMT4B that we have analyzed, myelin outfoldings do not correlate with elevated Akt phosphorylation.

The results of our investigation of Akt signaling might be viewed as in conflict with another study in which the investigators compared Akt activation in sciatic nerves of wild type and *Mtmr2*$^{-/-}$*Mtmr13*$^{-/-}$ double knockout mice [127]. The authors concluded that Akt phosphorylation was impaired in the mutant nerves, but that *Mtmr2*$^{-/-}$*Mtmr13*$^{-/-}$ double-knockout nerves contain higher levels of total Akt, apparently having compensated to maintain a wild type level of phospho-Akt. Our results are not directly comparable to those of this study [127], as while these authors examined double knockout mice, we have we examined *Mtmr2*$^{-/-}$ or *Mtmr13*$^{-/-}$ mice.

Mtmr2 and Mtmr13 partially localize to Schwann cell endomembrane compartments

The substrates of Mtmr2-Mtmr13, PI3P and PI(3,5)P_2, play key functions in endo-lysosomal membrane trafficking [76,91,92,93]. Accordingly, PI3P is most highly enriched on early endosomes and on the internalized vesicles of multi-vesicular endosomes [128].

The localization of $PI(3,5)P_2$ is less well understood, but experiments indicate roles for this lipid in endo-lysosomal membrane trafficking, notably in endosome to *trans*-Golgi network traffic [92,93,129,130].

When over-expressed in mammalian cell lines, MTMR2 exhibits a predominantly cytoplasmic localization [88,94,95,131]. In nerves, endogenous Mtmr2 was found to be present in both Schwann cells and neurons/axons [132]. Within myelinating Schwann cells, Mtmr2 was detected in all cytoplasmic compartments, including the paranode, and was excluded from the compact myelin [132]. The subcellular localization of MTMR13 is particularly poorly understood, with diffuse cytoplasmic localization reported in cell lines overexpressing the protein [94,95,133].

Our understanding of the functions of Mtmr2 and Mtmr13 in Schwann cells has been hampered by a lack of knowledge of the subcellular localization of the complex. To address this issue, we prepared rabbit antibodies to both Mtmr2 and Mtmr13 and demonstrated that these antibodies are specific for the endogenous mouse proteins. We then demonstrated that that both Mtmr2 and Mtmr13 localize to the Schwann cell cytoplasm and to punctate, presumably endomembrane, structures within the cytoplasm. Mtmr2 and Mtmr13 are excluded from the compact myelin and the nucleus. Our data represent the first report on the localization of the endogenous Mtmr13 protein. The localization we report here for Mtmr2 is consistent with a previous study's conclusion that endogenous Mtmr2 localizes to the Schwann cell cytoplasm [132], although the punctate nature of Mtmr2 localization has not been reported previously.

Although we have demonstrated that Mtmr2 and Mtmr13 partially localize to endomembrane compartments in the cytoplasm of myelinating Schwann cells, the identity of such structures remains unclear. We have attempted to determine if the Mtmr2- and Mtmr13-positive compartments are early endosomes, late endosomes/lysosomes or recycling endosomes, using antibodies to EEA1, Lamp1 and

Rab11, respectively. However, such studies been hampered by the poor performance of our rabbit Mtmr2 and Mtmr13 antibodies in teased fibers, possibly due to cross reactions with other myotubularin family members such as Mtm1, Mtmr1 and Mtmr5 [97,100]. In addition, difficulties in using mouse or rat Lamp1, EEA1 and Rab11 antibodies in frozen sciatic nerve cross sections have prevented effective co-labeling with our rabbit Mtmr2/13 antibodies in this preparation, highlighting the difficulties of determining the endogenous localizations of myotubularin phosphatases [84,97].

A recent study has provided significant insight into the functions of the *Drosophila* orthologs of mammalian MTMR2/MTM1/MTMR1 (Mtm in flies) and MTMR13/MTMR5 (Sbf in flies) [96]. Sbf was found to coordinate both PI3P turnover and Rab21 activation in a pathway that regulates endosomal trafficking and cell shape change in fly macrophages. Sbf scaffolds a complex (containing Pi3K68D and Mtm) that promotes endosomal PI3P turnover and membrane efflux to a Rab11-mediated recycling pathway that is essential for plasma membrane protrusions [96]. Future studies might be aimed at determining whether MTMR2 and MTMR13 perform analogous functions in Schwann cells, and also at assessing the role of phosphorylation in the regulation of MTMR2 localization [134].

Status of the endo-lysosomal pathway in the absence of Mtmr2 or Mtmr13

A number of studies have documented dramatic swelling of endo-lysosomal compartments when the relevant PI kinases or phosphatases are lost or inhibited [117,118,119,120,121,122]. In contrast, we found that the morphology of EEA1- and Lamp1-positive compartments appeared normal in *Mtmr13*$^{-/-}$ and *Mtmr2*$^{-/-}$ Schwann cells and fibroblasts. Our result stands in stark contrast to the dramatic upregulation of late endosomal/lysosomal membranes observed in fibroblasts and neurons that lack the

PI(3,5)P_2 5-phosphatase Fig4 [70,120]. In summary, our findings suggest that loss of either Mtmr2 or Mtmr13 does not cause wholesale dysregulation of the endo-lysosomal membrane system in Schwann cells. Future studies will examine PI3P and PI(3,5)P_2 levels in mouse models of CMT4B2 and determine the impact of loss of Mtmr2 and Mtmr13 on the trafficking of specific cargo proteins.

Mtmr2 and Mtmr13 reciprocally enhance each protein's abundance in peripheral nerve

Mutations in either *MTMR2* or *MTMR13* cause very similar forms of the pathologically distinctive CMT4B, suggesting that the two proteins share similar functions [46,47,83]. We have demonstrated that MTMR2 and MTMR13 physically associate [94]. An *in vitro* enzymatic analysis suggested that the Mtmr2-Mtmr13 complex possesses a higher specific activity for PI3P and PI(3,5)P_2 than does Mtmr2 [95]. However, the biological significance of Mtmr2-Mtmr13 association, particularly in cell types relevant to CMT4B, remains unclear.

Here, we have examined the Mtmr2-Mtmr13 protein relationship by focusing on protein stability and membrane association. We find that loss of either Mtmr2 or Mtmr13 decreases the other protein's abundance in sciatic nerve. Notably, in both brain and MEF cells, loss of either Mtmr2 or Mtmr13 has no impact on the abundance of the other. Thus, the mutual dependence of the two proteins appears to be specific for peripheral nerve, suggesting that it may be relevant to CMT4B disease. While we previously observed reduced Mtmr2 levels in nerve extracts from *Mtmr13*$^{-/-}$ mice, our initial study was performed using immunoprecipitation [72]. Here, we employ the more definitive approach of directly immunoblotting protein extracts. As an inactive phosphatase and likely scaffold protein [96], MTMR13 might have been viewed as a regulatory subunit of MTMR2. In contrast, our results indicate that Mtmr13 is even more dependent on Mtmr2

for its wild type level of protein abundance than the reverse. This raises the possibility that some aspects of CMT4B1 (MTMR2-deficiency) might result from decreased MTMR13 function, although we emphasize that our results were obtained in mouse models and cultured cells. In the absence of MTMR2, perhaps some MTMR13-specfic functions are impaired, such as the Rab-GEF activity of the DENN domain [96,135].

The regulation of membrane association is likely an important mechanism by which the function of MTMR2-MTMR13 is controlled, as this property dictates access to substrates. We have demonstrated that significant fractions of the endogenous MTMR2 and MTMR13 proteins are associated with membranes in cultured cell lines, that the pseudophosphatase domain of MTMR13 is sufficient for membrane association, and that the two proteins associate in a manner that requires coiled-coil motifs [94]. Here, we show that physical association with MTMR2 substantially enhances the abundance of MTMR13 on membranes in HEK293 cells. MTMR2 likely retargets MTMR13 from the cytosol to membranes, simultaneously stabilizing the pseudophosphatase. These findings may be relevant to sciatic nerve, as we consistently observe a 70% reduction in Mtmr13 levels in *Mtmr2*$^{-/-}$ extracts from this tissue. A recent study in *Drosophila* demonstrated that Sbf acts to recruit Mtm into stable complexes on vesicular and cortical membranes of fly cells [96]. Our data suggest an analogous, but reversed situation in mammalian cells, with MTMR2 acting to recruit MTMR13 to membranes while simultaneously stabilizing the pseudophosphatase.

The nature of the membrane trafficking events regulated by Mtmr2 and Mtmr13 in Schwann cells remains largely unknown. We have demonstrated that, at least at a morphological level, Schwann cell early endosomes and late/endo-lysosomes are not significantly altered by the loss of Mtmr2 or Mtmr13, indicating a more subtle disruption of traffic than that observed in cells lacking Fig4 [70,120]. Future studies will focus on the identification of specific membrane proteins that may be abnormally trafficked in the

absence of Mtmr2 or Mtmr13, as well as defining how PI3P and PI(3,5)P_2 are dysregulated by the loss of these proteins.

Materials and Methods

Antibodies

The anti-MTMR13 antibody (116-AN) was generated by immunizing rabbits with a recombinant protein consisting of the C-terminal PH domain from human MTMR13. The anti-MTMR2 antibody (119-AN) was generated by immunizing rabbits with full-length, recombinant, human MTMR2 containing an N-terminal His_6 tag. Anti-MTMR2 (119-AN) and Anti-MTMR13 (116-AN) antibodies were affinity purified from the serum of rabbits 119 and 116, respectively, using columns of His_6-MTMR2 and PH-MTMR13 proteins, respectively. Rabbit anti-Akt, anti-phospho-Akt (Ser473), anti-ERK1/2 and anti-EEA1 were obtained from Cell Signaling Technology. Rat anti-LAMP-1 (1D4B) and mouse anti-β-tubulin (E7) were obtained from the Developmental Studies Hybridoma Bank. Mouse anti-SAP97 (Dlg1) (K64/15) was obtained from the UC Davis/NIH NeuroMab Facility. Rabbit anti-MAG was from Santa Cruz Biotechnology. Rabbit anti-VPS26, anti-VPS35 and anti-SNX1antibody were from Abcam. Rabbit anti-NF-L and rat anti-MBP were obtained from Millipore. Mouse anti-FLAG (M2) and anti-c-myc (9E10) were from Sigma Aldrich and Roche Applied Science, respectively. Rabbit anti-PP-ERK1/2 (pT185-pY187) was from Invitrogen. Mouse anti-S100β was obtained from BD Biosciences.

Protein Analysis

Sciatic nerves (from sciatic notch to knee) were dissected and frozen using liquid nitrogen. Mice were mostly males and were between two and six months of age

(average age for all mice was 3.9 months). Each nerve extract resulted from the pooling and homogenizing of four or six sciatic nerves, with six nerves being more common. Each P4 nerve extract was generated by pooling six nerves. Nerves were pooled according to genotype and homogenized in ice-cold lysis buffer (120 mM NaCl/50 mM Tris, pH 8.0/0.5% Triton X-100/100 mM sodium fluoride/1 mM sodium orthovanadate, 2 mM sodium EDTA, supplemented with cOmplete, EDTA-free Protease Inhibitor Cocktail Tablets [Roche Applied Science] at a concentration of 1 tablet per 50 ml of buffer). Brain protein extracts were prepared by homogenizing freshly dissected brains in ice-cold lysis buffer. Monolayers of MEF cells were washed once with PBS and directly lysed in lysis buffer. Homogenates were cleared by centrifugation (17,000 *g* for 15 minutes at 4°C). Protein concentration was determined and lysates were suspended in NuPAGE LDS sample buffer (Invitrogen) containing 1 mM DTT. Protein extracts (17, 20, 17.5 and 7 µg per lane for sciatic nerve, brain, MEFs and P4 nerves, respectively) were resolved in 4-12% NuPAGE Bis-Tris gels (Invitrogen) in MOPS buffer, transferred to polyvinylidene difluoride membranes, and analyzed by immunoblotting. SuperSignal West Chemiluminescent Substrate (Thermo Scientific) was used for detection and quantitation was with a G:BOX Chemi imaging system using GeneSys software (Syngene). Protein levels are presented in arbitrary units with wild type set to 100, and data as mean ± standard error of the mean. Statistical significance was evaluated using unpaired T-tests.

Cell Culture and Transfection

Primary mouse embryonic fibroblasts (MEF) were cultured in Dulbecco's modified Eagle's medium (high glucose) supplemented with 10% fetal bovine serum (FBS) and 1% penicillin/streptomycin at 37°C, 5% CO_2. Cells were passaged no more than 7 times. HEK293 cells were cultured and transfected as previously described [94].

Primary mouse Schwann cells were prepared from single mouse embryos (P13.5) by a previously described method [136]. For routine culture, Schwann cells were maintained in Schwann cell growth medium (DMEM with 10% FBS supplemented with 10 ng/ml neuregulin [R & D Systems] and 5 µl/ml forskolin [Sigma-Aldrich]) at 37°C, 10% CO_2 and passaged no more than four times. Bright field images were taken on an AMG EVOS transmitted light microscope with a CaChN 10x/0.25 PhP objective.

Immunofluorescence

For cryosections, sciatic nerves were dissected and fixed in 4% paraformaldehyde (PFA)/4% sucrose in PBS on ice for 30 min, cryoprotected in 30% sucrose, embedded in OCT, and snap frozen in a dry ice/isopentane bath. Alternatively, mice were perfused with 4% PFA in PBS prior to nerve dissection, with nerves subsequently processed as described above. Nerves were cryosectioned into 8 µm transverse sections, mounted on glass slides, and stored at -20°C. Cryosections were washed once in PBS, permeabilized in 0.2% TRITON X-100 in PBS for 15 min, and blocked with 0.5% fish skin gelatin (Sigma Aldrich). Anti-MTMR2 and anti-MTMR13 primary antibodies were prepared in 0.05% fish skin gelatin at 1:1000 and incubated for 18 hours at 4°C. Cryosections were washed in PBST and, incubated with rabbit Alexa 488-conjugated secondary antibody at 1:500 for 1 hour. For fluorescent myelin staining, cryosections were permeabilized as described above and incubated for 20 minutes in PBS containing FluoroMyelin™ (Molecular Probes) at a 1:300 dilution.

For teased fiber immunofluorescence, sciatic nerves were dissected, fixed in 4% paraformaldehyde on ice for 30 min and washed 3 times in PBS. To tease individual fibers, the perineurium was removed and segments were subdivided on microscope slides using fine forceps. Slides were dried at room temperature for 18 hours and stored at -20°C. Slides were washed once in PBS, permeabilized as described above, and

blocked with 0.5% fish skin gelatin (Sigma Aldrich). Slides were incubated with primary antibodies prepared in 0.05% fish skin gelatin for 18 hours at 4°C, washed with PBST, and incubated with Alexa 488- or Cy3-conjugated secondary antibodies at 1:500 for 1 hr. MEF cells were plated on poly-D-lysine coated coverslips at 75% confluency. Coverslips were washed in PBS and cells were fixed in 4% PFA in PBS for 15min. Coverslips were then washed three times in PBS, permeabilized as described above and blocked with 10% normal goat serum (NGS; Jackson ImmunoResearch). Coverslips were incubated with primary antibodies prepared in 2% NGS for 18 hours at 4°C, washed with PBST, and incubated with Alexa488- or Cy3-conjugated secondary antibodies at 1:500 for 1hr. After secondary antibody treatment, coverslips or slides were washed with PBST, stained with DAPI (Molecular Probes) and mounted in Elvanol mounting medium. Schwann cells were plated on poly-L-lysine coated coverslips at 75% confluency. Coverslips were fixed and permeablized as described above and blocked with 0.5% fish skin gelatin (Sigma-Aldrich). Coverslips were incubated with primary antibodies prepared in 0.05% fish skin gelatin for 18 hours at 4°C, washed with PBST, and incubated with Alexa488- or Cy3-conjugated secondary antibodies at 1:500 for 1 hr. After secondary antibody treatment, coverslips or slides were washed with PBST, stained with DAPI (Molecular Probes) and mounted in Elvanol mounting medium.

The images were acquired on a wide field DeltaVison CoreDV deconvolution microscopy system (Applied Precision), built on an Olympus IX71 inverted microscope equipped with a Nikon Coolsnap ES2 HQ camera. Each image was acquired as a set of Z-stacks in a 1024x1024 format with a 60x 1.42 NA PlanApo objective using Cy3 and/or Alexa488 fluors. The pixel size was 0.107 x 0.107 x 0.2 μm. The images were deconvolved with the appropriate optical transfer function using an iterative algorithm of 10 iterations. The histogram was optimized for the brightest image and applied to all the other images for consistency before projection images were made from the Z-stack by

merging into a 24-bit TIFF file. The number of Z sections compressed in each image was the same for comparable images. Acquisition and deconvolution were accomplished using softWoRx software (Applied Precision). Post-acquisition imaging was accomplished using Volocity software (Perkin Elmer).

Fractionation

A 150 mm dish of HEK293 cells was transfected with FLAG-MTMR2, FLAG-MTMR2-ΔCC (Δcoiled-coil; Δ589-643), Myc-MTMR13, Myc-MTMR13-Δ1630-1682 (Δcoiled-coil, ΔCC) or Myc-MTMR13-Δ1683-1849 (ΔPH) as previously described [94]. Monolayers of cells were washed once with PBS and collected in 10 ml of PBS. Cells were pelleted by centrifugation (1000 *g* for 5 minutes at 4°C), resuspended in 3 ml of ice-cold hypotonic lysis buffer (10 mM Tris [pH 7.5], 1 mM NaF, 10 mM NaCl, 1 mM Na_2VO_4, 1 μg/ml Leupeptin, 10.5 μg/ml aprotinin, 1 μg/ml pepstatin, 1 mM PMSF, 1 mM benzamidine, 1 mM EDTA), and homogenized in a Dounce style homogenizer. Homogenates were centrifuged at 1000 *g* (10 minutes at 4°C) to pellet nuclei and unbroken cells. The resulting post-nuclear homogenate (~2.5 ml) was centrifuged for one hour at 100,000 *g* at 4°C, to yield a cytosolic (S100) fraction and a membrane pellet, which was resuspended in 1 ml of lysis buffer to yield the P100 membrane fraction. Protein concentration was determined for both fractions and these were resolved in SDS-PAGE gels (20 μg of protein per lane), and evaluated by immunoblotting.

Mice

All animal work was approved by and conformed to the standards of the Oregon Health & Science University Animal Care and Use Committee. *Mtmr13*$^{-/-}$ mice have been described previously [72]. The majority of the mice analyzed here had been backcrossed

for eight generations onto a C57BL/6 background. *Mtmr2*$^{-/-}$ mice contain a splice-accepting gene trap in intron 2-3 of *Mtmr2*, and will be described fully elsewhere.

Sciatic nerve morphology

Mice were perfused with EM fixative (1.5% glutaraldehyde, 1.5% paraformaldehyde, 0.05M sucrose, 0.25% $CaCl_2$ 0.1M Sodium cacodylate buffer [pH 7.4]). Sciatic nerves were dissected and further fixed overnight. To examine myelin morphology in postnatal day 3 (P3) mice, pups were euthanized and sciatic nerves were dissected and placed in EM fixative overnight. Toluidine blue semi-thin (1 μm) plastic cross sections were prepared from the mid sciatic nerve.

The entire transverse fascicular area (TFA) of the mid-sciatic nerve was imaged on an automated Olympus BX61 microscope with a motorized stage and OASIS controller. A 100x objective (U PLAN S-APO 100x oil, NA1.4) was used and images were acquired using a monochrome CCD F-View II camera controlled by MicroSuite software (Ver 3.3). The montage feature in MicroSuite was used to capture the entire TFA without duplication. Fixed nerves (above) were processed for EM in a Lynx II automatic processor. Ultrathin (70 nm) sections were cut and contrasted further with uranyl acetate and lead citrate, and grids were viewed and photographed by using an FEI Tecnai 12 transmission electron microscope that is interfaced to an AMT XR16M CCD camera.

To determine the ratio of normal to abnormal fibers, the entire TFA was counted. Axons with an area of ≥ 15.8 μm^2 (axonal diameter of ~4.5 μm) were selected using image thresholding and the MetaMorph (Ver. 7.5.3.0) integrated morphometry analysis tool. Selected axons were counted and scored as normal or abnormal. An abnormal fiber was defined as one having an infolding, outfolding, or deep invagination (~2/3 of axon diameter or more). For P3 sciatic nerves, the size selection protocol (above) was not

used. Instead, all myelinated axons were counted and scored as normal or abnormal. For P3 nerves, any axons that could not be clearly scored as normal or abnormal were scored as uncertain. These accounted for 0.5 to 1% of the fibers counted. To determine axon density, all visible myelinated fibers were counted in each 100x light image or 1200x EM image analyzed. The number of images analyzed was determined based on area, with 10% of total TFA being the target degree of coverage.

Images used for *g* ratio determination were taken at 100x with identical light/camera settings. Image analysis was performed in MetaMorph. Only reasonably round fibers lacking infoldings or outfoldings were analyzed. For *Mtmr13*$^{-/-}$ nerves, every suitable axon in an image was measured. For wild type animals, 10-15 of the rounder axons in each image were arbitrarily selected, with a goal of a roughly representative size distribution. Axons selected were generally between 2 and 11 μm in diameter and were not sectioned through Schmidt-Lanterman incisures. Axons were selected with the threshold tool (in MetaMorph) using the same threshold value for each image. At least 100 fibers per mouse were analyzed. Axon and myelin perimeters were measured using the integrated morphometry analysis tool. *G* ratio was calculated by dividing the axon perimeter by the myelin perimeter. Effective axon diameter was calculated by dividing the axon perimeter by pi.

Acknowledgements

The authors wish to thank Gary Banker, Gary Westbrook, Jau-Shin Lou, Peter Mayinger, and Sean Speese for helpful discussions and critical reading of the manuscript. Deconvolution microscopy and analysis were carried out in OHSU's Advanced Light Microscopy Core @ The Jungers Center for Neurosciences Research. The authors wish to thank Aurelie Snyder and Stefanie Kaech Petrie of the Advanced

Light Microscopy Core for expert advice. The DeltaVison CoreDV microscope was purchased with a Shared Instrumentation Grant from the National Institutes of Health-National Center for Research Resources (S10-RR023432 to Thomas Keller). The authors wish to thank Robert Kayton, Lisa Dirling Vecchiarelli and Sue Aicher for assistance with electron microscopy, nerve preparation and expert advice. The electron microscope was purchased through a grant from the Murdock Charitable Trust (to Sue Aicher). The 1D4B (LAMP-1) and E7 (β-tubulin) monoclonal antibodies, developed by Drs. J. Thomas August and Michael Klymkowsky, respectively, were obtained from the Developmental Studies Hybridoma Bank developed under the auspices of the National Institutes of Health-National Institute of Child Health & Human Development and maintained by The University of Iowa, Department of Biology, Iowa City, IA 52242.

Figures and Legends

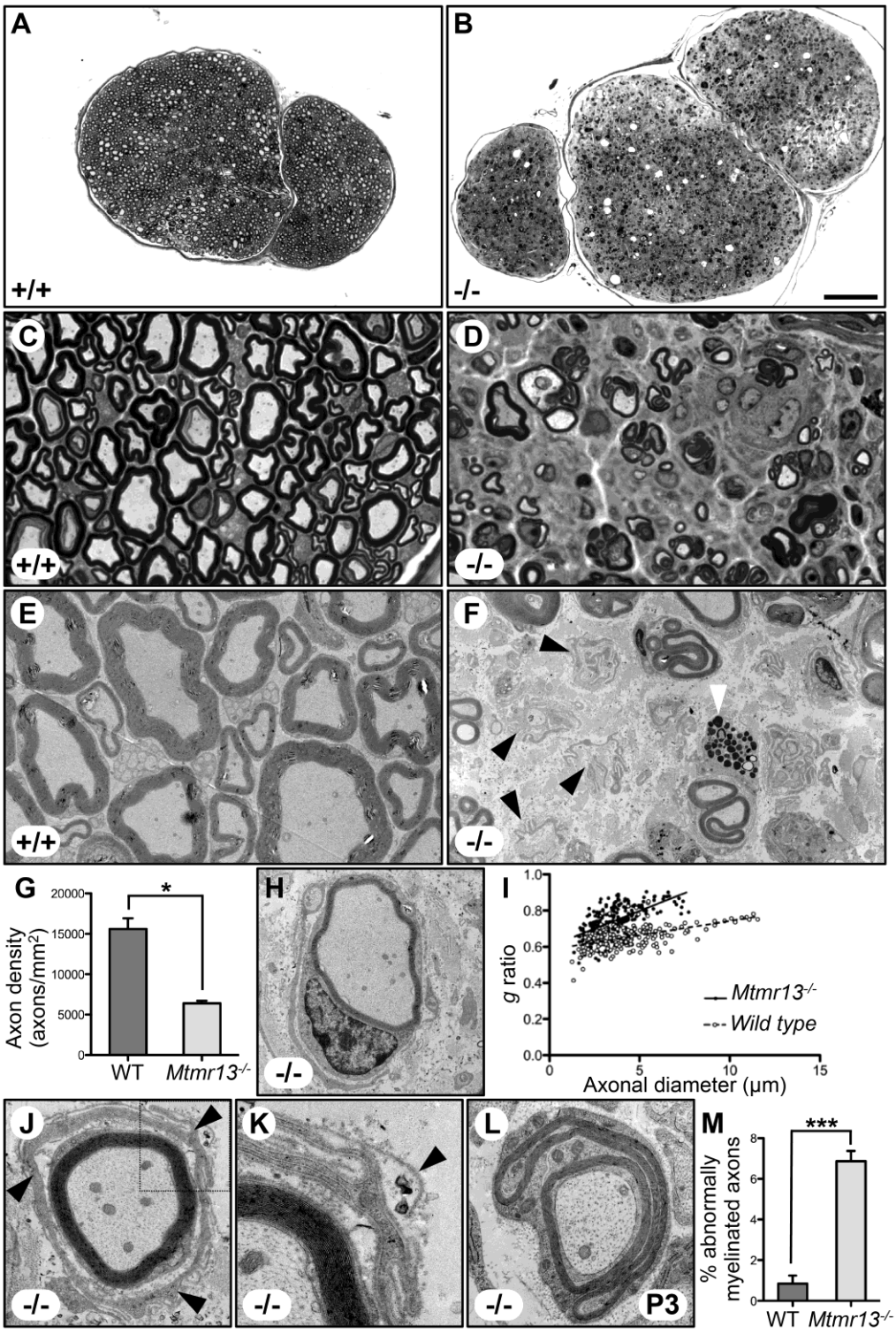

Figure 2.1. Axonal degeneration, hypomyelination and early dysmyelination in peripheral nerves of *Mtmr13*$^{-/-}$ mice. (**A-D**) Light microscopy analysis of sciatic nerves

from wild type and *Mtmr13*$^{-/-}$ mice at 28 months. Toluidine blue stained cross sections of the mid sciatic nerve are shown. *Mtmr13*$^{-/-}$ nerves show a reduction in toluidine blue staining (*black*), reflecting a significant reduction in the density of myelinated axons, as well as myelin outfolding and infolding (D). (**E, F**) EM analysis reveals evidence of axonal degeneration in *Mtmr13*$^{-/-}$ mice, namely remnants of axon-Schwann cell units (*arrowheads in F*). A mast cell is indicated with a white arrowhead. (**G**) Density of myelinated axons in sciatic nerve of wild type and *Mtmr13*$^{-/-}$ mice (15610 ± 1320 myelinated axons/mm^2 for wild type vs. 6402 ± 317.6 for *Mtmr13*$^{-/-}$, n = 2 mice for both genotypes, * P = 0.0211). (**H**) An example of a hypomyelinated axon in an *Mtmr13*$^{-/-}$ sciatic nerve. (**I**) Myelin thickness (*g* ratio) in wild type and *Mtmr13*$^{-/-}$ mice at 28 months (Average *g* ratio: 0.742 ± 0.017 for *Mtmr13*$^{-/-}$ vs. 0.654 ± 0.006 for wild type; n = 2; * P = 0.0395). (**J**) Examples of supernumerary Schwann cell processes and basal laminae (*arrowheads*) surrounding a myelinated axon in an *Mtmr13*$^{-/-}$ sciatic nerve. (**K**) A magnification of the indicated portion of (J) in which a detached basal lamina is marked with an arrowhead. (**L**) Myelin outfolding in sciatic nerves of *Mtmr13*$^{-/-}$ nice at postnatal day 3 (P3). (**M**) Frequency of abnormal myelination (outfolding) in P3 wild type and *Mtmr13*$^{-/-}$ sciatic nerves (0.8456% ± 0.3963 for wild type vs. 6.868% ± 0.5089 for *Mtmr13*$^{-/-}$; n = 3 for both; *** P = 0.0007). Scale bar: 100 μm (A & B), 10 μm (C & D), 4 μm (E & F), 3 μm (H), 1 μM (J), 520 nm (K), and 1 μm (L).

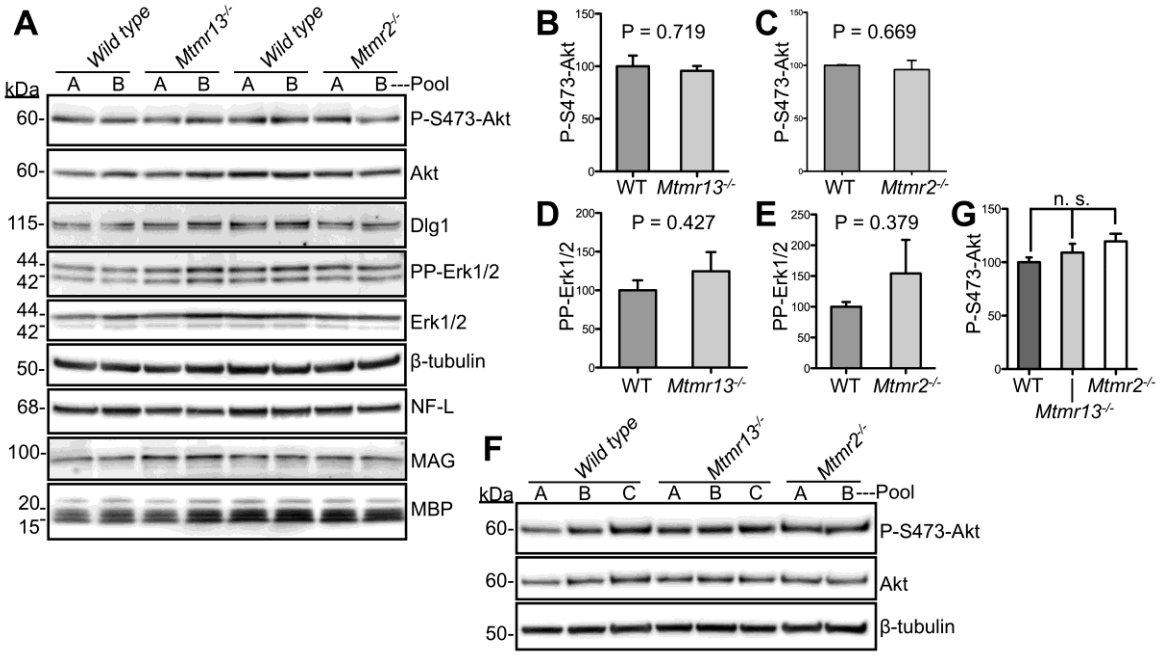

Figure 2.2. Akt and Erk1/2 activation, and Dlg1 protein levels in mouse models of CMT4B. (**A**) Sciatic nerve extracts were prepared from four-month-old mice of the indicated genotypes and examined by immunoblotting. Pools A and B denote independent (replicate) pools of nerves of the same genotype. (**B-E**) Quantification of protein levels in immunoblots. P-S473-Akt and PP-Erk1/2 values are normalized to the amount of total Akt and total Erk1/2 in each sample. Significant changes in the activation of Akt or Erk1/2 were not observed in *Mtmr13*$^{-/-}$ or *Mtmr2*$^{-/-}$ nerves. (B) P-S473-Akt (100.0 ± 10.21 for wild type vs. 95.67 ± 4.676 for *Mtmr13*$^{-/-}$; n = 3 for both; P = 0.7193). (C) P-S473-Akt (100.0 ± 0.5739 for wild type vs. 96.00 ± 8.680 for *Mtmr2*$^{-/-}$; n = 3 for both; P = 0.6695). (**D**) PP-Erk1/2 (100.0 ± 12.96 for wild type vs. 124.7 ± 24.75 for *Mtmr13*$^{-/-}$; n = 3 for both; P = 0.4272). (**E**) PP-Erk1/2 (100.0 ± 7.745 for wild type vs. for 154.3 ± 54.47 for *Mtmr2*$^{-/-}$; n = 3 for both; P = 0.3792). The levels of neurofilament light chain (NF-L) and myelin basic protein (MBP) were not significantly altered in *Mtmr13*$^{-/-}$ of *Mtmr2*$^{-/-}$ nerves. Myelin associated glycoprotein (MAG) levels were unchanged *Mtmr2*$^{-/-}$ nerves, but

appeared slightly elevated in *Mtmr13*$^{-/-}$ nerves. (**F**) Akt activation in mouse sciatic nerves at postnatal day 4 (P4). (**G**) Quantification of immunoblots in (F). P-S473-Akt values are normalized to the amount of total Akt in each sample. Significant changes in Akt activation were not observed. P-S473-Akt: 100.0 ± 4.615 for wild type vs. 109.1 ± 8.236 for *Mtmr13*$^{-/-}$ vs. 119.5 ± 7.147 for *Mtmr2*$^{-/-}$; n = 3 for wild type and *Mtmr13*$^{-/-}$; n = 2 for *Mtmr2*$^{-/-}$; P = 0.3915 for wild type vs. *Mtmr13*$^{-/-}$ and 0.0920 for wild type vs. *Mtmr2*$^{-/-}$.

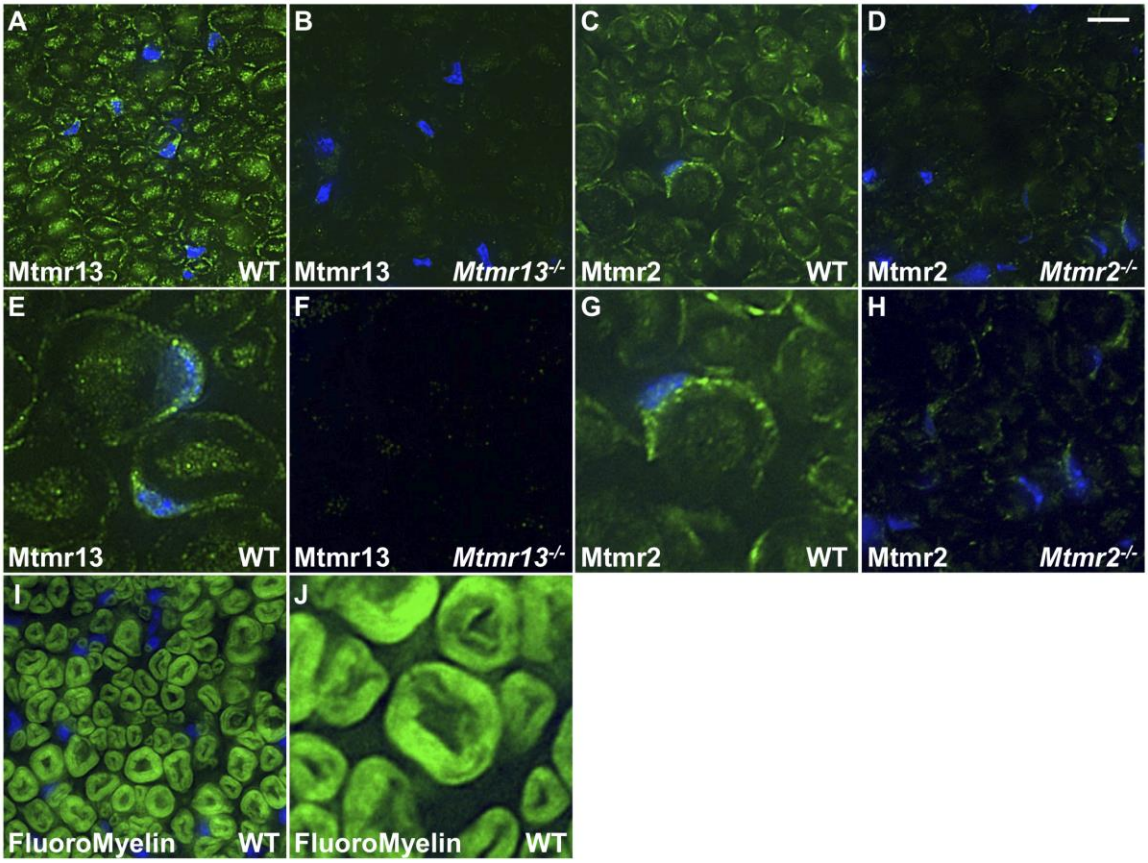

Figure 2.3. Specificity of anti-Mtmr13 and anti-Mtmr2 antibodies and localization within Schwann cells and axons. Cross sections of sciatic nerves from eight or nine month old mice were examined by immunofluorescence microscopy. (**A**) Anti-Mtmr13 immunofluorescence (*green*) is greatly reduced in sciatic nerve sections from *Mtmr13*$^{-/-}$ mice (**B**). (**C**) Anti-Mtmr2 immunofluorescence (*green*) is greatly reduced in sciatic nerve sections from *Mtmr2*$^{-/-}$ mice (**D**). Panels A-D depict representative data from one of four independent experiments. (**E**) Localization of Mtmr13 in wild type mouse sciatic nerve. Anti-Mtmr13 immunofluorescence (*green*) is detected in the Schwann cell cytoplasm and the axon, but is excluded from compact myelin and the Schwann cell nucleus. Punctate Mtmr13-positive structures are detected in the Schwann cell cytoplasm. (**F**) Anti-Mtmr13 immunofluorescence (*green*) is greatly reduced in an *Mtmr13*$^{-/-}$ nerve section

comparable to (E) under identical acquisition settings. (**G**) Localization of Mtmr2 in wild type mouse sciatic nerve. Anti-Mtmr2 immunofluorescence (*green*) is detected in the Schwann cell cytoplasm and the axon, but is excluded from compact myelin and the Schwann cell nucleus. Punctate Mtmr2-positive structures are detected in the Schwann cell cytoplasm. (**H**) Anti-Mtmr2 immunofluorescence (*green*) is greatly reduced in an *Mtmr2*$^{-/-}$ nerve section comparable to (G) under identical acquisition settings. (**I, J**) FluoroMyelin staining identifies compact myelin in sections comparable to those of A-D and E-H, respectively. Nuclei were labeled with DAPI (*blue*). Scale bar: 10 μm (A-D, I), 4 μm (E-H, J).

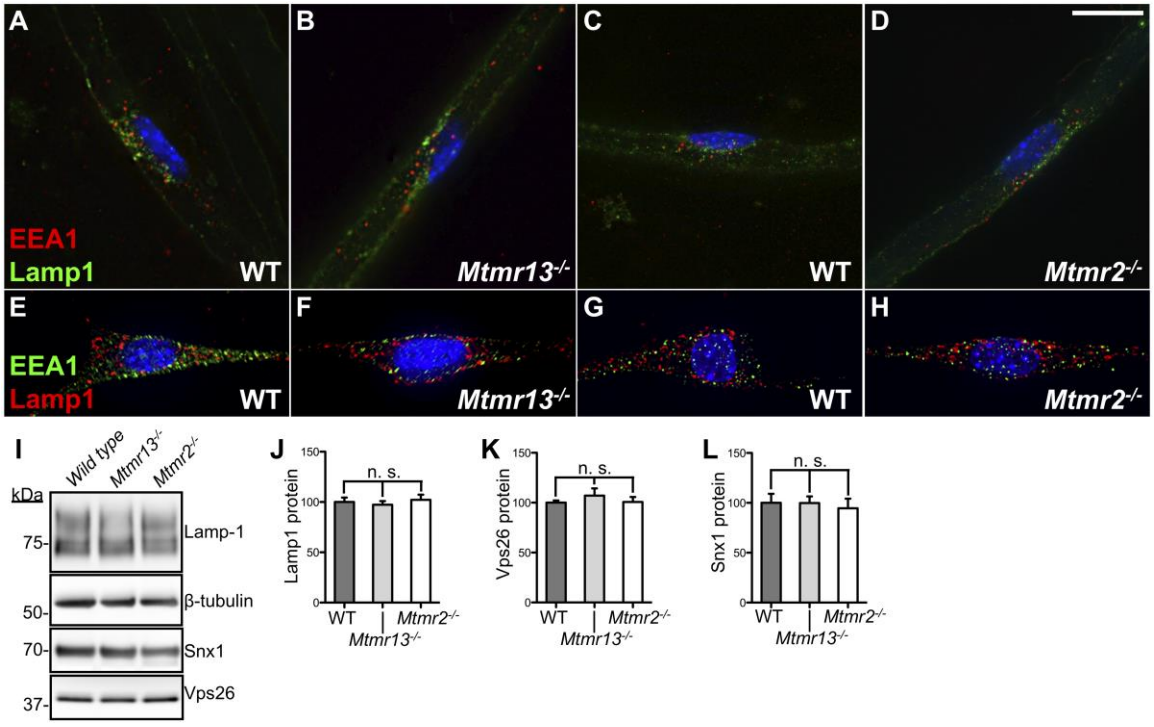

Figure 2.4. Status of endo-lysosomal membranes in CMT4B model Schwann cells and sciatic nerves. (**A-D**) Immunofluorescence was performed on teased myelinated fibers from sciatic nerves of wild type, *Mtmr13*$^{-/-}$ and *Mtmr2*$^{-/-}$ mice aged 110 days (A, B) or 58 days (C, D). Lamp1-positive late endosomes/lysosomes (*green*) and EEA1-positive early endosomes (*red*) in *Mtmr2*$^{-/-}$ and *Mtmr13*$^{-/-}$ Schwann cells appear similar to wild type, without evidence of endo-lysosomal swelling. (**E-H**) Immunofluorescence was performed on primary Schwann cells of the indicated genotypes. Lamp1-positive late endosomes/lysosomes (*red*) and EEA1-positive early endosomes (*green*) in *Mtmr2*$^{-/-}$ and *Mtmr13*$^{-/-}$ Schwann cells appear similar to wild type. Nuclei were stained with DAPI (*blue*). Scale bar: 15 μm (A-D), 17 μm (E, F) and 13 μm (G, H). (**I**) Sciatic nerve protein extracts were prepared from 4 month old mice of the indicated genotypes and examined by immunoblotting. (**J-L**) Quantification of immunoblots in (I). Lamp1, Vps26 and Snx1 values are normalized to the amount of β-tubulin in each sample. Significant changes in

Lamp1, Vps26 and Snx1 levels were not observed. Lamp1 protein levels: 100.0 ± 4.496 for wild type vs. 97.35 ± 3.613 for *Mtmr13*$^{-/-}$ vs. 102.2 ± 5.057 for *Mtmr2*$^{-/-}$; n = 3 for all genotypes; P = 0.6693 for wild type *vs. Mtmr13*$^{-/-}$; P = 0.7566 for wild type *vs. Mtmr2*$^{-/-}$. Vps26 protein levels: 100.0 ± 2.160 for wild type *vs*. 107.1 ± 7.155 for *Mtmr13*$^{-/-}$ *vs.* 100.7 ± 4.995 for *Mtmr2*$^{-/-}$; n = 2 for all genotypes; P = 0.4416 for wild type *vs. Mtmr13*$^{-/-}$; P = 0.9152 for wild type *vs. Mtmr2*$^{-/-}$. Snx1 protein levels: 100.0 ± 9.064 for wild type *vs.* 99.81 ± 6.647 for *Mtmr13*$^{-/-}$ *vs.* 94.60 ± 9.641 for *Mtmr2*$^{-/-}$; P = 0.9870 for wild type *vs. Mtmr13*$^{-/-}$; P = 0.7042 for wild type *vs. Mtmr2*$^{-/-}$; n = 3 for all genotypes.

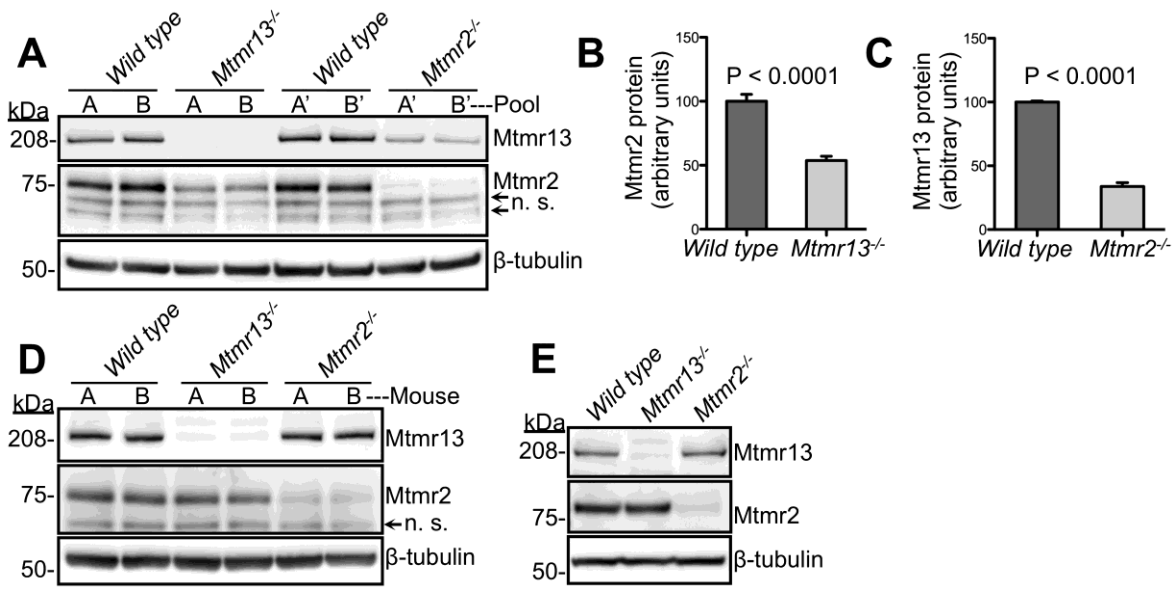

Figure 2.5. Reciprocal enhancement of protein abundance by Mtmr13 and Mtmr2 in mouse sciatic nerves. (**A**) Sciatic nerve protein extracts were prepared from 4 month old mice of the indicated genotypes and examined by immunoblotting. Pools A and B denote independent (replicate) pools of nerves of the same genotype. Non-specific (*n. s.)* bands are indicated in the MTMR2 blots. (**B & C**) Chemiluminescent quantification of protein levels in immunoblots. (B) Mtmr2 protein levels: 100.0 ± 5.493 for wild type vs. 53.73 ± 3.371 for *Mtmr13*$^{-/-}$, n = 5 for both, P < 0.0001. (C) Mtmr13 protein levels: 100.0 ± 0.7643 for wild type vs. 33.87 ± 2.942 for *Mtmr2*$^{-/-}$, n = 5 for both, P < 0.0001. (**D**) Mtmr13 and Mtmr2 proteins levels in brain extracts from 4 month old mice were examined by immunoblotting. Mtmr13 levels in brain: 100.0 ± 9.348 for wild type vs. 100.0 ± 7.331 for *Mtmr2*$^{-/-}$, n = 4 for both, P = 1.0000. Mtmr2 levels in brain: 100.0 ± 1.224 for wild type vs. 100.0 ± 5.254 for *Mtmr13*$^{-/-}$, n = 4 for both, P = 1.0000. (**E**) Protein extracts from MEF cells were examined by immunoblotting.

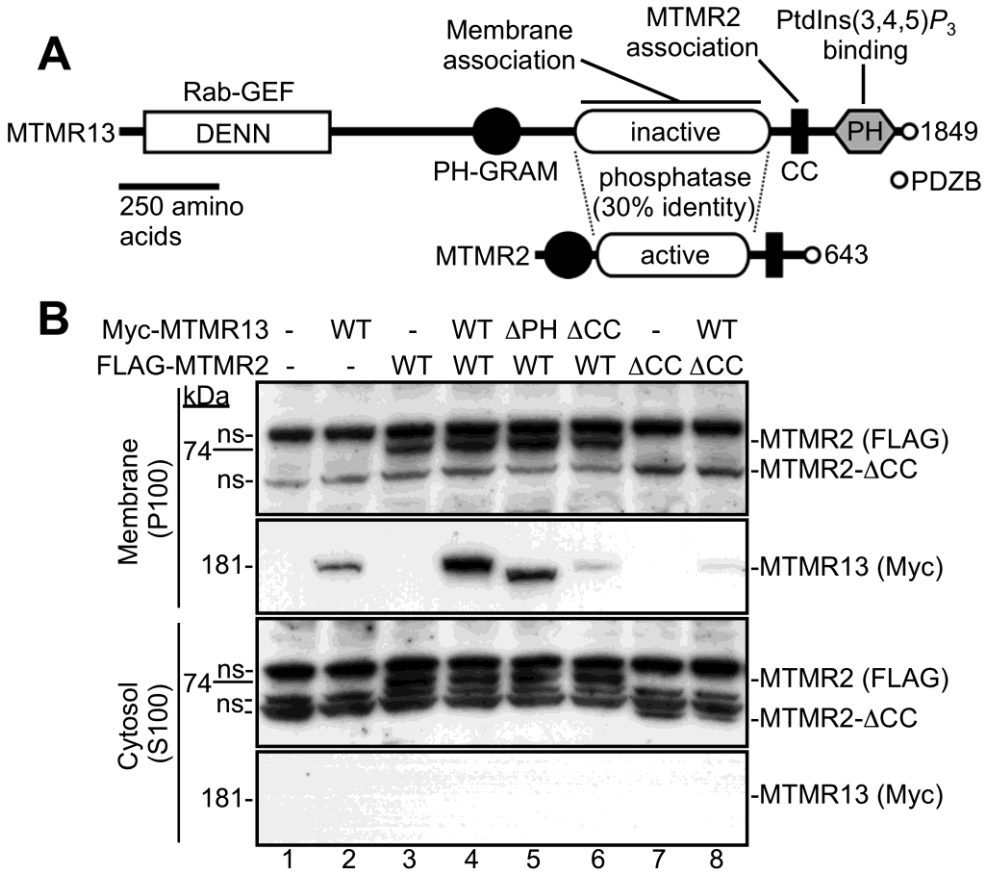

Figure 2.6. Mtmr13 is stabilized on membranes by Mtmr2. (**A**) A schematic of the composition of the MTMR13 and MTMR2 proteins, indicating functions attributed to specific domains of MTMR13. (**B**) Subcellular fractionation of MTMR13 and MTMR2 following exogenous expression in HEK293 cells. Transfected cells were fractionated into membrane (P100) and cytosolic (S100) fractions and examined by immunoblotting. The anti-FLAG antibody recognizes several nonspecific (*ns*) proteins that are present in both the P100 and S100 fractions. *Abbreviations*: PH, pleckstrin homology; DENN, differentially expressed in neoplastic versus normal cells; GRAM, glucosyltransferase Rab activator myotubularins; PDZB, PDZ domain binding motif; GEF, guanine nucleotide exchange factor; CC, coiled-coil.

Supplementary Data

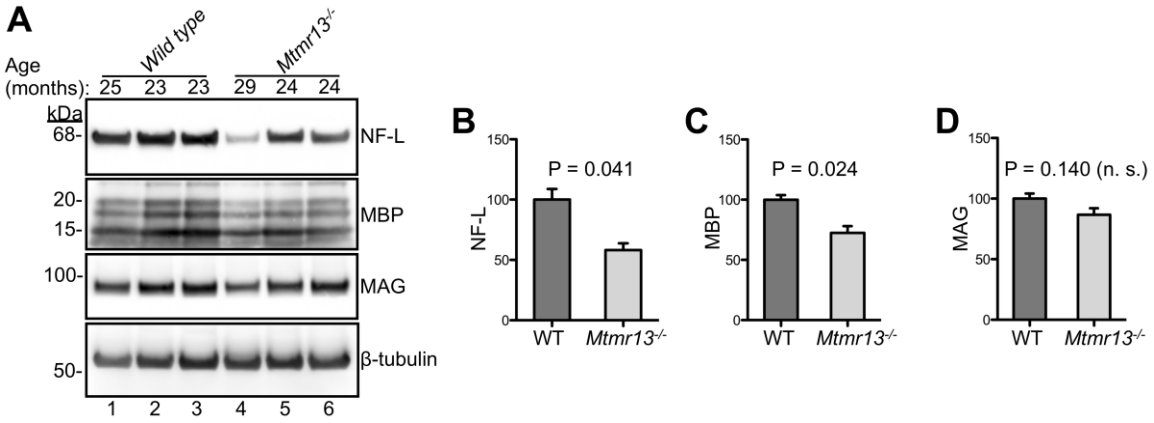

Supplemental Figure 2.7. Decreased abundance of neurofilament light chain and myelin basic protein in sciatic nerves of aged *Mtmr13*$^{-/-}$ mice. (**A**) Sciatic nerve extracts, prepared from individual male mice of the indicated age and genotype, were examined by immunoblotting. (**B-D**) Quantification of protein levels in immunoblots. The 29-month-old *Mtmr13*$^{-/-}$ mouse (*lane 4*) was excluded from the quantitative analysis, as an age-matched control was unavailable. Neurofilament light chain (NF-L), myelin basic protein (MBP) and myelin-associated glycoprotein (MAG) values were normalized to the amount of β-tubulin in each sample. (B) NF-L levels are reduced in sciatic nerves of two-year-old *Mtmr13*$^{-/-}$ mice (NF-L: 100.0 ± 8.777 for wild type vs. 58.15 ± 5.705 for *Mtmr13*$^{-/-}$; n = 3 for wild type and n = 2 for *Mtmr13*$^{-/-}$; P = 0.041). (C) MBP levels are reduced in sciatic nerves of two-year-old *Mtmr13*$^{-/-}$ mice (MBP: 100.0 ± 3.843 for wild type vs. 72.40 ± 5.616 for *Mtmr13*$^{-/-}$; n = 3 for wild type and n = 2 for *Mtmr13*$^{-/-}$; P = 0.024). (D) MAG levels are not significantly altered in sciatic nerves of two-year-old *Mtmr13*$^{-/-}$ mice (MAG: 100.0 ± 4.149 for wild type vs. 86.69 ± 5.350 for *Mtmr13*$^{-/-}$; n = 3 for wild type and n = 2 for *Mtmr13*$^{-/-}$; P = 0.1403).

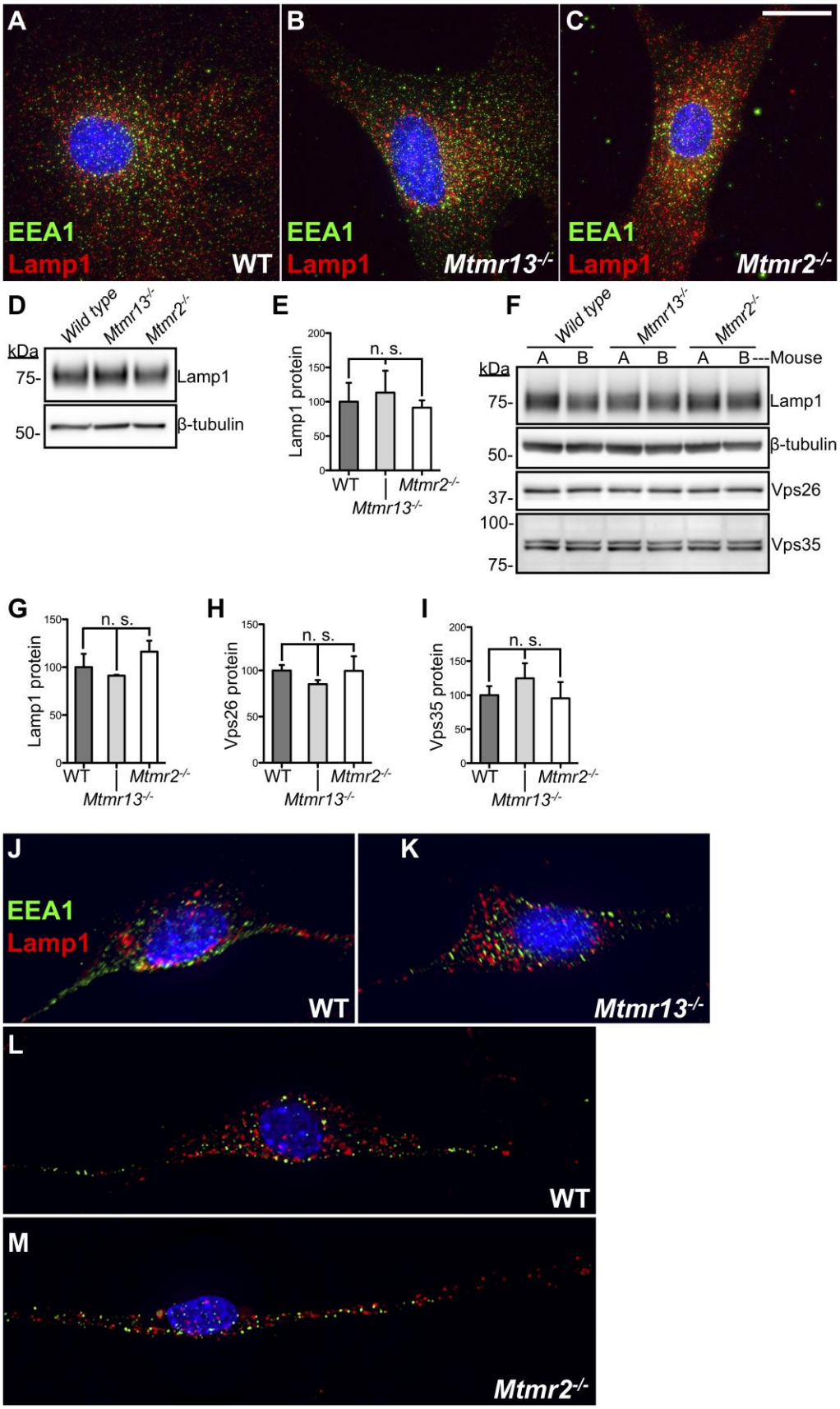
A
EEA1
Lamp1
WT
B
EEA1
Lamp1
Mtmr13-/-
C
EEA1
Lamp1
Mtmr2-/-
D
Wild type
Mtmr13-/-
Mtmr2-/-
kDa
75-
Lamp1
50-
β-tubulin
E
Lamp1 protein
n. s.
WT
Mtmr2-/-
Mtmr13-/-
F
Wild type
Mtmr13-/-
Mtmr2-/-
A B A B A B---Mouse
kDa
75-
Lamp1
50-
β-tubulin
37-
Vps26
100-
75-
Vps35
G
Lamp1 protein
n. s.
WT
Mtmr2-/-
Mtmr13-/-
H
Vps26 protein
n. s.
WT
Mtmr2-/-
Mtmr13-/-
I
Vps35 protein
n. s.
WT
Mtmr2-/-
Mtmr13-/-
J
EEA1
Lamp1
WT
K
Mtmr13-/-
L
WT
M
Mtmr2-/-

Supplemental Figure 2.8. Status of endo-lysosomal membranes in CMT4B model Schwann cells, fibroblasts and brain. (**A-C**) Immunofluorescence was performed on primary MEFs of the indicated genotypes. Lamp1-positive late endosomes/lysosomes (*red*) and EEA1-positive early endosomes (*green*) in *Mtmr2*$^{-/-}$ and *Mtmr13*$^{-/-}$ MEFs appear similar to wild type, without evidence of endo-lysosomal swelling. Nuclei were stained with DAPI (*blue*). (**D**) Lamp1 levels are not significantly changed in *Mtmr13*$^{-/-}$ or *Mtmr2*$^{-/-}$ fibroblasts (MEFs). Protein extracts from MEF cells were examined by immunoblotting. (**E**) Quantification of protein levels in immunoblots of (D). Lamp1 protein levels were normalized to the amount of β-tubulin in each sample. Lamp1: 100.0 ± 27.58 for wild type *vs.* 113.3 ± 31.91 for *Mtmr13*$^{-/-}$ *vs*. 91.44 ± 10.51 for *Mtmr2*$^{-/-}$; n = 3 for all genotypes; P = 0.7678 for wild type *vs*. *Mtmr13*$^{-/-}$; P = 0.7861 for wild type *vs*. *Mtmr2*$^{-/-}$). (**F**) Brain protein extracts were prepared from 4-month-old mice of the indicated genotypes and examined by immunoblotting. A and B denote independent (replicate) brains from mice of the same genotype. (**G-I**) Quantification of protein levels in immunoblots of (F). Lamp1, Vps26 and Vps35 protein levels are not significantly altered in *Mtmr13*$^{-/-}$ or *Mtmr2*$^{-/-}$ brains. Lamp1: 100.0 ± 13.88 for wild type *vs.* 91.21 ± 0.7732 for *Mtmr13*$^{-/-}$ *vs.* 116.2 ± 11.44 for *Mtmr2*$^{-/-}$; n = 2 for all genotypes; P = 0.5919 for wild type *vs. Mtmr13*$^{-/-}$; P = 0.4626 for wild type *vs. Mtmr2*$^{-/-}$. Vps26: 100.0 ± 5.972 for wild type *vs.* 85.22 ± 4.318 for *Mtmr13*$^{-/-}$ *vs.* 99.55 ± 15.85 for *Mtmr2*$^{-/-}$; n = 2 for all genotypes; P = 0.1828 for wild type *vs. Mtmr13*$^{-/-}$; P = 0.9811 for wild type *vs. Mtmr2*$^{-/-}$. Vps35: 100.0 ± 13.23 for wild type *vs*. 124.8 ± 22.08 for *Mtmr13*$^{-/-}$ *vs.* 95.42 ± 23.80 for *Mtmr2*$^{-/-}$; n = 2 for all genotypes; P = 0.4369 for wild type *vs. Mtmr13*$^{-/-}$; P = 0.8819 for wild type *vs. Mtmr2*$^{-/-}$. (**J-M**) Immunofluorescence was performed on primary Schwann cells from wild type, *Mtmr13*$^{-/-}$ and *Mtmr2*$^{-/-}$ mice (supplemental examples). Lamp1-positive late endosomes/lysosomes (*red*) and EEA1-positive early endosomes (*green*) in *Mtmr2*$^{-/-}$ and

Mtmr13$^{-/-}$ Schwann cells appear similar to wild type, without evidence of endo-lysosomal swelling. Scale bar: 25 μm (A-C), 12 μm (J-K).

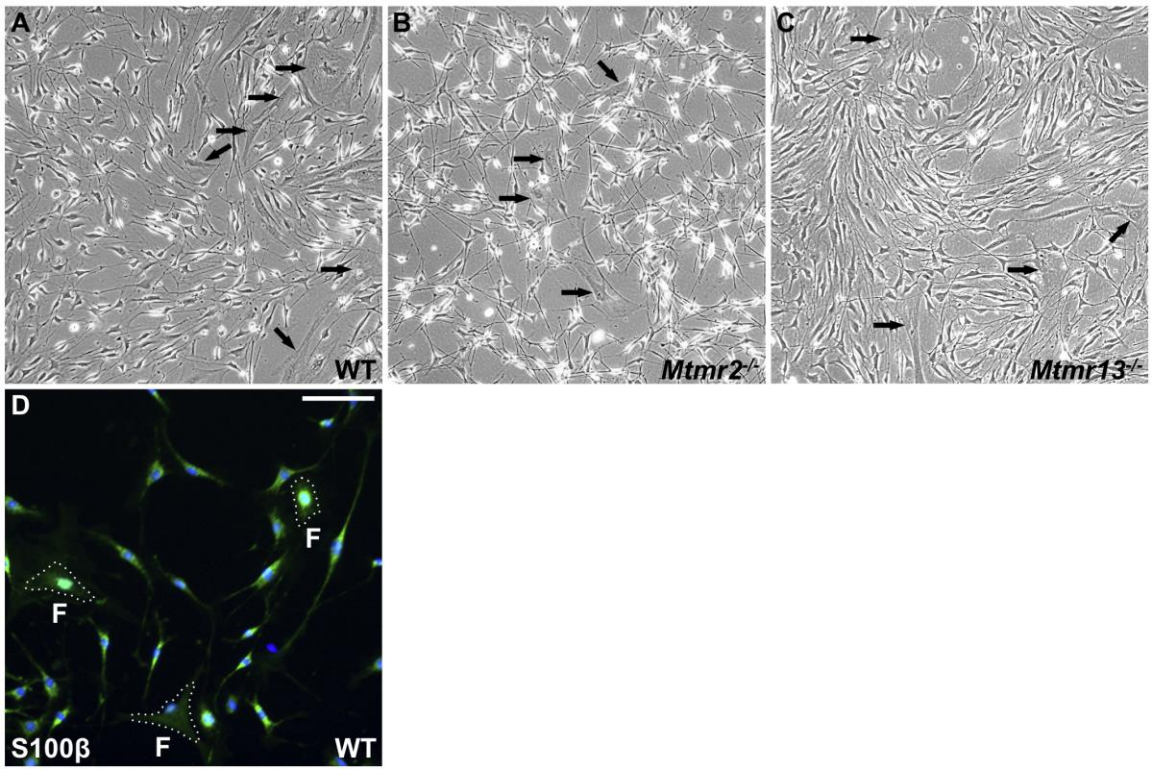

Supplemental Figure 2.9. Isolation of primary Schwann cells from wild type and CMT4B model mice. (**A-C**) After purification, cultured primary Schwann cells (passage 2 or 3) display a bipolar, spindle-like morphology. Contaminating fibroblasts (*arrowheads*) are larger and have a flat morphology. (**D**) Schwann cells are identified by cytoplasmic S100β immunofluorescence (*green*). Nuclei are stained with DAPI (*blue*). Contaminating fibroblasts (*F, outlined in white*) are larger, have a flat morphology, and lack S100β immunofluorescence in the cytoplasm. Scale bar: 200 μm (A-C), 100 μm (D).

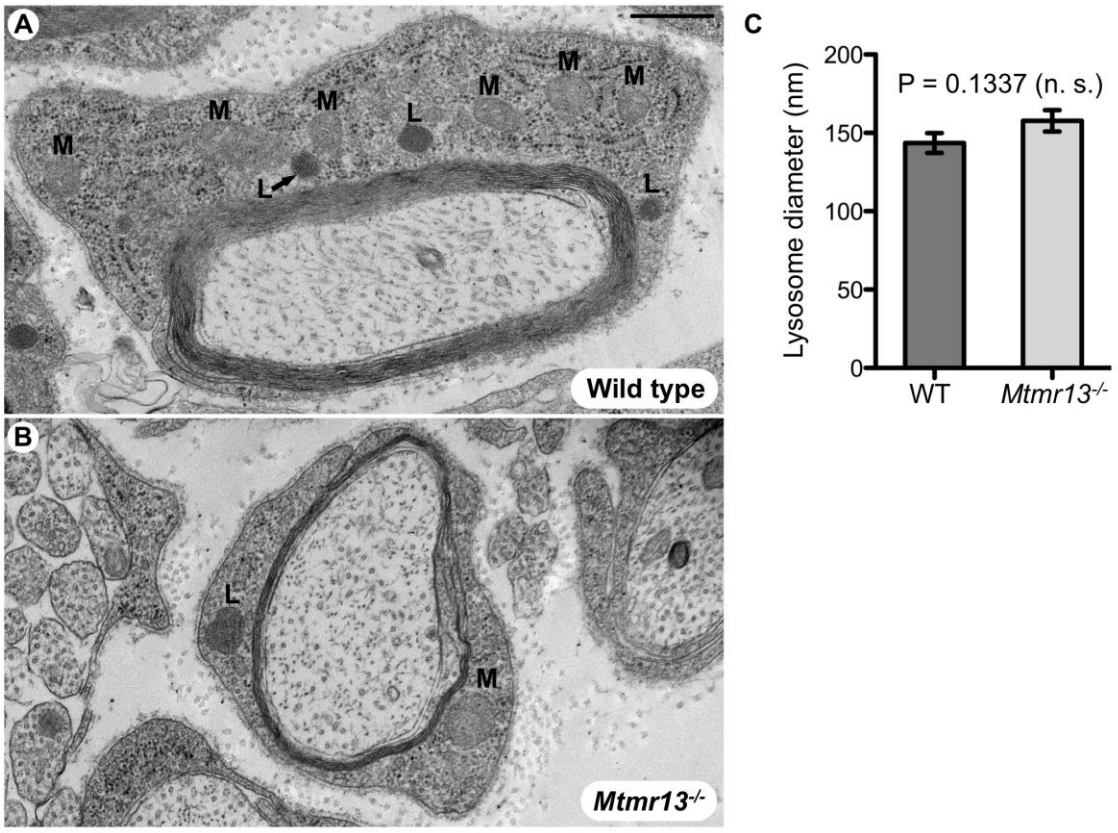

Supplemental Figure 2.10. Lysosomal size is not significantly altered in Schwann cells of *Mtmr13*$^{-/-}$ sciatic nerves. Electron microscopy (EM) was performed on wild type and *Mtmr13*$^{-/-}$ sciatic nerves at postnatal day 3 (P3) (two mice per genotype). Between 12 and 16 electron micrographs of between 4800x and 18500x direct magnification were examined per mouse. (**A,B**) Examples of lysosomes (*L*) in Schwann cells of wild type and *Mtmr13*$^{-/-}$ nerves. Mitochondria (*M*) are also indicated. Scale bar: 500 nm (A) and 455 nm (B). (**C**) Lysosomal diameter was determined using ImageJ software. A trend toward increased lysosomal diameter in *Mtmr13*$^{-/-}$ Schwann cells was not statistically significant (*n. s.*). Average lysosome diameter: 143.6 ± 6.393 nm for wild type (n = 98) *vs.* 157.7 ± 6.827 nm for *Mtmr13*$^{-/-}$ (n = 79); P = 0.1337. The possibility of peroxisomes being counted as lysosomes in this analysis cannot be excluded, as these organelles are similar in size to lysosomes and are also electron dense.

Chapter 3

Vps34 is required for completion and maintenance of Schwann cell myelination through its role in both endosomal and autophagic pathways

Anne M. Logan[1,2]**,** Alec Condon[1], Eric J. Schmidt[1] and Fred L. Robinson[1,†]. Vps34 is required for completion and maintenance of Schwann cell myelination through its role in both endosomal and autophagic pathways.

[1]The Jungers Center for Neurosciences Research, Department of Neurology, Oregon Health & Science University, 3181 SW Sam Jackson Park Road, Portland, OR 97239, USA.

[2]Neuroscience Graduate Program, Oregon Health & Science University.

[†]Corresponding Author: The Jungers Center for Neurosciences Research, Department of Neurology, Oregon Health & Science University, Mail Code L623, 3181 SW Sam Jackson Park Road, Portland, OR 97239, USA. Tel 503-494-8783; Fax 503-494-9161; Email: robinsof@ohsu.edu

Preface

The work is in preparation for submission to *The Journal of Neuroscience.*

Anne Logan designed the project and performed all the experiments, except for the morphology analysis of *Mtmr13*$^{-/-}$ *Pik3c2β*$^{-/-}$ mice, which was performed by Eric Schmidt. Anne Logan also performed the analysis of all data, with assistance from Alec Condon, and wrote the manuscript. Alec Condon also contributed to critical reading of the manuscript.

Fred Robinson contributed to the conception of the project and helped write and edit the manuscript.

Abstract

Phosphoinositides (PI) in eukaryotic cells are reversibly phosphorylated by a large network of PI-kinases and phosphatases, resulting in localized pools of PIs on stereotyped intracellular membranes. PI 3-kinases phosphorylate PI to make PI3P, and 3-phopshatases are capable of dephosphorylating both PI3P and $PI(3,5)P_2$. Regulation of PIs is critical for cell function, highlighted by the mutations in various PI metabolizing enzymes that lead to human disease. Here, we study the effect of manipulating PI levels in the Schwann cell. Using a P0-cre line to specifically ablate gene expression in Schwann cells, we knockout the class III PI 3-kinase Vps34, thus lowering PI3P levels only in the Schwann cell. Using this novel mouse, we find that Vps34 is required for completion of myelination and maintenance of an intact myelin sheath. At P3, no myelin, endosomal, or autophagic pathway defects are visible, but by P7 and persisting into adulthood there is dramatic dysregulation of all three. With this mouse, we also ask if we can rescue myelin outfoldings caused by mutations in the 3-phosphatase *Mtmr13* by re-balancing PI3P levels in the Schwann cell. We find that we are unable to change the prevalence of myelin outfoldings in these double-knockout mice, in either P3 or adult nerves. Class II PI 3-kinases also contribute to cellular PI3P; therefore, we crossed class II PI 3-kinase *β* knockout mice with $Mtmr13^{-/-}$ mice. We again found no changes in myelin outfolding prevalence in adult sciatic nerves.

Introduction

In eukaryotic cells, phosphoinositides (PIs) are regulated by PI kinases, phosphatases and lipases, a network of enzymes that control localization and turnover, thereby orchestrating compartmentalized signaling. PI phosphorylation and dephosphorylation plays an important role in the regulation of acute cellular signaling, membrane trafficking, and cytoskeletal dynamics[49,50].

Myelin is a multilayer wrapping of specialized plasma membrane that surrounds axons and makes possible efficient saltatory impulse propagation[2]. Myelin is produced by oligodendrocytes and Schwann cells in the central and peripheral nervous systems (CNS and PNS), respectively. PI signaling plays an important role in myelination in both the CNS and PNS[3]. PI(3,4,5)P_3, PI(3,5)P_2, and PI3P have each been demonstrated to play important roles in myelination [21,70,104,105,106,107]. Moreover, mutations in four PI phosphatases, myotubularin-related (MTMR) 2, MTMR5, MTMR13 and FIG4, have been identified as the causes of specific forms of demyelinating Charcot-Marie-Tooth (CMT) peripheral neuropathy[42,47,83,120].

Phosphatidylinositol 3-phosphate (PI3P) plays an important role in both endosomal trafficking and autophagy[137,138]. PI3P is highly enriched on early endosomes, where it recruits specific effector proteins, many of which contain FYVE or PX domains[139,140]. Depletion of PI3P delays the traffic of proteins through endosomes[137,141]. PI3P also plays a key role in autophagosome formation[138]. In mammalian cells, the majority of PI3P is thought to be generated via the phosphorylation of phosphatidylinositol (PI) by the class II and III PI 3-kinases (PI3Ks)[73,142].

CMT-causing mutations and studies with gene knockout mice have indicated that PI3P dysregulation and endosomal-lysosomal dysfunction may be a common trigger for dysmyelination in the PNS[143]. However, it is unclear which isoforms of PI3K are involved in generating PI3P in Schwann cells. Moreover, a number of distinct pools of

PI3P may be present in these cells. To begin to elucidate the roles of PI3P, endosomal trafficking, and autophagy in myelinating Schwann cells, we have examined the role of the PI3K Vps34 (*Pik3c3*) using mouse models.

Vps34 is the sole member of the class III PI3K sub-family, and a homolog has been identified in most eukaryotes[62,144]. Vps34 is involved in endosomal-lysosomal trafficking, autophagy, and cellular responses to nutrient availability[62]. The role of Vps34 in specialized mammalian cells and tissues, however, remains unclear. Recently, investigators have begun using conditional alleles of *Vps34* to examine protein function in specific mouse cell types[73,145,146,147,148,149,150,151].

Given the documented or implied roles of PI3P and autophagy in myelinating Schwann cells, we sought to determine the function of Vps34 in this unique cell type. We generated a mouse line in which *Vps34* is specifically deleted in Schwann cells and show that this mutation leads to incomplete myelination and radial sorting defects. Loss of Vps34 does not cause cell death, but prevents Schwann cells from completing the formation of a functional myelin sheath. We also found that both the autophagic and endosomal pathways are disturbed in Schwann cells that lack Vps34. Finally we examined whether lowering PI3P levels, via PI3K deletion, might improve the myelin abnormalities found in a mouse model of CMT neuropathy.

Results

Schwann cell-specific deletion of *Vps34/Pik3c3*

To selectively inactivate *Vps34* in Schwann cells, *Vps34*$^{flox/flox}$ mice[145] were crossed with myelin protein zero (P0)-Cre transgenic mice, which express Cre recombinase in Schwann cells beginning at embryonic (E) day 14.5[152] (Fig. 3.1A) (*see Materials and Methods*). *Vps34*$^{flox/flox}$ *P0-Cre*$^{+}$ mice are hereafter referred to as *Vps34-*

Schwann cell knockout (*Vps34*^{SCKO}). Loss of Vps34 protein in sciatic nerve extracts was confirmed by immunoblotting with an antibody recognizing the N-terminus of the kinase (Fig. 3.1D). Vps34 protein was reduced to about 37% of wild type levels in *Vps34*^{SCKO} sciatic nerves (Fig. 3.1D). The remaining Vps34 protein in *Vps34*^{SCKO} nerves can be accounted for by cell types other than Schwann cells, including axons, fibroblasts, and capillary endothelial cells (Fig. 3.1D). A similar degree of targeted protein persistence in sciatic nerves has been reported when using Schwann cell specific Cre drivers and whole nerve extracts[107,153]. Vps34 protein levels in *Vps34*^{SCKO} brain tissue were similar to wild type (Fig. 3.1E), consistent with the documented Schwann cell specificity of the P0-Cre transgene[152].

Vps34^{SCKO} mice are born and weaned at the expected rate based on Mendelian inheritance, however, by 28 days they are discernably smaller than wild type littermates. By 56 days, the body weight of *Vps34*^{SCKO} mice is about 73% that of wild type, sex-matched littermates, presumably due to secondary muscle atrophy (*data not shown*). Mice lacking Vps34 in Schwann cells survive well into adulthood, although they are typically euthanized by one year of age due to hind limb weakness.

Motor impairment in the absence of Schwann cell Vps34

Although *Vps34*^{SCKO} mice appear normal at birth, minor motor deficits, including a wide-based gait, become apparent by about 21 days. By 56 days, *Vps34*^{SCKO} mice display an unsteady gait, hind limb weakness, and have a slight tremor. Mutant animals often clench their hind paws when suspended by the tail and show wide placement of hind paws when standing, both suggestive of neuromuscular impairment. To assess ambulatory fitness, we evaluated *Vps34*^{SCKO} mice using an accelerating RotaRod test

(Fig. 3.1F). At 56 days, mutant mice were significantly impaired, with the average time to a fall being 33% that of wild type mice, indicative of motor nerve deficiency (Fig. 3.1F).

Loss of Schwann cell Vps34 causes myelination failure

To evaluate the role of Vps34 in myelination, we examined sciatic nerves from wild type and *Vps34*^{SCKO} mice at postnatal (P) days 3, 7, 21 and 56, using both light and electron microscopy (EM) (Fig. 3.2). In wild type nerves examined at P3, a significant amount of radial sorting has occurred, a majority of the large caliber axons are in 1:1 relationships with Schwann cells, and many large axons have thin myelin sheaths[154,155] (Fig. 3.2). At P3, *Vps34*^{SCKO} nerves were indistinguishable from those of wild type animals (Fig. 3.2). Neither myelin thickness (g ratio), nor the number of myelinated axons in the nerve was significantly altered (Fig. 3.3A-C). Nerve pathology becomes apparent in *Vps34*^{SCKO} mice at P7 (Fig. 3.2). Vacuoles are preset in the cytoplasm of many mutant Schwann cells (Fig. 3.2), and the number of axons ≥1 μm in the nerve is decreased by about 20% (Fig. 3.3C). We find an increase in both the size of Remak bundles and the number of large caliber axons in the bundles in *Vps34*^{SCKO} nerves (Fig. 3.3D,E), likely accounting for the 20% decrease in axons greater than 1 μm at P7. Slight hypomyelination is also suggested at P7, as evidenced by a small, albeit statistically insignificant, increase in g ratio (Fig. 3.3B).

We next examined *Vps34*^{SCKO} nerves at 21 days, a time at which myelination is complete in normal mice, with all axons larger than 1 μm myelinated. At P21, most *Vps34*^{SCKO} Schwann cells contain cytoplasmic vacuoles and myelin sheaths are thinner than in controls (Fig. 3.2), as indicated by a significant increase in g ratio (Fig. 3.3A,B). The decrease in number of axons ≥1 μm in diameter in the nerve remains similar to what was observed at P7; there is an approximately 25% decrease in *Vps34*^{SCKO} nerves at

P21 (Fig. 3.2 & Fig. 3.3C). Peripheral nerve pathology progressively worsens in adult *Vps34*^{SCKO} mice. At 56 days, myelin sheaths are thinner, and about 56% of the surviving large axons are completely demyelinated (Fig. 3.2 & Fig. 3.3A,B). In addition, the total number of axons ≥1 μm in the nerve remains decreased by around 25% (Fig. 3.3C).

To further explore the pathology caused by the loss of Vps34 in Schwann cells, we evaluated the relative abundance of myelin and axonal proteins in wild type and *Vps34*^{SCKO} nerves during postnatal development. The levels of neurofilament light chain (NF-L), a cytoskeletal constituent of axonal intermediate filaments, as well as those of myelin basic protein (MBP) and myelin-associated glycoprotein (MAG), compact and non-compact myelin proteins, respectively, were examined by immunoblotting. At P3, the levels of NF-L, MBP, and MAG proteins in sciatic nerve extracts from *Vps34*^{SCKO} animals were not significantly different from those of controls (Fig. 3.3F). At P7, evidence of dysmyelination or demyelination begins to emerge; MAG levels are decreased by about 43% and MBP levels are slightly lowered, albeit not to a statistically significant extent (Fig. 3.3F). NF-L protein abundance was not significantly altered in nerves from *Vps34*^{SCKO} mice at P7 (Fig. 3.3F), suggesting that no or little axon degeneration is occurring by P7, but instead that many axons greater than 1 μm in diameter are stuck in large Remak bundles in *Vps34*^{SCKO} sciatic nerve (Fig. 3.2 & Fig. 3.3C-E). By 21 days, the levels of the NF-L, MBP, and MAG proteins are all significantly decreased in *Vps34*^{SCKO} nerves (Fig. 3.3F), in accord with our morphological findings indicating hypomyelination (Fig. 3.2 & Fig. 3.3A-C).

Initiation of myelination in Schwann cells lacking Vps34

Our data indicate that the loss of Vps34 decreases the capacity of Schwann cells to complete and maintain myelin sheaths. To determine if *Vps34*-null Schwann cells

show impaired differentiation into the myelinating phenotype, we examined the expression of Sox10 and Krox20/Egr2, two transcription factors required for myelination. Sox10 is a key regulator of the differentiation of pluripotent neural crest cells into peripheral glia; mice lacking Sox10 fail to form Schwann cells [8,156]. Together with Oct6, Sox10 regulates progression of immature Schwann cells to the promyelinating stage by inducing the expression of *Krox20/Egr2*[157]. Sox10 expression is maintained in myelinating Schwann cells; immature Schwann cells express Sox10, but not Krox20[157]. Schwann cells lacking Krox20 fail to form myelin[17,158], and late myelin genes, such as P0 and MBP, are not expressed by *Krox20*-null Schwann cells[159]. After nerve injury, *Krox20* is down regulated, while other transcription factors, such as *c-Jun* and *Egr1/Krox24,* are induced[157,160].

At P21, the number of $Krox20^+$ nuclei per μm^2 is not significantly different in $Vps34^{SCKO}$ and wild type nerves (Fig. 3.4A *and not shown*), indicating that mutant Schwann cells transition to the myelinating phenotype efficiently. However, $Vps34^{SCKO}$ nerves show a 10-fold increase in the number of $Sox10^+$ cells that lack Krox20 expression (Fig. 3.4A *and not shown*). In wild type nerves, only about 10% of Schwann cells are immature ($Sox10^+$, $Krox20^-$); most are myelinating cells that express both Sox10 and Krox20 (Fig. 3.4A,B). However, $Sox10^+$, $Krox20^-$ cells account for over 40% of the Schwann cells present in $Vps34^{SCKO}$ nerves (Fig. 3.4A,B). Thus, while *Vps34*-null Schwann cells are capable of differentiation and the initiation of myelination, these cells are unable to complete and maintain a myelin sheath.

Autophagic and endosomal abnormalities in Schwann cells lacking Vps34

By generating PI3P, Vps34 plays a critical role in both endosomal trafficking and the initiation of autophagy [62,64]. To evaluate the status of the autophagic pathway in

Vps34^{SCKO} sciatic nerves, we examined the levels of the LC3 and p62/SQSTM1 proteins. When autophagy is activated, proLC3 is proteolytically processed to generate the LC3-I isoform, which is subsequently coupled to phosphatidylethanolamine to yield the membrane-associated LC3-II isoform [161]. LC3-II binds to the growing autophagosome membrane, and is therefore an indicator of the number of autophagosomes[161]. We examined the steady state levels of LC3-I and LC3-II in sciatic nerves at P3, P7, P21, and P56. At P3, the LC3-I and LC3-II levels in*Vps34*^{SCKO} sciatic nerves were indistinguishable from those of controls (Fig. 3.5A). However, by P7 the level of both LC3-I and -II was increased by about 60% in *Vps34*^{SCKO} nerves (Fig. 3.5B). Increased LC3 levels may indicate either a higher basal rate of autophagy initiation, with increased generation of autophagosomes, or a block of autophagosome maturation and the completion of autophagy[161]. p62 (SQSTM1) is a cargo receptor which promotes the degradation of ubiquitinated proteins by the autophagosome[162]. We observed elevated levels of p62 in the nerves of *Vps34*^{SCKO} mice beginning at P7 (Fig. 3.5A), suggesting a defect in autophagic protein degradation[161]. *Vps34*^{SCKO} mice older than 7 days also showed elevated levels of LC3-I/II and p62 in sciatic nerves (Fig. 3.5C,D). The observed increases in LC3-I/II and p62 indicate that the loss of Vps34 in Schwann cells leads to defective autophagic flux, which may begin to impair myelination and axon survival after day 3.

PI3P production by Vps34 also plays a key role in endosomal/lysosomal membrane traffic in many eukaryotic cells types[144,163,164,165]. To assess the importance of Vps34 function for endosomal traffic in Schwann cells, we compared the levels of the early and late endosomal/lysosomal proteins in the nerves of wild type and *Vps34*^{SCKO} mice. The Rab5 effector early endosome antigen 1 (EEA1) binds to PI3P and facilitates homotypic fusion of early endosomes, a process essential for trafficking[166,167]. Lysosomal-associated membrane protein 1 (LAMP1) is integral to

late endosomes and lysosomes and can be used to assess the abundance and morphology of these membranes. At P3, EEA1 and LAMP1 levels were similar in wild type and *Vps34*^{SCKO} sciatic nerves (Fig. 3.5A). In contrast, mutant nerves analyzed at day 7 contained significantly elevated levels of LAMP1 (Fig. 3.5B), a trend that continued at P21 and P56 (Fig. 3.5C,D). EEA1 levels were also significantly elevated in *Vps34*^{SCKO} nerves examined at P21 and P56 (Fig. 3.5C,D). These data indicate that loss of Schwann cell Vps34 triggers an expansion of endosomal and lysosomal membranes, which is first evident at P7, a time of active developmental myelination.

Elimination of PI 3-kinase isoforms that generate PI3P does not alter myelin abnormalities associated with loss of PI 3-phosphatases

It remains unclear how the balance of PI 3-kinase and 3-phosphatase activities maintains appropriate levels of PI3P, particularly in specialized mammalian cell types (Fig. 3.6)[168]. Given the human genetic data indicating that the regulation of PI3P and $PI(3,5)P_2$ is critical for myelination[42,47,83,120], we considered whether abnormalities caused by loss of the PI 3-phosphatase MTMR2, or the associated pseudophosphatase MTMR13, might be ameliorated by reducing the activity of the relevant PI 3-kinase(s) in Schwann cells (Fig. 3.6). It is predicted that CMT4B-causing, *loss of function* mutations in *MTMR13* or *MTMR2* may lead to pathogenic elevation of PI3P in Schwann cells[169]. We therefore investigated whether reducing PI3P levels in *Mtmr13*$^{-/-}$ Schwann cells would reduce the severity of the myelin abnormalities (outfoldings) characteristic of CMT4B, presumably by normalizing endosomal trafficking or other cellular functions. To do so, we generated *Mtmr13*$^{-/-}$ *Vps34*^{SCKO} mice and compared the nerves of these animals to those from *Mtmr13*$^{-/-}$ mice. When examined at day 3, sciatic nerves from *Mtmr13*$^{-/-}$ and *Mtmr13*$^{-/-}$ *Vps34*^{SCKO} mice showed a similar frequency of myelin

outfoldings (~12%) (Fig. 3.7A,B). Consistently, myelin outfoldings were observed at a similar frequency when *Mtmr13*$^{-/-}$ and *Mtmr13*$^{-/-}$ *Vps34*^{SCKO} nerves were compared at P18 (Fig. 3.7A,B). This finding suggests that, in Schwann cells, Vps34 is not responsible for generating a pool of PI3P that is dephosphorylated by the Mtmr2-Mtmr13 phosphatase complex.

In addition to Vps34, the class II PI 3-kinases are candidates for the enzymes that generate PI3P in Schwann cells[142]. Therefore, we considered whether PI3K-C2β might be responsible for generating a pool of PI3P targeted by MTMR phosphatases. To test this, we generated *Mtmr13*$^{-/-}$ *Pik3c2β*$^{-/-}$ mice and compared the nerve pathology of these animals to that of *Mtmr13*$^{-/-}$ mice. To assess myelin outfoldings, we analyzed 8-month old mouse sciatic nerves, and found that there was no change in the prevalence of myelin outfoldings (Fig. 3.8A,B). PI3K-C2β appears to be dispensable for myelination and nerve development (Fig. 3.8A). To confirm that *Pik3c2β* deletion does not impact myelin outfoldings in younger mice, we examined nerves from 2-month-old mice, again finding no significant difference in the prevalence of myelin outfoldings (Fig. 3.8A,B). Thus, genetic elimination of Vps34 or PI3K-C2β, two manipulations that lower PI3P levels, has no impact on the prevalence of myelin outfoldings in *Mtmr13*$^{-/-}$ mice, a model of CMT4B dysmyelination.

Discussion

We sought to determine the role of the class III PI3K Vps34 in myelinating Schwann cells, and test whether we could alter MTMR13-related myelin outfoldings by manipulating PI3K expression. We found that although Vps34 plays a critical role in myelination, we were unable to alter myelin outfoldings by crossing *Vps34*^{SCKO} mice with *Mtmr13*$^{-/-}$ mice. To determine whether PI3K-C2β depletion would impact myelin

outfoldings we also made *Mtmr13*$^{-/-}$ *Pik3c2β*$^{-/-}$ mice and found that lowering PI3P levels through *Pik3c2β* knockout again had no effect.

Using our *Vps34*^{SCKO} mouse model, we found that Schwann cells lacking Vps34 are able to proliferate adequately to support the initiation of myelination. At P3, we saw no myelin abnormalities in *Vps34*^{SCKO} nerves. By P7, however, *Vps34*-null Schwann cells were no longer able to maintain wild type levels of myelination. There was a decrease in the number of axons greater than 1 μm in *Vps34*^{SCKO} nerves, likely due to incomplete radial sorting (Fig. 3.3D,E), and the percentage of axons myelinated was significantly decreased (*data not shown*). At P21 and P56, significant hypomyelination was observed in *Vps34*^{SCKO} nerves.

We found a striking increase in Sox10-positive cells in P21 *Vps34*^{SCKO} nerves, but no change in Krox20 expression. The large increase in Sox10-positive cells in this mouse line could be due, in part, to the state of P21 nerves. Morphological analysis of the sciatic nerve at P21 shows there is loss of axons ≥1 μm in diameter, due to incomplete radial sorting, most Schwann cells are highly vacuolated (Fig. 3.2). In a peripheral nerve injury state, Schwann cells are able to switch off their myelination program, re-enter the cell cycle and divide, and adopt a phenotype that is reminiscent to immature Schwann cells[160]. P21 *Vps34*^{SCKO} nerves could therefore be similar to a nerve injury state, where Schwann cells are de-differentiating and proliferation, causing an increase in Sox10-positive Schwann cell nuclei in *Vps34*^{SCKO} sciatic nerves.

Vps34 is a critical regulator of vesicular trafficking events including endosomal trafficking and autophagy[62]. We found that Vps34 in the Schwann cell is critical in both the endosomal-lysosomal system and in regulating autophagy, but not until after day 3, when the demands of myelination are substantial. At P3, endosomal and autophagic protein levels in *Vps34*^{SCKO} nerves are similar to wild type levels. By P7, however, we see increased expression of the endosomal and lysosomal proteins EEA1 and LAMP1

and autophagy-related proteins by Western blotting *Vps34*^{SCKO} sciatic nerve lysates. These changes persist into adulthood in *Vps34*^{SCKO} sciatic nerves, suggesting that Vps34 in Schwann cells contributes to both the endosomal-lysosomal and autophagic pathways.

In yeast, loss of Vps34 is lethal, but the role of Vps34 in specialized mammalian cells appears to be significantly more complicated. For example, the cellular defects of *Vps34*-null liver and heart tissue can be partially explained by defective autophagy, because aspects of the phenotype are identical to *Atg5*- or *Atg7*- (two proteins required for the initiation of autophagy) knockout mice[146]. However, the resulting phenotype in *Vps34*-null hepatocytes and cardiomyocytes is more severe than *Atg5*- or *Atg7*-knockouts alone. This indicates that loss of autophagy-independent functions of Vps34, such as endosomal trafficking and endocytosis[146], are contributing to the *Vps34* knockout phenotype. In contrast, studies performed in T lymphocytes show that Vps34 is completely dispensable for autophagy, but is critical in regulating T cell homeostasis by modulating IL-7R trafficking, signaling, and recycling[147]. No autophagy defects were found in *Vps34*-null T lymphocytes, suggesting that Vps34 is not required for autophagy initiation in this cell type. Additional studies have been performed in a variety of specialized mammalian cell types, and findings from autophagy being severely affected to not affected at all have been reported, and disruptions in the endosomal pathway have been both reported and not[145,146,147,148,149,150,151]. A Schwann cell-specific deletion of the autophagy gene *Atg7* was reported to have minor myelin defects compared to our *Vps34*^{SCKO} mice[170]. Therefore, we conclude that the phenotype of *Vps34*^{SCKO} mice is due to a combination of dysfunction of both the autophagic and endosomal pathways, however the myelination abnormalities are likely due to dysfunction of the endosomal pathway since *Atg7* knockout mice do not exhibit myelination defects.

Studies performed in cultured MEF cells have quantified the contribution of Vps34 and the class II PI3Ks, PIK3-C2α and PIK3-C2β, to PI3P production[73]. In control cells treated with class II PI3K shRNAs (to both C2α and C2β), a 20% decrease of PI3P levels was observed[73]. Additionally, *Vps34*$^{-/-}$ MEF cells had only one third the amount of PI3P as control cells, indicating that Vps34 makes the bulk of PI3P in MEF cells[73]. From these studies it was determined that the contribution of Vps34 and class II PI3Ks to total PI3P levels are additive and non-compensatory. Therefore, we hypothesized that the class II PI3Ks may be contributing to PI3P production in Schwann cells, making PI3K-C2β a valid kinase to study.

We asked if lowering Schwann cell PI3P levels, by *Vps34*- or *Pik3c2β*-knockout, in a CMT4B2 model (*Mtmr13*$^{-/-}$) could improve dysmyelination. We found that neither kinase was able to change the prevalence of myelin outfoldings in *Mtmr13*$^{-/-}$ mice. However, there are other sources of PI3P in the cell that have not been ruled out, including type I and II 4-phosphatases that dephosphorylate PI(3,4)P_2 to PI3P[171]. There could also be PI3Ks compensating; when one kinase is removed, another PI3K could be upregulated. The fact that neither *Vps34*- nor *Pik3c2β*-knockout impacted the prevalence of myelin outfoldings could also suggest that there are different pools of PI3P in the Schwann cell, and that PI3Ks may act on distinct pools of PI3P in Schwann cells.

Our study highlights the critical role PIs play in myelinating glial cells, and the complexity of PI regulation in Schwann cells. The PI3K Vps34 has a critical role in completion of myelination, as loss of expression is detrimental to the sciatic nerve. The pool of PI3P Vps34 catalyzes is involved in completion of myelination and maintenance of a myelin sheath. This pool of PI3P, however, does not appear to be the pool that is dysregulated with loss of Mtmr13. PI3K-C2β also does not appear to be responsible for catalyzing the bulk of PI3P that is related to Mtmr13 outfoldings, but interestingly is dispensable for myelination, since loss *Pik3c2β* does not cause any myelin or sciatic

nerve abnormalities (Fig. 3.7C and *data not shown*). Future studies will allow us to conclude which PIs and which specific subcellular pools of PIs are dysregulated in *Mtmr13*$^{-/-}$ mouse models of CMT, as well as which kinases are responsible for making these pools of PIs, with implications towards treating CMT patients in the future.

Materials and Methods

Schwann cell specific inactivation of Vps34

The mouse *Pik3c3* (*Vps34*) gene consists of 25 exons strung over about 75 kilobases (kb) of DNA on the forward strand of chromosome 18 (Gene: *Pik3c3* ENSMUSG00000033628). The corresponding mRNA transcript of 3102 base pairs (bp) (NM_181414.5, Transcript: Pik3c3-001 ENSMUST00000115812 – 3257 bp) encodes a protein of 887 amino acids (aa) (NP_852079.2). All 25 exons associated with the above referenced mRNA transcript code for protein. *Pik3c3/Vps34*$^{flox/flox}$ mice were a generous gift from Fan Wang. This line of mice contains an engineered allele of *Pik3c3* in which exons 17 and 18, which encode the ATP binding sequences of the kinase, are flanked with *loxP* sites[145]. In the presence of Cre recombinase, exons 17 and 18 are removed and the Vps34 protein is not expressed[73,145]. Genotyping of *Vps34*$^{flox/flox}$ mice was carried out using by PCR (40 cycles) using primers ALO-18 (Vps34 F; GCCACCCATTGCTGCCT) and ALO-21 (Vps34 R; CCCTCACTGGCTGTGGC) and genomic (g) DNA from mouse tails. These primers amplify bands of 291 and 251 base pairs (bp), respectively, when wild type and *floxed Vps34* alleles are present. To generate mice with a Schwann cell-specific deletion of *Vps34, Vps34*$^{fl/fl}$ mice were crossed with mP$_0$TOTA(Cre) (P0-Cre) transgenic mice[152,172]. The P0-Cre transgene was detected by PCR with oligonucleotides ALO-5 (P0-F; CACCACCTCTCCATTGCAC) and ALO-6 (P0-R; GCTGGCCCAAATGTTGCTGG). *Vps34*$^{fl/fl}$ mice were previously found

to be indistinguishable from wild type mice[145]. Control mice, referred to as wild type, were either *Vps34*$^{fl/fl}$ (*P0-Cre*$^{-}$) or *Vps34*$^{+/fl}$ (*P0-Cre*$^{-}$) littermates of *Vps34*$^{fl/fl}$ *P0-Cre*$^{+}$ (*Vps34*^{SCKO}) mutant mice. *Mtmr13*$^{-/-}$ mice have been described previously[72,173]. All work with animals was approved by and conformed to the standards of the Oregon Health & Science University Institutional Animal Care and Use Committee.

Generation of Pik3c2β$^{-/-}$ and Mtmr13$^{-/-}$Pik3c2β$^{-/-}$ mice

Pik3c2β$^{+/fl}$ mice [174] were obtained from the Jackson Laboratory (Strain: B6.129-Pik3c2btm1Pkha/J). To generate a *null* allele of PI3K-C2β, *Pik3c2β*$^{+/flox}$ mice were crossed with *CMV-Cre* mice (Jackson Laboratory strain B6.C-Tg[CMV-cre]1Cgn/J). The resulting *CMV-Cre*$^{+}$*; Pik3c2β*$^{+/flox}$ progeny were crossed with C57BL/6 mice to accomplish germ line deletion of *floxed Pik3c2β* exons 3-5. *Pik3c2β*$^{+/\Delta}$ progeny were intercrossed to generate *Pik3c2β*$^{\Delta/\Delta}$ mice, which were subsequently crossed with *Mtmr13*$^{-/-}$ mice (N8 on C57BL/6) to yield *Pik3C2β*$^{+/\Delta}$; *Mtmr13*$^{+/-}$ double heterozygotes, which were then intercrossed to generate *Pik3c2β*$^{\Delta/\Delta}$*Mtmr13*$^{-/-}$ mice. A three-primer PCR reaction using oligonucleotides EJS-003 (GGCACACACTAACCACAGCACC), EJS-004 (TCGATGCACGTCTCTCCGC) and EJS-005 (ACACTGGGGTGAGCTGAGCTAGG) was used to genotype mice for *Pik3c2β*. Using these primers, the wild type, *floxed* and deleted (*Δ*) alleles of *Pik3c2β* yield PCR products of 568, 618 and 404 bp, respectively.

Morphology

Adult mice were perfused with electron microscopy (EM) fixative (1.5% glutaraldehyde, 1.5% PFA, 0.05 M sucrose, 0.25% $CaCl_2$, 0.1 M sodium cacodylate buffer [pH 7.4]). Sciatic nerves were dissected and further fixed overnight. To examine myelin morphology of P3 and P7 mice, pups were euthanized and sciatic nerves dissected and fixed in EM fixative overnight at 4°C. Ultra-thin (70 nm) EM sections and

semi-thin (1 μm) toluidine blue stained plastic cross-sections were prepared from the mid-sciatic nerve. EM images were acquired using a FEI Tecnai 12 Biotwin transmission electron microscope at 80 kV. Toluidine blue sections were imaged at 63x on a Zeiss ApoTome microscope. Two cross sections of the sciatic nerve (one each from the left and right nerve) were analyzed per mouse, and 4-7 mice of each genotype were analyzed at each time point. The pixel size of acquired images was 0.086 μm^2 and images were calibrated accordingly. The entire sciatic nerve cross-section was imaged using a tiling function and the acquired images were stitched together using Zen Blue software (Zeiss), and subsequently analyzed using MetaMorph software.

Toluidine blue stained cross-sections were used to determine g ratio by measuring the axonal circumference and dividing that number by the circumference of the outer edge of the myelin sheath. The diameter of each corresponding axon was found by dividing axon circumference by π, and the data points were plotted as a scatter plot of axon diameter (μm) versus g ratio. For g ratio analysis, axons from throughout the entire nerve cross-section were sampled. In each cross section analyzed, 50 round axons were measured (100 total per mouse). In P3 nerves, g ratio on all possible round, myelinated axons was measured (60-100 axons per mouse).

For total axon counts, toluidine blue stained cross sections were analyzed. At P56, four cross sectional areas (2 each from the left and right nerve) of 100 μm^2 per animal were analyzed (4-5 animals of each genotype). Images were calibrated using the pixel dimensions indicated above, and axons ≥1 μm in diameter and in a 1:1 relationship with a Schwann cell were counted, whether myelinated or not. For P56, about 20-28% of the entire transverse fascicular area (TFA) was counted. For P21 axon counts, total axons ≥1 μm in ~30% of the entire TFA were counted for each mouse (n = 4) on two cross sections (left and right sciatic nerve). For axon counts in P3 and P7 mice, the entire TFA was counted in 4-7 mice per genotype. Every axon that was in a 1:1

relationship with a Schwann cell was counted in two cross-sections (right and left sciatic nerve), and the average of the two sections was calculated. The total fascicular area (TFA; in μm^2) was determined for all nerves analyzed using MetaMorph software.

An additional analysis of total large caliber axon number at P7 was performed using EM images (890x magnification; 8-16 images per animal). The total number of axons in 1:1 relationships with Schwann cells (myelinated or not) was determined. In wild type mice at P7, nearly all axons in 1:1 relationships with Schwann cells are ≥1 μm in diameter. As a single 890x EM image captured a nerve area of 2457 μm^2, analysis of 8-16 such images resulted in 26-62% of the TFA being analyzed per mouse. On average, 42% of the TFA was analyzed for each mouse (n = 5 for wild type; n = 4 for *Vps34*^{SCKO}). Once the axon count for a significant fraction of the nerve was established, this number was scaled based on total nerve area to generate a predicted total axon count for the nerve.

For analysis of myelin outfoldings at P18, four 50 μm^2 areas of the nerve (8-13% of the entire TFA) for each animal were counted for axons containing a myelin outfolding/infolding and total myelinated axons (n = 5). For analysis of myelin outfoldings at P3, five EM images (890x; 63 μm X 39 μm), from each mouse were counted for the number of outfolding/infoldings and total myelinated axons, and subsequently averaged (n = 4). On average, about 35% of the total TFA was analyzed per P3 nerve section. Sciatic nerve morphology analysis of *Mtmr13*$^{-/-}$ *Pik3c2β*$^{-/-}$ mice was as described previously (Ng et al., 2013).

For analysis of bundles of axons at P7, EM images of 890x magnification were analyzed. A bundle was defined as any assortment of axons in contact with, but not in a 1:1 relationship with a Schwann cell. The area of the axonal portion of the bundle was measured; the area of the associated Schwann cell nucleus, cytoplasm and any significant processes was excluded. An average of 74 bundles were measured per

mouse (5 wild type and 4 *Vps34*^{SCKO} mice). The number of large caliber axons per bundle was also determined in P7 sciatic nerves. An average of 30 bundles per mouse were analyzed from five wild type and four *Vps34*^{SCKO} mice. A large caliber axon was defined as such if the average of long and short axes was above 1 μm and the smallest measure was above 0.35 μm.

Rotarod test

Six to seven week old male and female (no significant difference between the sexes was detected) mice were placed on an elevated, accelerating rotating rod (Economex model 0207-003M, Columbus Instruments; rod diameter, 7 cm; elevated 45 cm), which began rotating at 5 rpm at the start of the test. The rotation speed of the rod accelerated at a rate of 0.5 rpm/sec and the latency to a fall in seconds was recorded. Each mouse underwent three trials per day, with no delay between trials, on three consecutive days. On the 3rd day, the 3 trials were averaged and plotted on a bar graph (n = 5 wild type; n = 13 for *Vps34*^{SCKO}*).*

Immunofluorescence

P21 mice were perfused with 4% paraformaldehyde (PFA) and nerves were post-fixed in 4%PFA/4% sucrose in phosphate buffered saline (PBS) for 30 minutes. Nerves were placed in 10% sucrose in 0.1M phosphate buffer (PB), pH 7.5 overnight at 4°C. The solution was changed to 30% sucrose in 0.1M PB, pH 7.5 the following day, and stored at 4°C. Nerves were snap frozen in Optimal Cutting Temperature compound in a dry ice/isopentane bath and stored at -80°C. Longitudinal sections (10 μm) were cut on a cryostat and examined by immunofluorescence. Slides were rinsed once in PBS, permeabilized in 0.2% Triton X-100 for 15 minutes at room temperature and washed again in PBS. Nerve sections were blocked for 1 hour at room temperature in 10%

normal goat serum (NGS) in PBS. Primary antibodies (guinea pig anti-Sox10, a gift from Dr. Michael Wegner, and rabbit anti-Krox20 [Covance]) were diluted in 2% NGS in PBST (PBS with 0.1% Tween-20) and incubated overnight at 4°C. Slides were washed 3 times in PBST, secondary antibodies (Jackson ImmunoResearch) were added in 2% NGS in PBST, and incubated for 1 hour at room temperature. Finally, slides were washed 3 times in PBST, stained with 4',6-diamidino-2-phenylindole (DAPI), and cover slips were applied using Elvanol. Images were acquired on Zeiss Apotome microscope using the tiling function (as described above) to image the entire nerve. Krox20-positive nuclei, Sox10-positive nuclei, and total nuclei (DAPI-positive) were counted in 7-8 entire nerve sections from each mouse (both left and right nerve) from 2 mice from each genotype. The area of the entire nerve was determined using MetaMorph to allow for calculation of the number of nuclei/μm^2.

Immunoblotting

Immunoblotting of sciatic nerve and brain extracts were performed as previously described[173]. Antibodies used were rabbit polyclonal anti-MAG and anti-p62 (Santa Cruz Biotechnology), rat monoclonal anti-MBP and rabbit monoclonal anti-NF-L (Millipore), rabbit monoclonal anti-Vps34 and anti-EEA1 (Cell Signaling Technology), rat monoclonal anti-Lamp1 (1D4B) and mouse monoclonal anti-β-tubulin (E7) (Developmental Studies Hybridoma Bank), and rabbit polyclonal anti-LC3 (Novus Biologicals). Sciatic nerve and brain extracts were prepared as previously described[173]. For each P3 and P7 nerve lysate, three mice of the same genotype (6 nerves total) were pooled. For P21 and P56, a single mouse was used (2 nerves) for each lysate. Each time point/antibody combination was run in triplicate (3 lysates per genotype per time point). 20-25 µg of protein per lane was resolved in 4-12% NuPAGE

Bis-Tris gels (Invitrogen), and chemiluminescent quantitation of immunoblots was as previously described[173].

Statistics

Prism 6 was used for all statistical analyses.

Acknowledgements

The authors wish to thank Aurelie Snyder and Stefanie Kaech Petrie of the Advanced Light Microscopy Core at The Jungers Center for Neurosciences Research for their expert advice in imaging and analyzing nerve morphology. The authors also wish to thank Melissa Williams, Sue Aicher, Lisa Dirling Vecchiarelli, and Robert Kayton for assistance with electron microscopy. Melissa Williams was invaluable in the processing and imaging of the sciatic nerves for morpohology analysis. The Sox10 antibody was a generous gift from Dr. Michael Wegner, the Vps34-floxed mice were a gift from Dr. Fan Wang, and the P0-cre line was generously given to us by Dr. Laura Feltri. The 1D4B (LAMP-1) and E7 (β-tubulin) monoclonal antibodies, developed by Drs. J. Thomas August and Michael Klymkowsky, respectively, were obtained from the Developmental Studies Hybridoma Bank developed under the auspices of the National Institutes of Health-National Institute of Child Health & Human Development and maintained by The University of Iowa, Department of Biology, Iowa City, IA 52242.

Figures and Legends

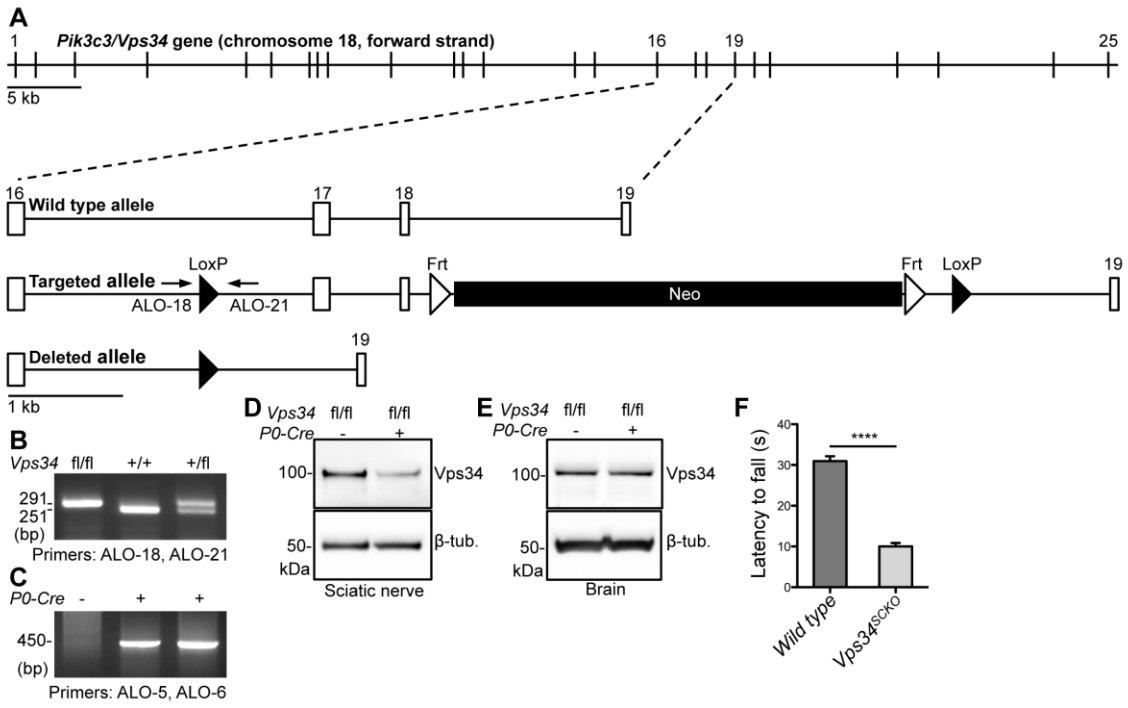

Figure 3.1. Schwann cell-specific deletion of *Pik3c3/Vps34*. (**A**) A schematic representation of the mouse *Pik3c3/Vps34* gene and conditional deletion allele[145]. The positions of oligonucleotide primers used for PCR genotyping are indicated. Schwann cell-specific expression of *Cre* Recombinase from the *P0-Cre* transgene (*Tg*) triggers deletion of *Pik3c3/Vps34* exons 17 and 18, as well as the neomycin expression cassette. (**B**) PCR genotyping of $Vps34^{fl/fl}$, wild type, and $Vps34^{+/fl}$ mice. The presence of the *LoxP* site results in a 45 base pair (bp) increase in the size of the ALO-18, ALO-21 PCR product. (**C**) Detection of *P0-Cre* transgene (Chromosome 15) via PCR with primers ALO-5 and ALO-6. (**D**) Immunoblot analysis of Vps34 protein abundance in sciatic nerve extracts from $Vps34^{fl/fl}$ (wild type) and $Vps34^{fl/fl};P0\text{-}Cre^{+}$ ($Vps34^{SCKO}$) mice at P56, using an antibody specific for the amino terminus of Vps34. Arbitrary Vps34 protein levels: 100

± 14.22% in *Vps34*$^{fl/fl}$ vs. 37 ± 4.07% in *Vps34*$^{fl/fl}$*;P0-Cre*$^{+}$, p = 0.01, n = 3 mice per genotype. Vps34 levels are normalized to β-tubulin and wild type mean was set to 100%. (**E**) Immunoblot analysis of brain extracts from *Vps34*$^{fl/fl}$ (wild type) and *Vps34*$^{fl/fl}$*;P0-Cre*$^{+}$ (*Vps34*^{SCKO}) mice at 14 weeks (n = 3 mice per genotype). In the brain, there was no significant change in Vps34 protein levels. (**F**) Rotarod testing of wild type and *Vps34*^{SCKO} mice was carried out at 6-7 weeks on an accelerating Rotarod. The average time to fall (in seconds [s]) was determined for each mouse. The average time to fall was 30.95 ± 1.2 s for wild type (n = 13 mice) vs. 10.00 ± 0.86 s for *Vps34*^{SCKO} (n = 5 mice) (****p < 0.0001). The data are presented as mean ± SEM; unpaired t tests were used to evaluate significance.

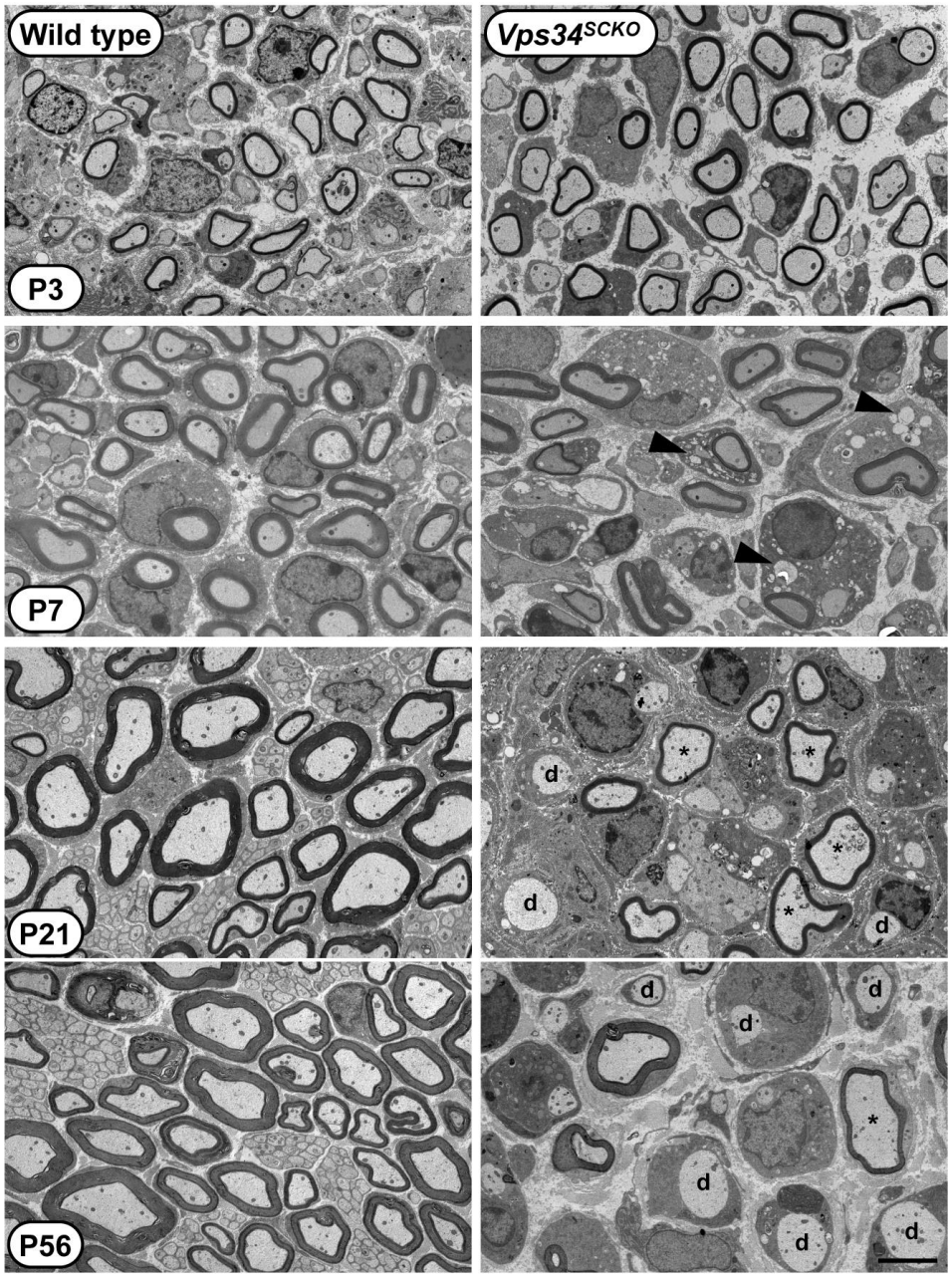

Figure 3.2. Abnormal myelination following deletion of *Vps34* in Schwann cells. EM analysis of mid-sciatic nerve cross sections of wild type and *Vps34*^{SCKO} mice at P3, P7, P21, and P56. At P3, the morphology of *Vps34*^{SCKO} nerve appears normal compared to wild type controls (n = 7 mice per genotype). By P7, nerve pathology is evident, including slight hypomyelination, loss of axons greater than 1 μm, and vacuoles in the

Schwann cytoplasm (*black arrowheads*) (n = 4 or 5 mice per genotype). At both P21 and P56, nerve pathology worsens; severe axon loss, hypomyelination (*asterisk*), and demyelination (*d*) are evident (n = 4 or 5 mice per genotype). Scale bar: 4 μm.

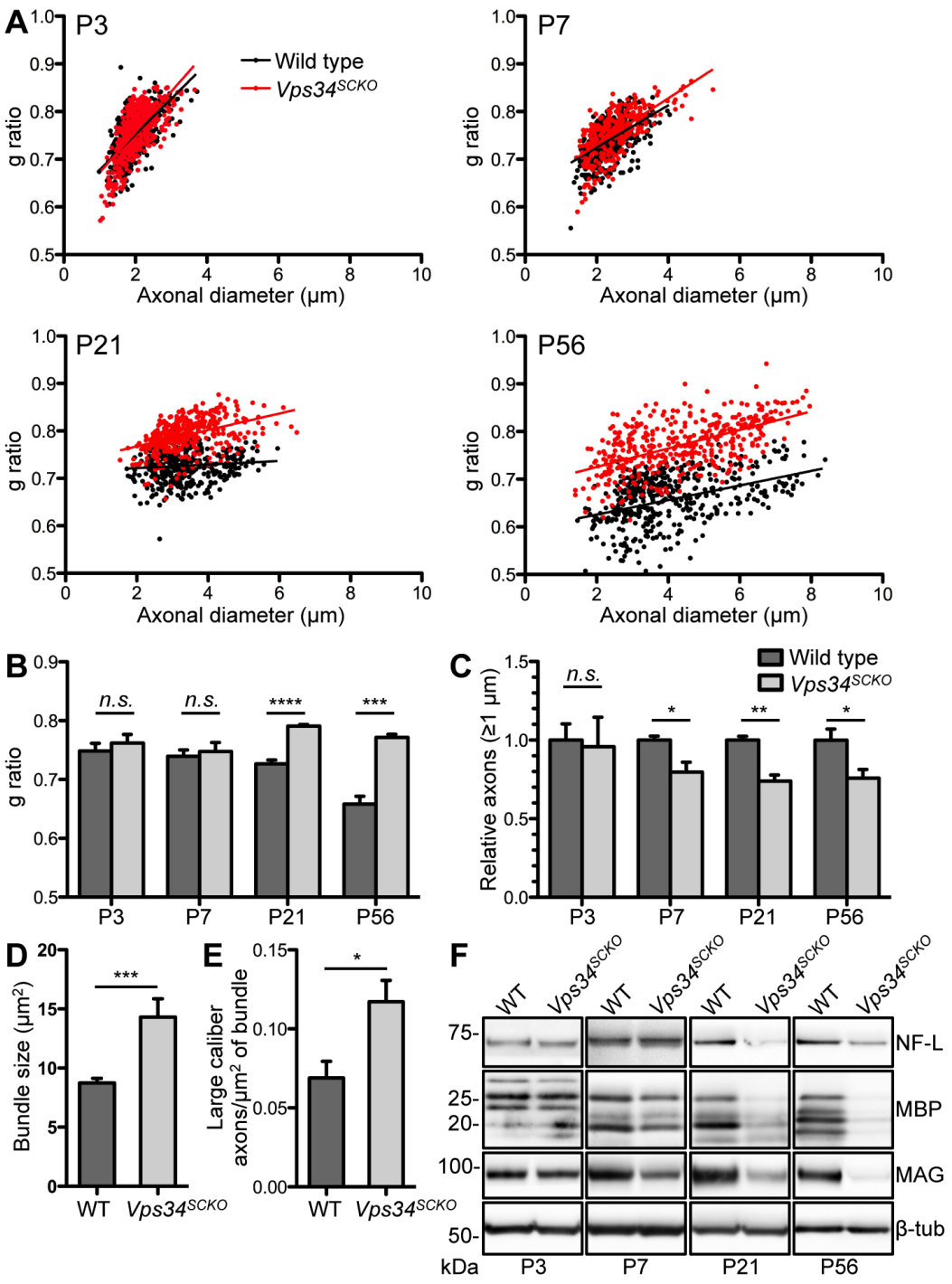

Figure 3. Schwann cells lacking Vps34 fail to complete myelination. (**A**) G ratio analysis of myelin thickness in wild type and *Vps34*^{SCKO} sciatic nerves, evaluated at P3, P7, P21, and P56. 100 myelinated axons per mouse were measured, and the g ratio is

plotted versus axonal diameter (μm), with the best-fit line shown. (**B**) Average g ratios. At P3 and P7 there is no significant difference in average g ratio between wild type and *Vps34*^{SCKO} mice. P3 average g ratio: 0.75 ± 0.013 for wild type vs. 0.76 ± 0.015 for *Vps34*^{SCKO} (n = 7 mice). P7 average g ratio: 0.74 ± 0.011 for wild type vs. 0.75 ± 0.015 for *Vps34*^{SCKO} (n = 4-5 mice). At both P21 and P56, there is a significant increase in the average g ratio of *Vps34*^{SCKO} mice, indicating hypomyelination. P21 average g ratio: 0.73 ± 0.006 for wild type vs. 0.79 ± 0.003 for *Vps34*^{SCKO} (n = 4 mice). P56 average g ratio: 0.66 ± 0.013 for wild type vs. 0.77 ± 0.005 for *Vps34*^{SCKO} (n = 4-5 mice). (**C**) The relative number of large caliber axons (≥1 μm) axons in a 1:1 relationship with a promyelinating Schwann cell, whether myelinated or not, was analyzed in wild type and *Vps34*^{SCKO} sciatic nerves. The mean wild type relative axon number for each age group is normalized to 1. At P3, the number of axons in *Vps34*^{SCKO} nerves is not significantly different from that of the wild type. Relative axons: 1.00 ± 0.1029 for wild type vs. 0.9587 ± 0.1865 for *Vps34*^{SCKO} (P = 0.8494; n = 7 mice). At P7, a significant reduction in axons in 1:1 relationships with Schwann cells is observed in *Vps34*^{SCKO} sciatic nerves. Relative axons: 1.000 ± 0.02509 for wild type vs. 0.7965 ± 0.06279 (n = 4-5 mice). Similar reductions in the relative proportions of axons in 1:1 relationships with Schwann cells are observed in *Vps34*^{SCKO} nerves at P21 and P56. P21 relative axons: 1.000 ± 0.02461 for wild type vs. 0.7399 ± 0.03790 for *Vps34*^{SCKO} (n = 4 mice). P56 relative axons: 1.000 ± 0.07082 for wild type vs. 0.7583 ± 0.05520 for *Vps34*^{SCKO} (n = 4-5 mice). (**D**) Increased bundle size in *Vps34*^{SCKO} nerves at P7 (n = 4-5 mice). **(E)** Increased number of large caliber axons (≥ 1 μm) per μm^2 of bundle area in *Vps34*^{SCKO} nerves at P7 (n = 4-5 mice). (**F**) Immunoblot analysis of myelin and axonal proteins in sciatic nerves of wild type and *Vps34*^{SCKO} mice. For all four ages, n = 3 lysates per genotype. The level of NF-L is not significantly changed in *Vps34*^{SCKO} nerves analyzed at P3 or P7. However, by P21, NF-L protein abundance is significantly decreased in *Vps34*^{SCKO} nerves. At P3, the levels of

the myelin proteins MBP and MAG are similar in wild type and *Vps34*^{SCKO} nerves. By P7, mutant nerves contain slightly reduced levels of MBP and a significant decrease in the abundance of MAG. Both MBP and MAG levels are significantly reduced at P21 and P56. The data are presented as mean ± SEM; unpaired t tests were used to evaluate significance (*n.s.*, not significant; **p < 0.01; ***p < 0.001; ****p < 0.0001).

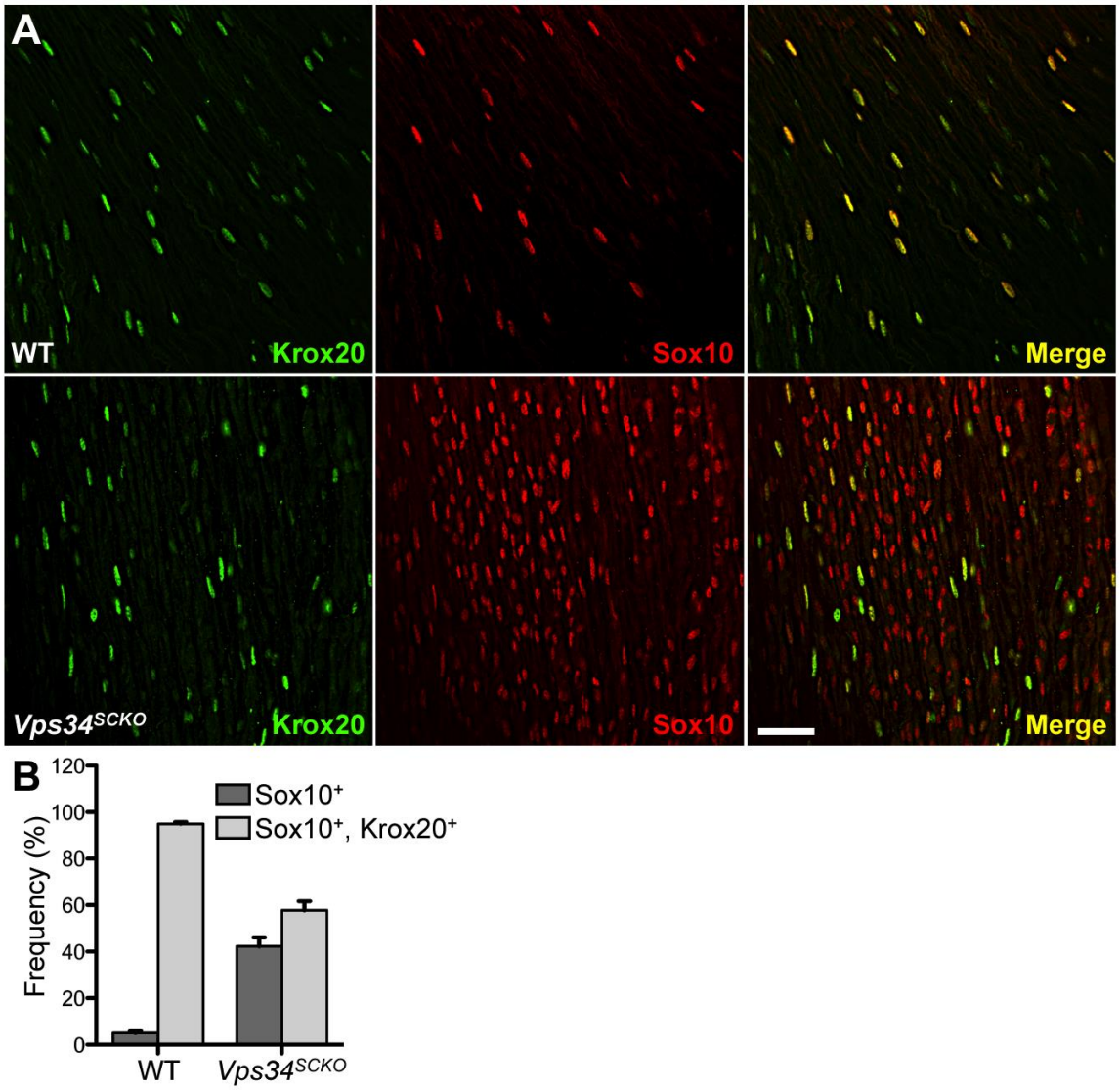

Figure 3.4. Loss of Vps34 does not impact Schwann cell differentiation. (**A**) Longitudinal sections of sciatic nerves of P21 wild type (*upper*) and *Vps34*^{SCKO} (*lower*) mice were examined by immunofluorescence with antibodies for Krox20 (*green*) and Sox10 (*red*). The number of Krox20-positive nuclei/μm^2 is not significantly different between wild type and *Vps34*^{SCKO} nerves ($p = 0.29$, n = 7-8 whole nerve sections per genotype, 2 animals per genotype), indicating that Schwann cell differentiation to the myelinating phenotype is unimpaired. The number of Sox10-positive nuclei/μm^2 is increased about 9-fold in *Vps34*^{SCKO} sciatic nerves (0.0001 ± 0.00004 for wild type vs.

0.0011 ± 0.0004 for *Vps34*^{SCKO}, p = 0.0335, n = 7-8 whole nerve sections per genotype, 2 animals per genotype). (**B**) The percentage of Sox10^{+} versus Sox10^{+}Krox20^{+} Schwann cells at P21 in wild type and *Vps34*^{SCKO} nerves is graphed. In wild types, most Schwann cells are mature, myelinating cells expressing Krox20. Only 5.03 ± 0.76% of the wild type nerve Schwann cells express Sox10 alone. However, in *Vps34*^{SCKO} nerves, 42.23 ± 3.9% of the total Schwann cells are immature, expressing Sox10 alone. Although the number of cells expressing Krox20 is not decreased in *Vps34*^{SCKO} nerves, this large increase in Schwann cells expressing only Sox10 indicates that there is a large population of immature, possibly de-differentiated, Schwann cells in the *Vps34*^{SCKO} sciatic nerve. Scale bar: 40 μm. The data are presented as mean ± SEM; unpaired t tests were used to evaluate significance.

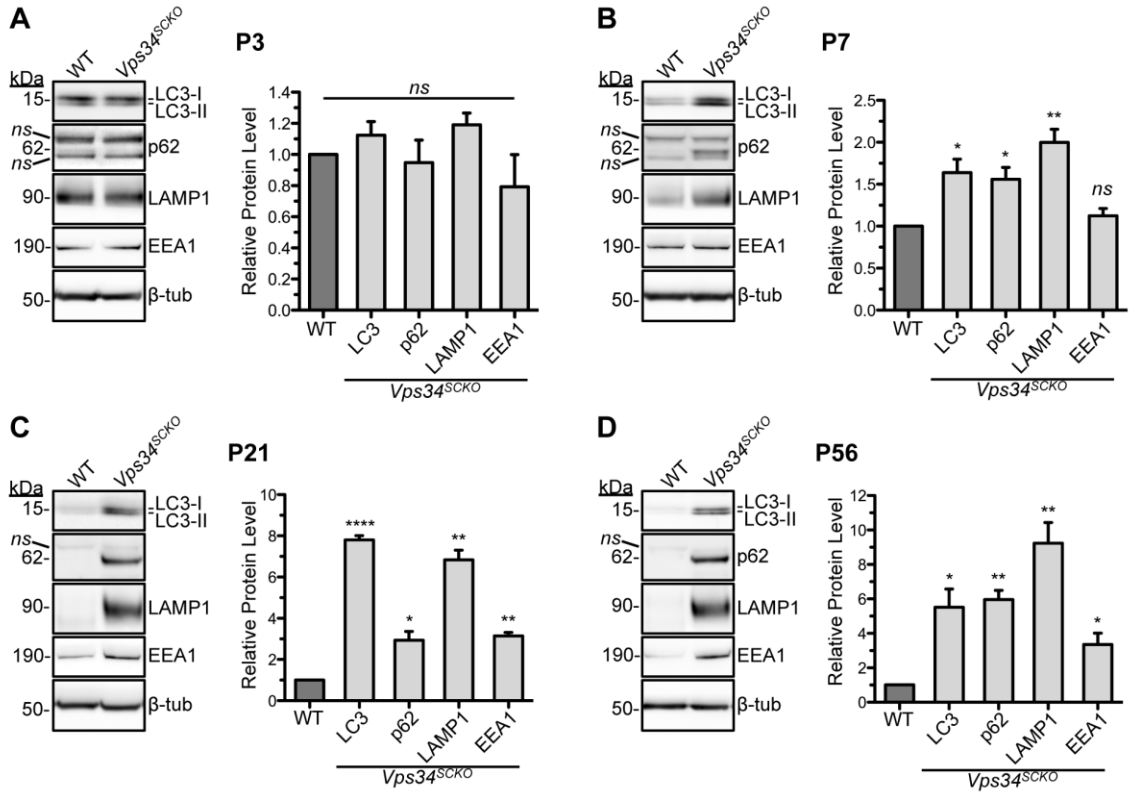

Figure 3.5. Autophagic and endosomal protein expression level is altered in *Vps34*^{SCKO} nerves. The levels of LC3-I and -II, p62, Lamp1, and EEA1 in sciatic nerve extracts were examining by immunoblotting at P3, P7, P21 and P56 (**A-D**). The abundance of each protein relative to that of the wild type is presented graphically. (A) At P3, the levels of the examined proteins were not significantly altered in mutant nerves. (B) By P7, there is a significant increase in LC3-I/II, p62, and Lamp1 levels in *Vps34*^{SCKO} nerve extracts (LC3: p = 0.045; p62: p = 0.02; Lamp1: p = 0.003; EEA1: p = 0.27). (C & D) At P21 and P56, significant increases in the levels of LC3-I/II, p62, Lamp1, and EEA1 protein were observed in *Vps34*^{SCKO} nerves (P21 LC3: p < 0.0001; P21 p62: p = 0.01; P21 Lamp1: p = 0.004; P21 EEA1: p = 0.002; P56 LC3: p = 0.02; P56 p62: p = 0.001; P56 Lamp1: p = 0.003; P56 EEA1: p = 0.03). At each age, the average wild type value for a given protein was normalized to 1. The data are presented as mean ± SEM;

unpaired t tests were used to evaluate significance (*n.s.*, not significant; *p < 0.05; **p < 0.01; ***p < 0.001; ****p < 0.0001). For all four ages, n = 3 lysates per genotype.

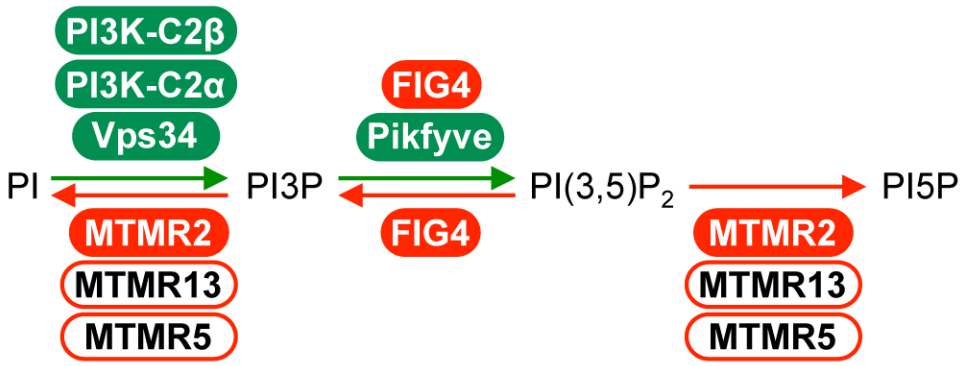

Figure 3.6. Model for the regulation PI3P, PI(3,5)P_2 and PI5P abundance in Schwann cells by PI kinases and PI phosphatases. Phosphorylation reactions and kinases are indicated with green; dephosphorylation reactions and phosphatases are indicated with red. Although the PI 5-phosphatase FIG4 is capable of dephosphorylating PI(3,5)P_2, the predominant role of this enzyme in mammalian cells is the promotion of PIKfyve kinase activity.

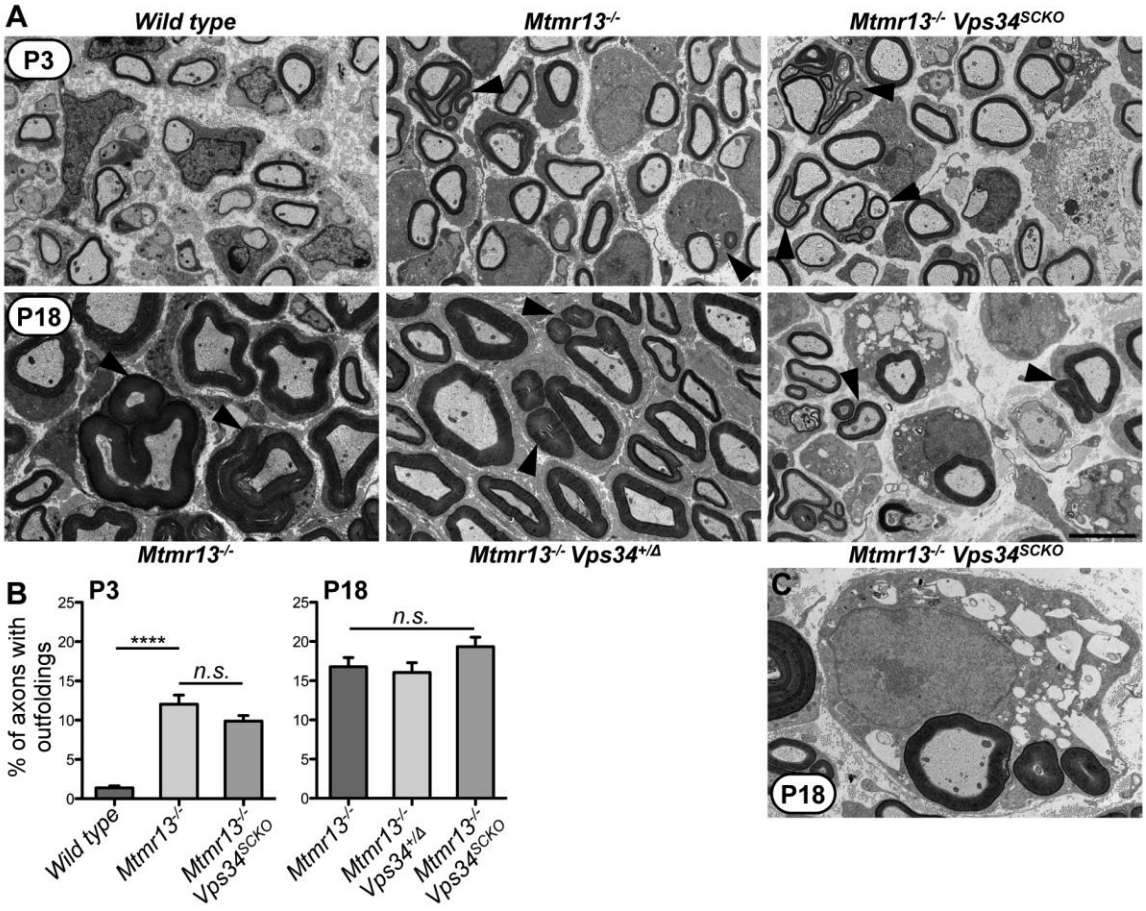

Figure 3.7. Loss of Vps34 does not alter the myelin abnormalities caused by Mtmr13 deficiency. (**A**) EM morphology of mid-sciatic nerves from P3 wild type, *Mtmr13*$^{-/-}$, and *Mtmr13*$^{-/-}$ *Vps34*^{SCKO} mice (*upper panels*) and P18 *Mtmr13*$^{-/-}$, *Mtmr13*$^{-/-}$ *Vps34*$^{+/\Delta}$, *and Mtmr13*$^{-/-}$ *Vps34*^{SCKO} mice (*lower panels*). Myelin outfoldings (*arrowheads*) are observed in both *Mtmr13*$^{-/-}$ and *Mtmr13*$^{-/-}$ *Vps34*^{SCKO} nerves. (**B**) Quantification of myelin outfoldings observed in (A). The percentage of myelinated fibers containing outfoldings is presented as mean ± SEM. At P3, the frequency of myelin outfoldings was not significantly different between *Mtmr13*$^{-/-}$ and *Mtmr13*$^{-/-}$ *Vps34*^{SCKO} nerves (12.04 ± 1.17% for *Mtmr13*$^{-/-}$ vs. 9.88 ± 0.71% for *Mtmr13*$^{-/-}$ *Vps34*^{SCKO}; $p > 0.05$ using a one-way ANOVA with Sidak's multiple comparisons test to evaluate significance. ****$p \leq 0.0001$). Likewise, at P18, the frequency of myelin outfoldings was not significantly different

between *Mtmr13*$^{-/-}$, *Mtmr13*$^{-/-}$ *Vps34*$^{+/\Delta}$, or *Mtmr13*$^{-/-}$ *Vps34*^{SCKO} nerves (16.78 ± 1.16% for *Mtmr13*$^{-/-}$ vs. 16.05 ± 1.26% for *Mtmr13*$^{-/-}$ *Vps34*$^{+/\Delta}$ vs. 19.35 ± 1.21% for *Mtmr13*$^{-/-}$ *Vps34*^{SCKO}; p = 0.1739; n = 5 for *Mtmr13*$^{-/-}$ and *Mtmr13*$^{-/-}$ *Vps34*^{SCKO}; n = 4 for *Mtmr13*$^{-/-}$ *Vps34*$^{+/\Delta}$). A one-way ANOVA was used to evaluate significance. (**C**) A higher magnification EM image of an *Mtmr13*$^{-/-}$ *Vps34*^{SCKO} Schwann cell containing both cytoplasmic vacuoles and myelin outfoldings (analyzed at P18). Scale bar: 4 μm (A and B), 2.5 μm (C).

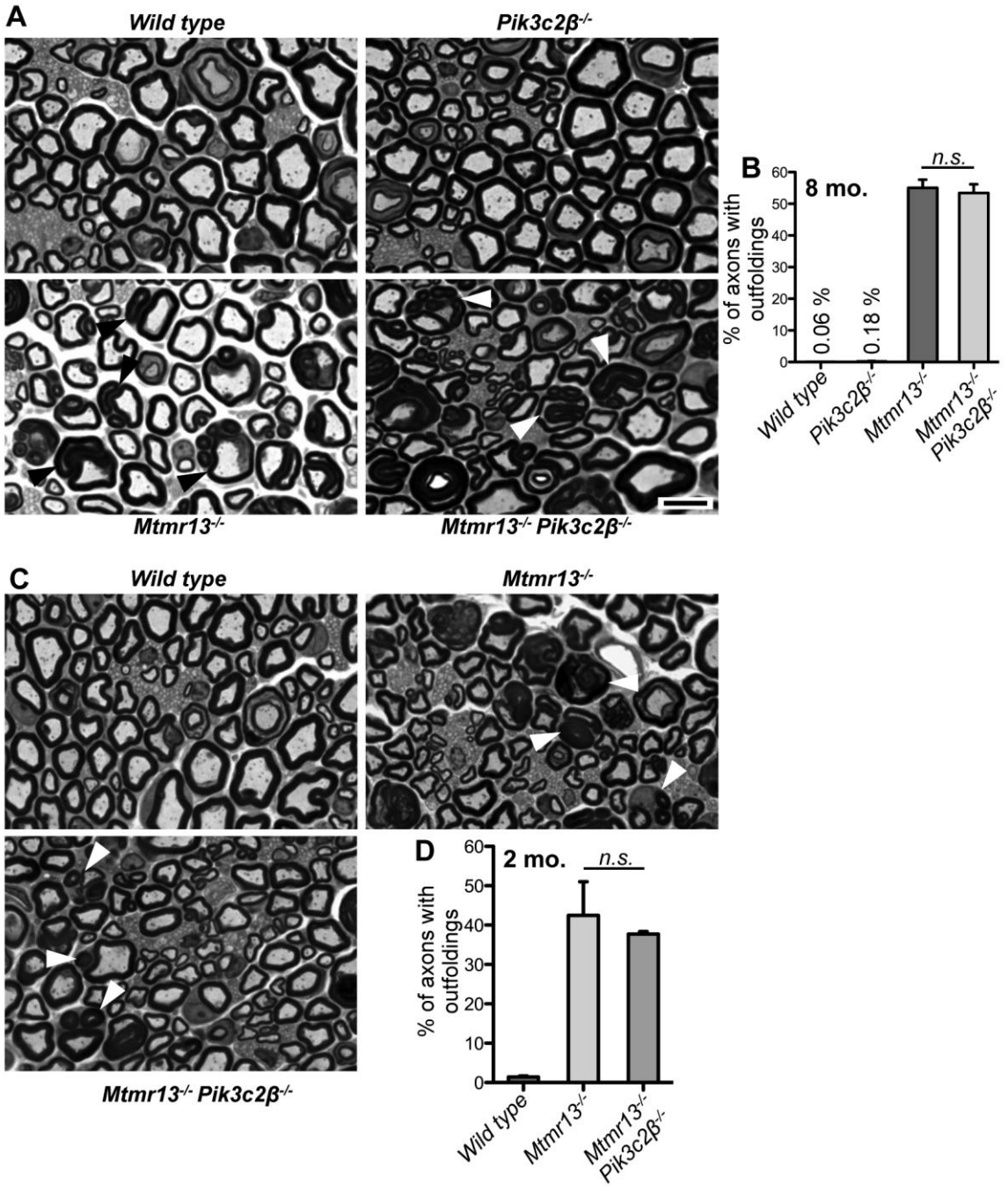

Figure 3.8. Loss of PI 3-kinase C2β does not affect peripheral nerve myelination or alter the myelin abnormalities caused by Mtmr13 deficiency. (**A**) Toluidine blue stained cross sections of the mid-sciatic nerve from 8-month-old wild type, *Pik3c2β*$^{-/-}$, *Mtmr13*$^{-/-}$, and *Mtmr13*$^{-/-}$ *Pik3c2β*$^{-/-}$ mice. Peripheral nerve myelination and axonal

integrity in *Pik3c2β*$^{-/-}$ nerves was similar to wild types, whereas nerves from *Mtmr13*$^{-/-}$ and *Mtmr13*$^{-/-}$ *Pik3c2β*$^{-/-}$ mice contain numerous myelin outfoldings (*black or white arrowheads*). (**B**) Quantification of myelin outfoldings observed in (A). At 8 months, the frequency of myelin outfoldings was not significantly different between *Mtmr13*$^{-/-}$ and *Mtmr13*$^{-/-}$ *Pik3c2β*$^{-/-}$ nerves (55.1 ± 2.6% for *Mtmr13*$^{-/-}$ vs. 53.5 ± 2.7% for *Mtmr13*$^{-/-}$ *Pik3c2β*$^{-/-}$; p = 0.71; n = 4-8 mice per genotype). (**C**) Toluidine blue stained cross sections of the mid-sciatic nerve from 2-month-old wild type, *Mtmr13*$^{-/-}$, and *Mtmr13*$^{-/-}$ *Pik3c2β*$^{-/-}$ mice. (**D**) Quantification of myelin outfoldings observed in (C). The frequency of myelin outfoldings was not significantly different between *Mtmr13*$^{-/-}$ and *Mtmr13*$^{-/-}$ *Pik3c2β*$^{-/-}$ nerves (42.5 ± 8.5% for *Mtmr13*$^{-/-}$ vs. 37.7 ± 0.7% for *Mtmr13*$^{-/-}$ *Pik3c2β*$^{-/-}$; p = 0.63; n = 2 mice per genotype). The data are presented as mean ± SEM; unpaired t tests were used to evaluate significance (*n.s.*, not significant). Scale bar: 6 μm.

Chapter 4

New tools for studying CMT4B dysmyelination: An *in vitro* culture model, a genetically-encoded PI3P detector, and a lentiviral construct expressing Cre recombinase in Schwann cell primary cultures

The contents of chapter four are unpublished.

Abstract

Demyelinating Charcot-Marie-Tooth (CMT) type 4B2 is caused by mutations in myotubularin-related protein 13 (*MTMR13*), resulting in peripheral neuropathy and serious disability in human patients. Although the disease-causing gene is known, the cellular etiology that leads to Schwann cell demyelination remains unknown. Based on the known localization and roles of its phosphoinositide substrates, MTMR13 is thought to function in the endosomal-lysosomal pathway. To examine the endo-lysosomal trafficking defects that may result from loss of MTMR13, we have established an *in vitro* culture model system. This system will allow us to look mechanistically at the effects of loss of MTMR, and provide a system where, in the future, high-throughput screening of potential therapeutic compounds for treating CMT may be possible. In addition, we describe two tools we have developed that can be used in combination with the culture model of CMT4B2: a lentirviral construct expressing the phosphatidylinositol 3-phosphate (PI3P) detection probe 2xFYVE, and a lentiviral construct expressing Cre recombinase. Together, the tools described here will complement the work being done with *in vivo* mouse models of CMT to further the understanding of how mutations in *MTMR13* lead to dysmyelination.

Introduction

The myotubularin (MTMR) family of phosphoinositide (PI) 3-phosphatases specifically catalyze the dephosphorylation of phosphatidylinositol 3-phosphate (PI3P) and 3,5-bisphosphate ($PI(3,5)P_2$), two lipids that regulate membrane traffic within the endosomal-lysosomal pathway[51,175]. A number of studies have shown that phosphoinositide regulation in endosomal-lysosomal pathways is critical for functional myelination, highlighted by seven mutations (*FIG4*, *MTMR2*, *MTMR5*, *MTMR13*, *FRABIN/FGD4*, *SH3TC2* and *SIMPLE/LITAF*) that cause demyelinating forms of the peripheral neuropathy CMT[77]. Peripheral neuropathy is estimated to have a worldwide total prevalence of 2.4% (8% in individuals 55 years or older)[176]. Although CMT is the cause of a small percentage of total peripheral neuropathies, this disorder is a significant clinical challenge. Loss of MTMR2, MTMR5, or MTMR13 causes CMT type 4B1, 2 and 3, respectively, in humans[45,47,177]. CMT4B is a severe recessive form of demyelinating CMT, characterized by dysmyelination and secondary axonal degeneration, which leads to disability. Nerves from CMT4B patients show distinctive myelin outfoldings, a hallmark of the condition thought to represent localized hypermyelination[40].

The study of CMT genes is a powerful strategy for unlocking the basic neurobiology of Schwann cells. The identification of genes that cause CMT tells us which proteins are indispensable *only* in the peripheral nerves and glia, as most other tissues are normal in CMT patients. Our challenge is to determine why loss of MTMR13, which causes CMT4B2, is selectively detrimental to myelinating Schwann cells, despite ubiquitous *MTMR13* expression in most human tissues. Despite the availability of excellent mouse models of CMT4B[68,72,178], the cellular mechanisms of disease – in particular, how dysregulation of PI3P affects endosomal trafficking in the Schwann cell – remain unknown. Here, I present three new tools I have developed for studying CMT: 1)

Mtmr13 knockout myelinating co-cultures, 2) a novel strategy for detecting PI3P in myelinating Schwann cells, and finally, 3) lentiviral mediated transduction of primary cell cultures with a Cre recombinase construct.

To study *MTMR13* mutations, we use mouse models of CMT4B2 that faithfully model the characteristic myelin outfoldings and secondary axonal degeneration[72,173]. However, *in vivo* models are not ideal to study the underlying cellular etiology, as study of subcellular trafficking is impractical. To complement our *in vivo* CMT4B2 mouse model, we sought to establish an *in vitro* system that could be pharmacologically manipulated and modified with transgene expression. The myelinating dorsal root ganglion (DRG) and Schwann cell co-culture that we have established provides an *in vitro* model of CMT4B2 dysmyelination. This system will enable us to address important mechanistic questions *in vitro*. For example, regulation and localization of PI3P is likely critical to CMT4B because PI3P is a substrate of MTMR13, and thus PI3P levels are likely elevated in CMT4B2 patients and mouse models. To address this, we have made and validated a novel PI3P reporter that can be used in *in vitro.* This reporter will be used in future experiments to examine subcellular pools of PI3P in myelinating Schwann cells, which will provide clues about the underlying trafficking defects in CMT4B2 patients. Our novel PI3P reporter provides a way to fluorescently visualize PI3P in myelinating Schwann cells through lentiviral expression of the EGFP-2xFYVE protein, which binds specifically to the headgroup of PI3P in cells.

We have also made a lentiviral construct expressing Cre recombinase and tested its effectiveness in Schwann cell primary cultures. Using Schwann cell cultures, we have established that Cre recombinase lentivirus efficiently leads to recombination and decreased expression of the floxed gene in culture. Together, these tools will be used to ask critical endosomal trafficking questions, with the hope of elucidating the link between *MTMR13* mutations, the levels of PI3P, and endosomal trafficking in the Schwann cell.

Results

Mtmr13$^{-/-}$ myelinating co-cultures recapitulate the myelin outfoldings in *Mtmr13*$^{-/-}$ mice and humans with CMT4B2

In order to study how mutations in *MTMR13* lead to disrupted membrane trafficking and myelin outfoldings, we created a system in which pharmacological manipulations and fluorescent reporters can be used to visualize Schwann cell trafficking in the wild type and diseased states. Myelinating co-cultures from *Mtmr13*$^{-/-}$ mice model the hallmark myelin outfoldings caused by *MTMR13* mutations (Fig. 4.1). To validate our system, we stained myelinating co-cultures from wild type and *Mtmr13*$^{-/-}$ mice for axons, using an antibody for neurofilament heavy chain (NF-H, a member of the intermediate filament family and a major component of neuronal cytoskeletons), and for myelin, using an antibody for myelin basic protein (MBP, a major constituent of the compact myelin sheath in the peripheral nervous system). We found that wild type and *Mtmr13*$^{-/-}$ cultures both myelinate robustly, indicating that loss of Mtmr13 does not decrease the amount of overall myelination *in vitro* (Fig. 4.2A). We then quantified myelin outfoldings in wild type and *Mtmr13*$^{-/-}$ cultures. 26% of myelinated MBP-positive segments contain a myelin outfolding, while in the control wild type cultures only 2% of myelin segments contain one or more outfoldings (Fig. 4.2B-D). In our *Mtmr13*$^{-/-}$ mouse model, at P3 we find around 7% of the myelinated fibers contain a myelin outfolding, and in adult mice, about 30% of myelinated fibers contain a myelin outfolding[72,173], indicating that our myelinating co-culture system is a good model for studying *Mtmr13* mutations *in vitro*.

2xFYVE is a reporter of PI3P levels and localization in myelinating Schwann cells

PI3P is primarily localized to early endosomes. Historically, it has been difficult to visualize and quantify PI3P. In 2000, Gillooly et al. built a probe consisting of two FYVE domains from the Hrs protein linked to EGFP[140]. PI3P is a key regulator of transport in the endocytic pathway and its function is conserved back to yeast[179]. The EGFP-2xFYVE reporter was shown to bind selectively to PI3P both *in vivo* and *in vitro[140]*. As expected, EGFP-2xFYVE colocalizes extensively with EEA1, a protein known to localize exclusively to early endosomes[140]. Additionally, 2xFYVE was observed to localize to a pool of PI3P present on internal membranes of multivesicular late endosomes in cultured cells[140]. How loss of MTMR13 may affect these specific pools of PI3P remains an unanswered question. Visualization of PI3P may offer critical insight and contribute to the advancement of the understanding of CMT. As MTMR13 dephosphorylates PI3P, we hypothesize that a specific pool of PI3P may be increased in the absence of MTMR13, thus leading to a disruption of PI3P-mediated membrane trafficking.

In order to examine PI3P in myelinating Schwann cells, we made the 2xFYVE reporter into a lentivirus (LVPG-EGFP-2xFYVE) (Fig. 4.3A). This will allow us to transduce and visualize Schwann cell PI3P once myelination has been initiated *in vitro*. To first verify that LVPG-EGFP-2xFYVE behaves as the 2xFYVE reporter plasmid is reported to, we transduced wild type mouse embryonic fibroblast (MEF) cells with the lentivirus. LVPG-EGFP-2xFYVE exhibits an endosomal-like pattern in MEF cells, confirming that 2xFYVE is localizing to PI3P pools on early endosomes as expected (Fig. 4.3B-C).

We next wanted to look at the distribution and pattern of 2xFYVE in myelinating co-cultures to confirm that the reporter would bind specifically to PI3P in this culture setting. We saw EGFP expression in the stereotyped early-endosomal pattern in both axons and Schwann cells (Fig. 4.4C-D) as expected, since lentivirus has the ability to

transduce during any stage of the cell cycle. From these experiments, we conclude that our lentivirus expressing 2xFYVE is a reliable reporter for PI3P localization in myelinating co-cultures, and provides us with a valuable tool needed to perform future experiments that will look closely at PI3P level and localization in wild type compared to *Mtmr13*$^{-/-}$ myelinating co-cultures.

Vps34-floxed primary Schwann cell cultures transduced with Cre-expressing lentivirus leads to efficient loss of Vps34 protein expression

To study Vps34 function in Schwann cells, we need the ability to ablate Schwann cell expression of Vps34 in primary cultures. This tool will be useful for studying the role of Vps34 in Schwann cell autophagy, since *in vivo* experiments studying the stages and progress of autophagy are not possible with the current tools available. Cre lentivirus can also be used to reduce expression of other floxed genes, and is thus a valuable tool for the lab.

Using a lentivirus expressing Cre recombinase, we show high transduction efficiency in MEF cells (Fig. 4.5A) and efficient deletion of Vps34 in Vps34-floxed Schwann cell cultures. Lentivirus expressing the control catalytically inactive Cre (ΔCre) shows that expression of Vps34 remains in the Schwann cell, as is also the case when no virus is added (Fig. 4.5B). In the lane where no virus was added to the cells, robust expression of Vps34 persists, but it is important to note that the increase in beta-tubulin loading control in this lane compared to the other five lanes indicates that adding virus to the Schwann cell cultures does lead to some cell death. However, this figure confirms that the lentiviruses I have developed and presented here will be useful tools in future studies of the role of Vps34 in Schwann cell autophagy, as well as other genes in the lab.

Discussion

Despite the availably of excellent mouse models of CMT4B, the cellular origins of this dysmyelinating condition remain unknown. In particular, the details of MTMR13 involvement in PI3P regulation, and how endosomal trafficking might be disrupted in the disease state, are unclear. We have developed an *in vitro* culture system that reproduces the distinctive myelin outfoldings of CMT4B2. This model will allow us to study the underlying cellular defects of *MTMR13* mutations in a simplified system and allow us to make pharmacological manipulations with the goal of exploring treatments for CMT. Additionally, we have developed a novel strategy for detecting PI3P in myelinating Schwann cells by expressing EGFP-2xFYVE using lentiviral transduction. This tool may allow us to determine how PI3P localization and abundance are altered in myelinating Schwann cells that lack Mtmr13.

This novel *in vitro* model of CMT4B2 can be used to address another important and outstanding question in the field: whether PI3P levels can be rebalanced in Schwann cells with *MTMR13* mutations, thus restoring normal myelination. It has been suggested that knocking down PI 3-kinases in an MTMR13 deficient setting may be a therapeutic approach to treating CMT[180]. PI 3-kinases phosphorylate PI to make PI3P in the cell[62,144,181], but it is unclear whether balancing a phosphatase deficient system with kinase knockdown would improve cellular outcomes in the disease model. Therefore, future experiments in our lab will use our *in vitro* myelination system to attempt to renormalize levels of PI3P in *Mtmr13*$^{-/-}$ Schwann cells by transducing cultures with lentivirus encoding shRNAs to knockdown the class III PI 3-kinase Vps34, as well as the class II PI 3-kinases: PI3K-C2α and PI3K-C2β, two PI 3-kinases that may also contribute to PI3P production[182]. We anticipate that the knockdown of Vps34, PI3K-

C2α, and/or PI3K-C2β, in the context of *Mtmr13*$^{-/-}$ cultures, will decrease myelin outfoldings. We already know that Vps34 knockout alone in Mtmr13-deficient cells is not sufficient to rescue myelin outfoldings, so perhaps there is compensation by other PI 3-kinases to make up for decreased PI3P in Vps34 deficiency. We therefore propose that successful rescue of myelin outfoldings may involve knocking down two or more of the three potential kinases. We would interpret such a rescue result as strong evidence that specific PI 3-kinase isoforms are responsible for generating the pool of PI3P that is the key target of Mtmr13.

Lentiviral-mediated transduction of Cre recombinase into primary Schwann cell cultures and myelinating co-cultures will provide the opportunity to temporally knockdown expression of certain genes of interest. This tool will complement the systems described above. Transduction of Cre lentivirus in Schwann cell primary cultures successfully reduces expression of Vps34 protein in Schwann cells made from mice with the Vps34 allele floxed. Vps34 has been suggested as a potential PI 3-kinase that may be responsible for making a bulk of the PI3P in the cell, which is the substrate of MTMR13. Many groups have suggested that knocking down Vps34 in an *MTMR13*$^{-/-}$ background may rescue myelin abnormalities. Using the myelinating co-culture system described above, in combination with the lentiviral Cre construct, we will be poised to test whether knockdown of Vps34, in combination with the class II PI 3-kinases, can rescue outfoldings *in vitro*.

Finally, the use of Vps34$^{fl/fl}$ Schwann cells in combination with the lentiviral Cre construct can be used in a myelinating co-culture setting to study the necessity of the Vps34 in myelination. From our *Vps34*^{SCKO} mouse model, we know that Vps34 is required for Schwann cell myelination. It would be interesting to study whether loss of Vps34 in adult mice causes dysregulation of myelination, or if Vps34 is only required for initial myelination and not myelin maintenance. This experiment can now be performed

in the lab with the tools in hand, and will be something the Robinson lab will follow up on in the future.

The work presented in this section are tools that I have developed during my PhD work which will allow us to better understand how the critical regulation of PI3P is achieved in myelinating Schwann cells, and may form the basis of a rational therapy for CMT4B2. Future studies in the lab will use these tools to address various questions that remain in the field.

Materials and Methods

DRG myelinating co-cultures

DRGs were dissected from E13.5 pups in L15 + FBS media (L-15 media Life Technologies #11415-064 + 10% FBS + 0.04% pen/step) (Day1). DRGs from the whole litter were pooled and kept at 37°C in L15 + FBS, then washed once in L15 – FBS. The DRGs were then trypsinized (0.25%) for 45 minutes at 37°C. Equal part L15 + FBS was added to neutralize the trypsin, and the tube was spun at 1000 rpm for 10 minutes. Supernatant was removed, and replaced with pre-warmed M1/NGF media (MEM media Life Technologies #11095-080 + 10% FBS + 1.2 M D-glucose (final concentration 4.3 g/L) + NGF Life Technologies #13257-019 (final concentration 1 µg/µL)). DRGs were triturated with a P200 pipette to break up the ganglia into a single cell suspension; cells were spun at 1000 rpm for 5 minutes. Media was removed and replaced M1/NGF. Cells were counted and plated on collagen coated glass coverslips at a density of 130,000 cells per well in 160 µL media in a 6-well dish. Cultures were incubated at 37°C, 5% CO_2.

The next day (Day 2), wells were flooded with 1 mL M1/NGF media. Media was changed to 2 mL M1/NGF every other day. On Day 9, media was changed to 2 mL C-

medium (MEM media + 1.2 M D-glucose (final concentration 4.3 g/L) + 10% FBS + L-glutamine Life Technologies #25030-149 (final concentration 2 mM) + NGF (final concentration 50 ng/mL) + Ascorbic Acid (final concentration 50 µg/mL)). Ascorbic acid was prepared fresh each time, sterile filtered, then added to C-medium. C-Medium was changed every 2 days.

On Day 22, cells with fixed with 4% PFA in 1X phosphate buffered saline (PBS) for 15 minutes at room temperature, then washed three times in 1X PBS. Cultures were permeabilized in 0.2% Triton X-100 in 1X PBS for 15 minutes at room temperature, then washed in 1X PBST (1X PBS + 0.1% Tween-20). Cultures were blocked in 10% NGS in 1X PBST for 30 minutes at room temperature, then changed to primary antibody diluted in 2% NGS in 1X TBST. MBP was used to visualize myelin (Millipore, MAB386, rat) @ 1:250, NF-H was used to visualize axons (Abcam, AB4680, chicken) @ 1:10,000. Primary antibodies were incubated at 4°C overnight.

The following day, coverslips were rinsed in 1X TBST three times. Secondary antibodies were added @ 1:500 in 2% NGS in 1X TBST (Alexa Flour 488 Goat Anti-Rat IgG (H+L) [Jackson IR # 112-545-167] and Alexa Flour 647 Goat Anti-Chicken IgY [Jackson IR #103-605-155]), and incubated for one hour at room temperature. Coverslips were washed three times in 1X TBST. Nuclei were stained with DAPI (Invitrogen, #D1306) @ 1:40,000 in 1X TBST for one minute, then coverslips were washed twice for five minutes in 1X TBST. Coverslips were rinsed in deionized water, and mounted on slides in Elvanol mounting media. Slides were stored at 4°C.

Images were acquired on a wide-field DeltaVision CoreDV deconvolution microscopy system (Applied Precision), built on an Olympus IX71 inverted microscope equipped with a Nikon Coolsnap ES2 HQ camera. Each image was acquired as a set of Z-stacks in a 1024 X 1024 format with a 60X 1.42 NA PlanApo objective. The pixel size was 0.107 X 0.107 X 2 μm^3. Images were deconvolved with the appropriate optical

transfer function using an iterative algorithm of 10 iterations. The histogram was optimized for the brightest image acquired, and applied to all other images analyzed for consistency. Images were made from the Z-stack by merging into a 24-bit TIFF file, and the number of Z-sections compressed in each image shown and analyzed was the same for comparable images. Acquisition and deconvolution were accomplished using the softWoRx software (Applied Precision). Post-acquisition imaging was accomplished using the Volocity software (Perkin Elmer).

For analysis, slides were blinded and each was divided into four quadrants and two images were taken from each of the quadrants (8 images total per slide). This was done on 6 slides from each genotype (wild type and *Mtmr13*$^{-/-}$). Total number of MPB-positive fibers was counted for each image, as well as the number of MBP-positive myelin sheaths containing one or more myelin outfoldings. The average was calculated for each genotype, and the result is presented as the percent of MBP-positive myelin sheaths containing one or more myelin outfoldings.

2xFYVE Lentivirus

PCR was used to amplify EGFP-2xFYVE out of the EGFP-C2 vector, run on a 0.7% agarose gel, and the DNA was gel purified. Infusion cloning was used to clone EGFP-2xFYVE product into linearized lentiviral plasmid (LVPG). Infusion clone reaction was plated on LB-amp plates and grown overnight at 30°C (to prevent recombination). Colonies were picked the following day, and grown in LB broth + ampicillin at 30°C overnight, then mini-prepped (Qiagen). Restriction enzyme digests of mini-preps were performed with the enzymes SalI and XbaI to check insertion length and confirm no recombination took place.

Once correct size was confirmed, maxi-prep (Qiagen) was performed to obtain a high concentration of LVPG-EGFP-2xFYVE plasmid for viral packaging. To package

LVPG-EGFP-2xFYVE, 293FT cells were grown on 0.1 mg/mL Poly-L-Lysine coated flasks and transfected with the 27 µg experimental vector (LVPG-EGFP-2xFYVE) + 9 µg pVSVG + 7 µg pREV + 17 µg pMDL in Optimem using Lipofectamine 2000. Transfection complex was allowed to incubate on cells at 37°C for 8 hours, then media was replaced with 14 mL 293 FT medium (DMEM (Gibco #11965-092) + 10% FBS + 0.1 mM MEM Non-Essential Amino Acid (Gibco #11140-050) + 6 mM L-glutamine (Gibco #25030-081) + 1 mM MEM Sodium Pyruvate (Gibco #11360-070) + 1% pen/strep). At 48 and 80 hours post-transfection, media was collected and combined, spun at 1000 x g for 5 minutes, then sterile filtered using a disposable vacuum filter (Millipore #SE1M000M00). Viral supernatant then was aliquoted and stored at -80°C.

LVPG-EGFP-2xFYVE transduction of MEF cells

Wild type MEF cells were plated at a concentration of 1.0 X 10^5 cells/mL in cell culture medium (DMEM (Life Technologies #11995-065) + 10% FBS + 1% pen-strep) on glass coverslips in a 6 well tissue culture dish. Cells were grown at 37°C overnight, and the following morning 100 µL, 250 µL, 500 µL, and 1.0 mL LVPG-EGFP-2xFYVE viral supernatant was added to culture medium. Cells were grown for 48 hours, then fixed in 4% PFA in 1X PBS for 15 minutes at room temperature, and rinsed in 1X PBS. Coverslips were stained with DAPI, washed, rinsed in deionized water, and mounted on slides in Elvanol mounting media. Slides were stored at 4°C, and imaged on the wide-field DeltaVision CoreDV deconvolution microscopy system (Applied Precision) (*see methods above*).

LVPG-EGFP-2xFYVE transduction of myelinating co-cultures

To transduce myelinating co-cultures, the same methods as described above were followed with minor changes. On Day 5, 500 µL LVPG-EGFP-2xFYVE viral

supernatant was added to 1.5 mL M1/NGF. Twenty-four hours later, virus-containing media was removed and a quick wash with 2 mL C-medium (without ascorbic acid) was done to ensure virus was removed entirely, then cultures were returned to M1/NGF media. On Day 8, media was changed to 2 mL C-medium + Ascorbic Acid; every 2 days thereafter media was replaced with fresh media, using formula as described above. Cells were fixed on Day 22, and the protocol described above was followed.

Viral transduction of Schwann cell primary cultures with Cre recombinase and catalytically inactive Cre

Viral plasmids were a generous gift from Dr. Fredrik Sterky at Stanford University. Viral plasmids were packaged using 293FT cells as described above. 1.0 mL or 1.5 mL viral supernatant of Cre and catalytically inactive Cre (ΔCre) was added to primary Schwann cell cultures made from $Vps34^{fl/fl}$ mice (primary Schwann cell cultures were prepared as previous described[173]), then cultured for four days. On day 4, the viral media was replaced with fresh Schwann cell culture media. At day 7, cells were lysed and raw lysates were prepared for Western blotting.

Western blots were performed as previously described[173]. Primary antibody against Vps34 (Cell Signaling, rabbit, #3358, used @ 1:1000) was used to check for loss of Vps34 protein in the presence of Cre virus, and beta-tubulin was used as a loading control (Developmental Studies Hybridoma Bank, #E7, used @ 1:1000).

Acknowledgements

The work done to establish the *Mtmr13*$^{-/-}$ myelinating co-cultures would not have been possible without the help of a technician in the lab, Aubree Ng. Her knowledge and experience in tissue and cell culture was invaluable in getting this difficult culture

technique up and running in our lab. I am very grateful for her help and assistance in the years we worked together in the lab.

Figures and Legends

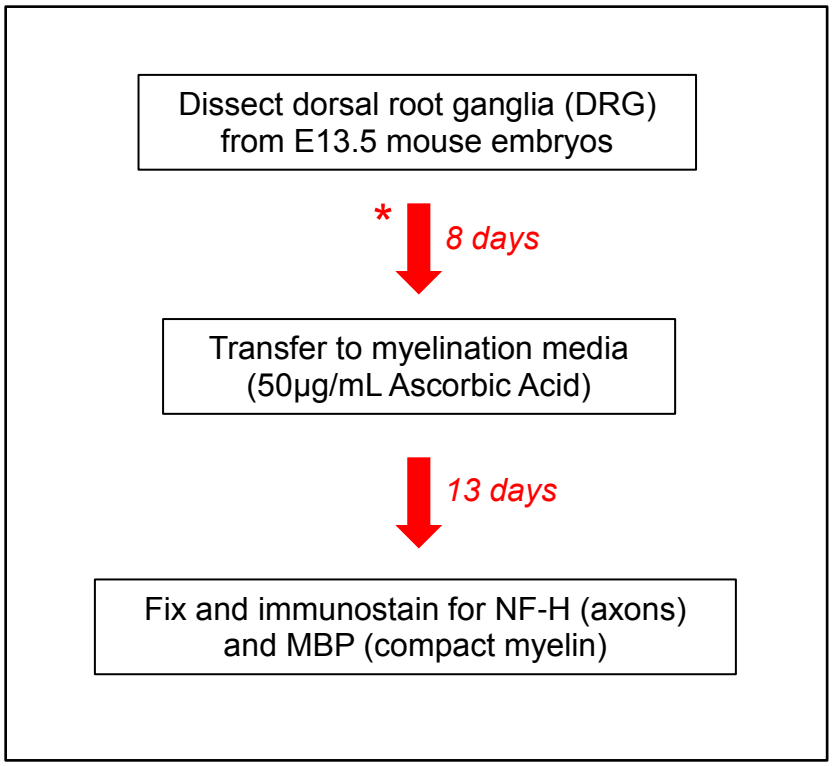

Figure 4.1: Schematic of protocol for growing DRG myelinating co-cultures. When transducing co-cultures with lentivirus, viral supernatant is added to cultures on day 5 (red asterix), then the remainder of the protocol is followed as normal.

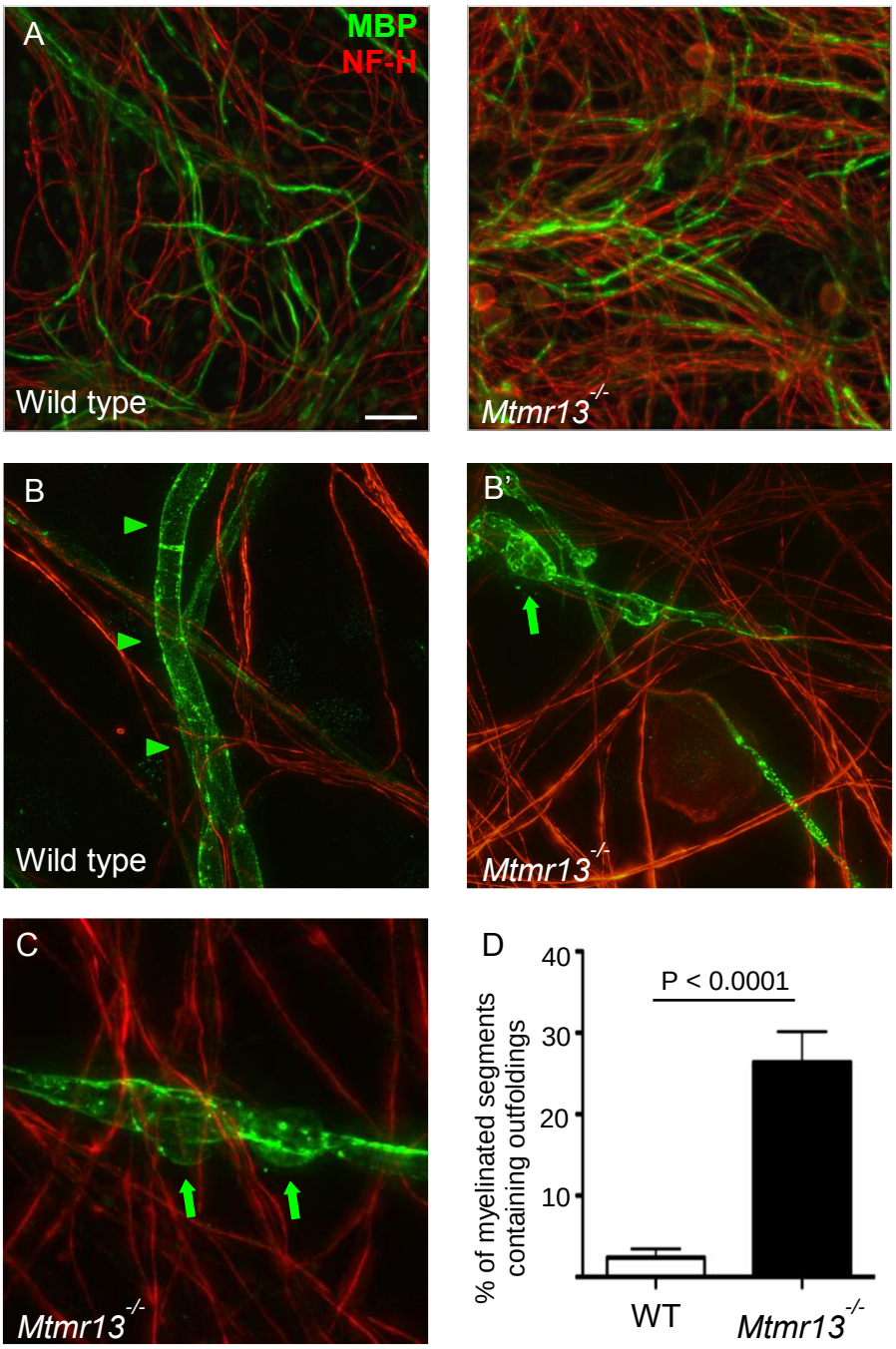

Figure 4.2: *Mtmr13*$^{-/-}$ Schwann cells produce CMT4B-like myelin outfoldings *in vitro*. (**A**) Efficiency of myelination in *Mtmr13*$^{-/-}$ co-cultures is similar to that of wild type (10X). (**B**) Higher magnification (60X) images of wild type and (**B'**) *Mtmr13*$^{-/-}$ *co*-cultures. Green arrowheads show thick, uniform myelin segments in wild type. Green arrows

highlight myelin outfoldings in *Mtmr13*$^{-/-}$ cultures, shown at higher magnification in (**C**). (**D**) Quantification of myelin outfoldings shows that 26.35 ± 3.8% of myelinated segments contain a myelin outfolding in *Mtmr13*$^{-/-}$ co-cultures, whereas in wild type control cultures, only 2.4 ± 1.1% of myelinated segments contain an outfolding. Scale bar: 80 μm (A), 10 μm (B-C).

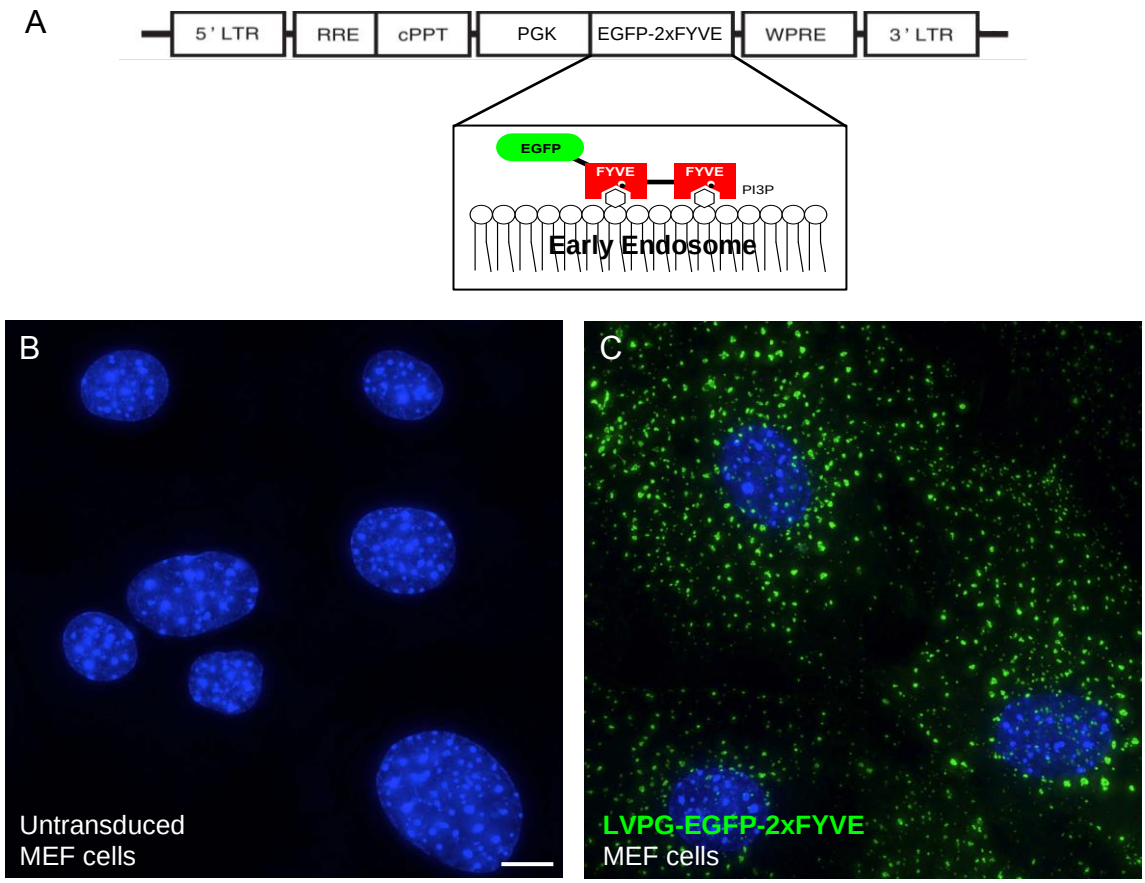

Figure 4.3: Lentiviral expression of EGFP-2xFYVE exhibits an endosomal-like pattern in MEF cells. (**A**) Schematic showing the LVPG lentiviral backbone vector expressing 2xFYVE under the control of the PGK promoter. (**B**) Untransduced MEF cell nuclei stained with DAPI (blue). (**C**) MEF cells 48 hours post transduction with LVPG-EGFP-2xFYVE shows endosomal-like pattern. Scale bar: 10 μm.

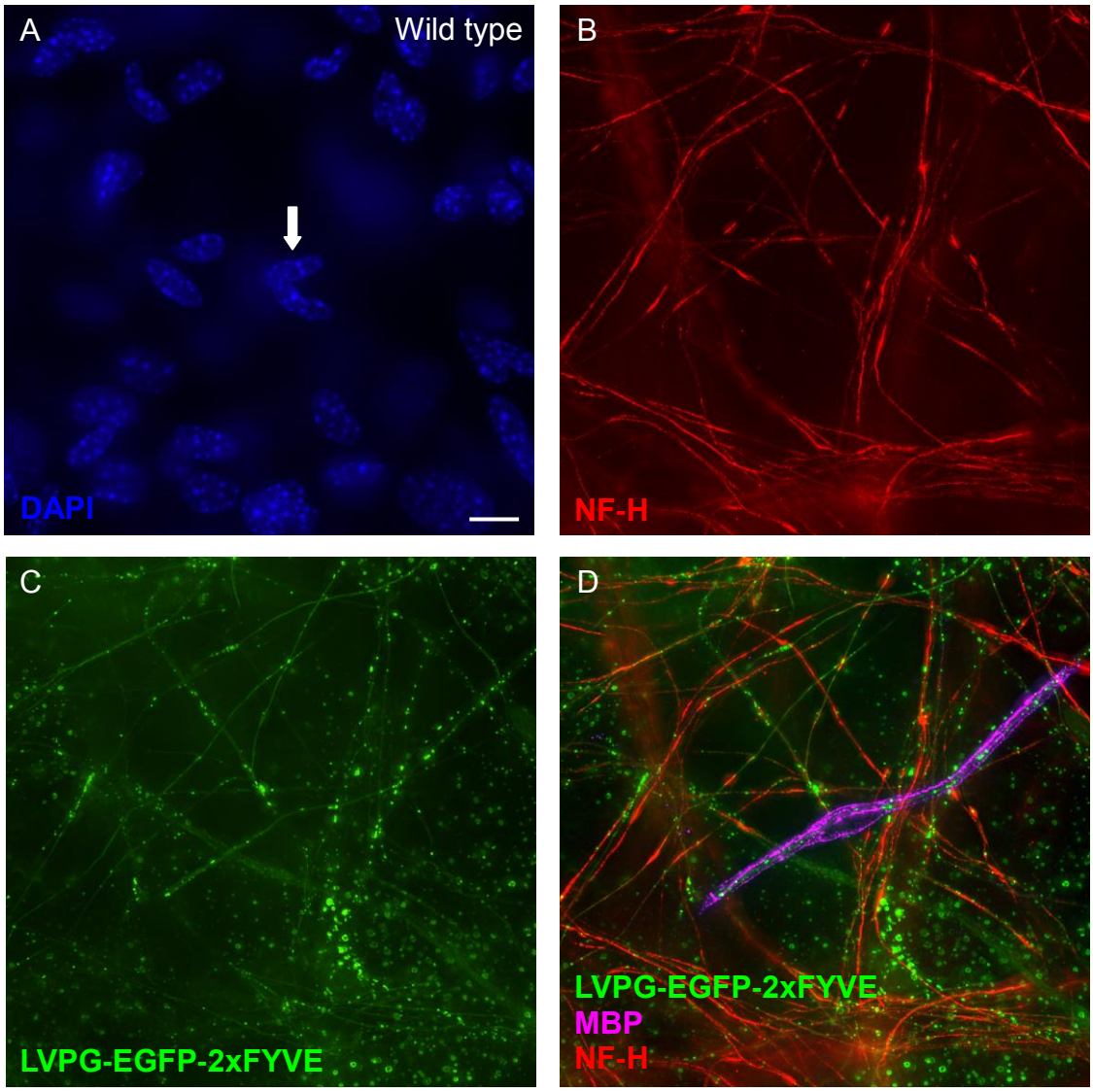

Figure 4.4: LVPG-EGFP-2xFYVE expression in myelinating co-cultures shows endosomal-like pattern in both neurons and Schwann cells. (A-D) Wild type myelinating co-cultures transduced with LVPG-EGFP-2xFYE show endosome-like pattern of expression in both the axons and a myelinating Schwann cell. (**A**) DAPI showing contaminating fibroblast nuclei and Schwann cell nucleus (white arrow). (**B**) NF-H-positive axons, (**C**) LVPG-EGFP-2xFYVE. (**D**) Merge of B+C, plus MBP immunofluorescence showing a Schwann cell myelinated segment with EGFP-2xFYVE expression. Scale bar: 80 μm.

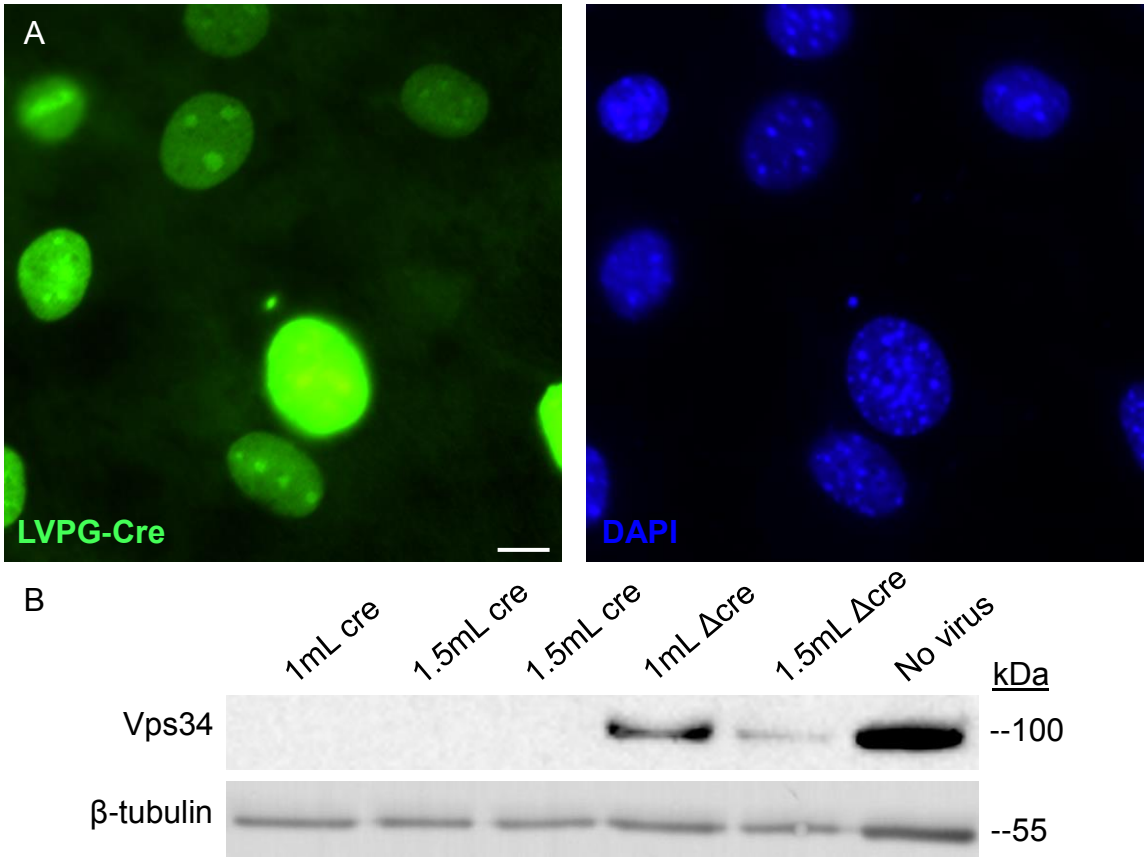

Figure 4.5: LVPG-Cre and -ΔCre expression in MEF cells and Schwann cell primary cultures. (**A**) Representative immunofluorescent image of wild type MEF cells transduced with LVPG-Cre showing nuclear expression of Cre, as expected. DAPI staining in the right panel shows the high transduction efficiency of the LVPG-Cre virus. Scale bar: 10 μm. (**B**) Western blot of cell lysates made from cultured Vps34$^{fl/fl}$ Schwann cells transduced with either 1.0 or 1.5 mL of Cre or ΔCre virus shows efficient loss of Vps34 protein in the presence of Cre recombinase. Beta-tubulin is used as a loading control and shows that addition of LVPG virus leads to some minor Schwann cell death, demonstrated by the slightly elevated level of beta-tubulin in the control lane where no LVPG virus was added.

Chapter 5

Concluding Remarks and Future Directions

General Summary and Conclusions

The study of genetic peripheral neuropathies has expanded over the past 20 years through advancements in next generation molecular sequencing and better access to sequencing for neuropathy patients[38]. As a result, more than 1000 mutations in 80 different genes have been identified that cause CMT[39]. Still, inherited peripheral neuropathies are challenging to treat. The study of CMT genes and their normal function in Schwann cells and axons is critical for advancing the understanding of the molecular pathogenesis of CMT, and is a window into the basic neurobiology of Schwann cells and myelination. Understanding the basic biology and mechanism of disease is ultimately necessary to develop therapies to treat CMT. The study of demyelinating CMT genes is also of great interest to those seeking an understanding of why such genes are critical specifically in Schwann cells, which may shed light on other cell type-specific diseases.

Many researchers studying CMT4B (myotubularin family mutations) hypothesize that such mutations result in loss of a critical PI balance in Schwann cells, leading to sub-cellular trafficking defects and abnormal myelination. I based my dissertation work on investigating this hypothesis, focusing my research projects on examining the contribution of PI 3-kinases and 3-phosphatases to overall PI balance in Schwann cells.

Using our mouse model for CMT4B2, my thesis work contributed to an understanding of the molecular pathogenesis resulting from loss of MTMR13. We found that not only do the Mtmr2 and Mtmr13 proteins partially localize to endomembrane compartments in Schwann cells, they also reciprocally enhance expression level of one another[67]. Further studies showed that reciprocal enhancement of expression was most dramatic in the sciatic nerve, one of the affected tissues in CMT4B patients, but not in MEF cells or whole brain tissue lysates[67]. Taken together, these findings highlight the interdependence of Mtmr2 and Mtmr13 in Schwann cells.

The localization and stabilization of Mtmr2 and Mtmr13 proteins is likely key to CMT pathogenesis. It is possible that loss of wild type localization and expression level of either binding partner alters PIs in specific regions in the Schwann cell. Both PI3P and $PI(3,5)P_2$ are dephosphorylated by the Mtmr2/Mtmr13 complex, therefore localization and levels of these PIs may be dysregulated with loss of MTMR13. The status of endo-lysosomal membranes in the cell may be a potential readout for PI3P and $PI(3,5)P_2$ dysregulation. PI3P and $PI(3,5)P_2$ function in endosomal trafficking, each with a described function in movement and processing of endosomal membranes. We therefore studied the status of the endosomal and lysosomal systems in diseased Schwann cells (*Mtmr13*$^{-/-}$), by light and electron microscopy, as well as biochemical methods[67]. Other loss of function studies of PI kinases and phosphatases (such as FIG4[183]) have shown dramatic changes in endosomal or lysosomal membranes. However, we found no upregulation in endosomal or lysosomal membranes[67]. Our findings suggest that dysregulation of membrane trafficking in *Mtmr2*$^{-/-}$ and *Mtmr13*$^{-/-}$ Schwann cells may be more nuanced, likely disrupting trafficking of specific proteins or receptors rather than total dysregulation of endomembrane trafficking.

AKT activation in CMT models and models of myelin dysregulation is a hotly debated topic. It has been suggested that elevated $PI(3,4,5)P_3$ levels contribute to localized hypermyelination, causing both myelin outfoldings and tomacula[126]. However we examined the state of AKT singling in CMT4B mice (both *Mtmr2*$^{-/-}$ and *Mtmr13*$^{-/-}$) and found no change in AKT activation in these models[67]. AKT is activated by class I PI 3-kinase-mediated phosphorylation of $PI(4,5)P_2$ to $PI(3,4,5)P_3$ at the plasma membrane, which in turn leads to activation of AKT[64]. Our findings suggest that AKT activation, and thus PI 3-kinase signaling and PIP3 production, is appropriately regulated in mouse models of CMT4B. Based on our hypothesis that mutations in *MTMR13* disrupt the critical PI balance and are the driving force behind disease development in the Schwann

cell, it is likely that $PI(3,4,5)P_3$ is not the major PI dysregulated in CMT. Instead, perhaps the PIs directly regulated and controlled by myotubularin phosphatases are dysregulated, contributing to disease development and progression. For example, it is possible that levels of $PI(3,5)P_2$ are dysregulated in Schwann cells, similar to Mtmr2 knockout mice[70], leading to disruption of cellular functions and in turn myelin abnormalities.

In recent years, the study of class II and III PI 3-kinases and their contribution to cellular PI3P production has increased greatly. It has been proposed that PI 3-kinase function is central to the molecular pathogenesis of CMT4B. As AKT production of $PI(3,4,5)P_3$ appears unaffected in our models, we examined the effect of manipulating PI3P levels in Schwann cells. Myotubularin proteins catalyze PI3P dephosphorylation, the opposite of Vps34 function; therefore it has been proposed that selective inhibition of class II or III PI 3-kinases might provide clinical benefits to patients. In late 2014, two independent groups published highly specific Vps34 inhibitors, and suggested that these inhibitors may be of interest for the treatment of CMT4B neuropathies[180,184]. We proposed a similar hypothesis, but instead of chemical inhibition of Vps34 to modify PI3P levels, we used a genetic approach.

Using a conditional knockout strategy, we specifically ablated Vps34 expression in Schwann cells late in embryonic development. Vps34 makes the majority of PI3P, although the class II PI 3-kinases can contribute to PI3P production in some cell types. Because of the contribution of class II PI 3-kinases, we expanded our studies to investigate the class II PI 3-kinase PI3K-C2β. Interestingly, we found that Vps34 is critical for Schwann cell myelination, but PI3K-C2β is dispensable. Schwann cells lacking PI3K-C2β myelinate normally, whereas loss of Vps34 causes significant myelination defects. To directly examine if knocking down a kinase in a phosphatase-deficient system can be of therapeutic benefit, we made two double-knockout mouse

lines with *Mtmr13* knocked out in combination with *Vps34* or *Pik3-c2β*. In both mouse lines the prevalence of myelin abnormalities was unaltered. This finding suggests that targeted inhibition of Vps34 is probably not a viable therapeutic option for treating CMT. It also suggests that that manipulating PI3P levels through a single PI 3-kinase knockout is not sufficient to rescue myelin abnormalities in the context of the *Mtmr13*$^{-/-}$ mouse model of CMT4B2.

Our central hypothesis predicts that PI balance in Schwann cells is critical for myelination and this balance is altered in CMT. With the mouse lines we made, we found that PI3P must be properly regulated for normal myelination. However, we were unable to alter myelin outfoldings caused by *Mtmr13* mutations, suggesting that the PI3P pools catalyzed and regulated by either Vps34 or PI3K-C2β are not contributing to myelin abnormalities. This result does not rule out the possibility that PI balance in Schwann cells is critical, instead it suggests we have not yet discovered the specific PI pool that is dysregulated in CMT. Additionally, it is still possible that PI3P is involved in disease pathogenesis. There are two other PI 3-kinases that produce PI3P that may compensate for the absence of Vps34 or PI3K-C2β[64]. Another possibility is that PI3P levels and localization are in fact not dysregulated in CMT models. Perhaps one of the other PIs is dysregulated in the Schwann cell, likely PI(3,5)P_2 or PI5P.

With the *Vps34*^{SCKO} mouse line we also found that in Schwann cells, Vps34 contributes to both autophagic and endosomal pathways. This finding is important to the overall understanding of Vps34 function in mammalian cell types. Vps34 has been studied extensively in yeast, but the role of this kinase is much more complicated in specialized mammalian cell types. Various groups have studied Vps34 in mammalian cell types, including sensory neurons, hepatocytes, and cardiomyocytes, and found the function of Vps34 varies greatly from cell type to cell type[145,146,147]. In some mammalian cells, Vps34 is required for autophagic function, whereas in other cell types

it appears to be completely dispensable. In endosomal trafficking, the role of Vps34 also varies depending on cell type. We found that both autophagic and endosomal pathways are affected by loss of Vps34 in Schwann cells, and future experiments performed in the lab should determine exactly what stages in these pathways Vps34 are necessary.

Our lab has proposed a "dual output" model of MTMR13 function where MTMR13 may have two critical roles in the Schwann cell, both involved in the control of endo-lysosomal trafficking as well as myelination. MTMR13 may control PI levels and the cellular balance of PIs through its dimerization with MTMR2 and dephosphorylation of PI3P and PI(3,5)P_2. It may also contribute to Schwann cell myelination through its DENN domain, activating Rabs required for intracellular trafficking. The Robinson lab is taking various approaches to study these two functional outputs of the MTMR13 protein. Taken together with the findings of my thesis work, we suggest that loss of MTMR13 might not be disrupting only the PI balance; it may also be disrupting Rab activation in Schwann cells.

Future Directions

The findings of my thesis have raised many new questions relating to the molecular pathogenesis of CMT4B. I focused my thesis work on the effects of manipulating PI levels on myelination, and found that lowering PI3P levels through Vps34 knockout is detrimental to Schwann cell myelination. Interesting, *Pik3-c2β* is dispensable for myelination, suggesting that Vps34-mediated PI3P regulation, but not PI3K-C2β, is necessary for normal myelination. The exact role of Vps34 in autophagy progression and endosomal trafficking requires more experiments, however. Future experiments performed in the lab will address at what stages of autophagy progression and endosomal trafficking Vps34 is required. *In vitro* experiments with primary cultured

Schwann cells would be a perfect system for answering such questions because use of inhibitors that block specific stages of autophagy and live cell imaging of labeled receptors known to traffic through the endosomal system in Schwann cells is possible.

The findings of this dissertation work will steer the direction of the Robinson lab as future members study the pathomechanisms of CMT. I have shown that MTMR2 and MTMR13 localize to endomembrane structures in Schwann cells, and they reciprocally enhance the expression of one another in the sciatic nerve[67]. I have also shown that Vps34 is required for myelination, and have performed a thorough morphological analysis of these novel knockout mice. I found that PI3K-C2β is not required for Schwann cell myelination, and that loss of PI3K-C2β or Vps34 protein expression is not sufficient to rescue myelin outfoldings in *Mtmr13*$^{-/-}$ mice. The conclusions presented here form the basis of future experiments the lab will conduct, and provide valuable insight into understanding the molecular changes in the Schwann cell that lead to CMT.

Figures and Legends

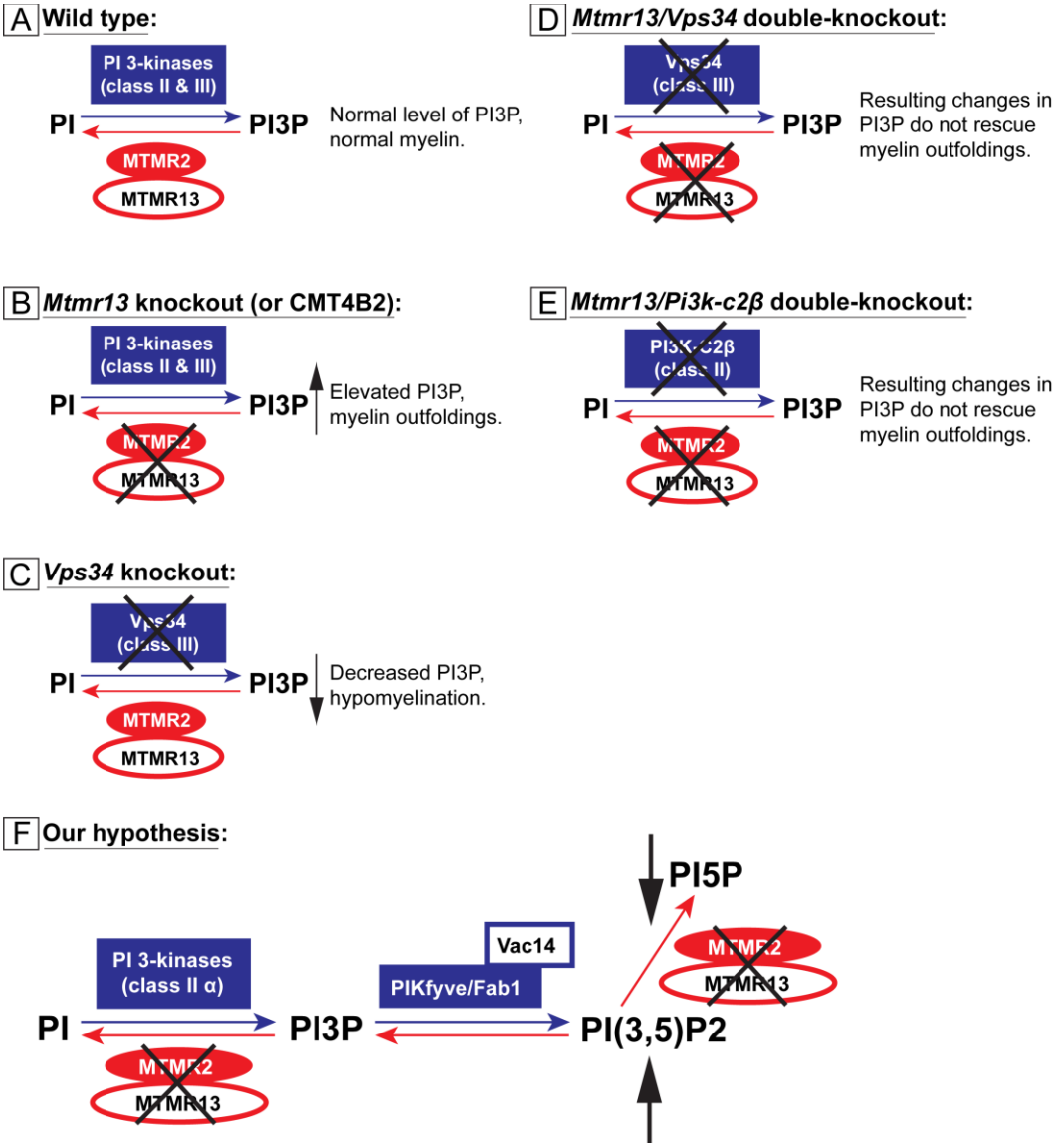

Figure 5.1: Summary of experiments and our hypothesis for future experiments to probe PI balance in Schwann cells. This figure illustrates the hypothesized status of PI3P levels and the observed state of myelination in the peripheral nerve in (**A**) "normal" wild type mice, followed by four experimental knockout mice presented in this thesis work: (**B**) *Mtmr13* knockout, (**C**) *Vps34* knockout, (**D**) *Mtmr13/Vps34* double-knockout,

and (**E**) *Mtmr13/Pi3k-c2β* double-knockout. Manipulating PI3P levels in *Mtmr13* knockout mice by the additional knockout of either *Vps34* or *Pi3k-c2β* did not alter the prevalence of myelin outfoldings in the nerve. (**F**) We therefore hypothesize that other PIs may be the critical lipids dysregulated in *Mtmr13*$^{-/-}$ mice and CMT4B2. We hypothesize that PI(3,5)P_2 levels may be elevated, contributing to myelin abnormalities. It is also possible that PI5P levels are low in *Mtmr13*$^{-/-}$ Schwann cells, which may be leading to myelin dysregulation. Finally, it is possible PI3P levels may be dysregulated in *Mtmr13*$^{-/-}$ Schwann cells, but we have not yet found the relevant PI 3-kinase. The class II PI 3-kinase α has never been studied in Schwann cells and myelination, and could be contributing to the pool of PI3P that MTMR2/MTMR13 dephosphorylate.

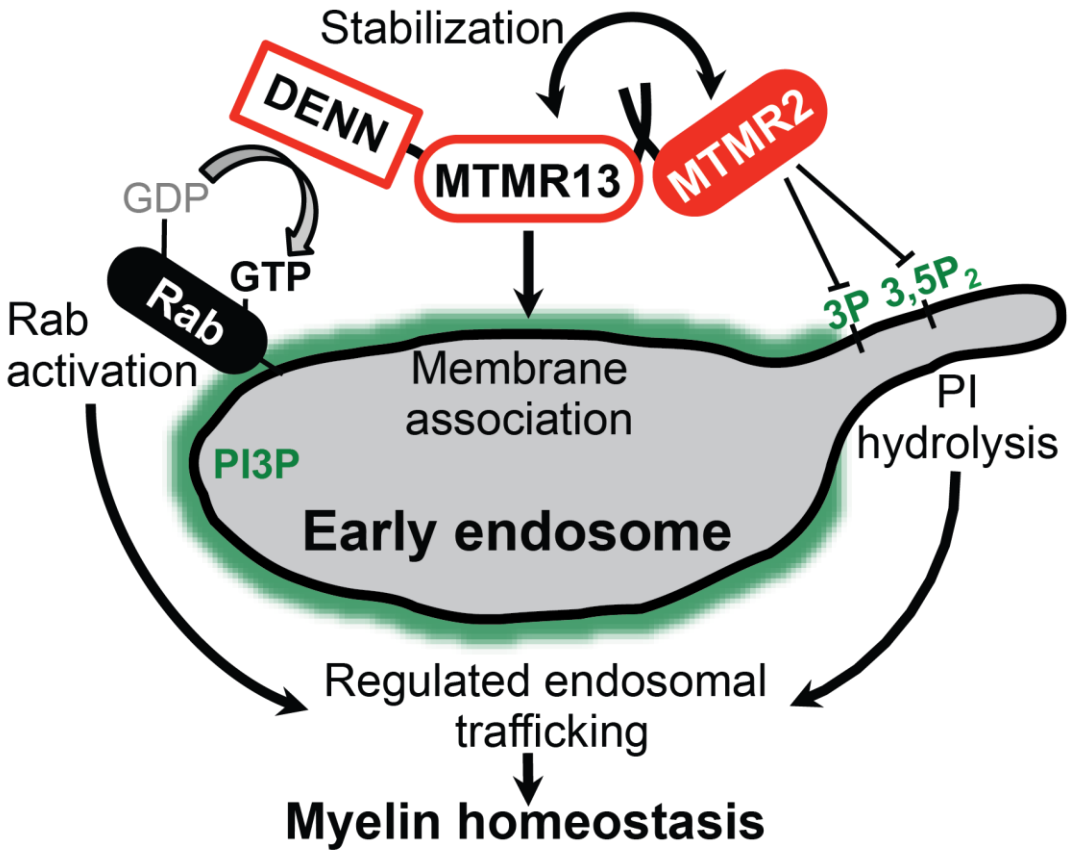

Figure 5.2: The "dual output" model of MTMR13 function in Schwann cells. Our lab hypothesizes that MTMR13 is playing a larger role than simply regulating PI3P and PI(3,5)P_2 levels (through its dimerization with and stabilization of MTMR2). MTMR13 may simultaneously be controlling the activation of specific Rabs in the Schwann cell through its DENN domain. Together, through Rab activation and PI hydrolysis to maintain a critical PI balance in the cell, we propose that MTMR13 functions to regulate endosomal trafficking, which contributes to myelin membrane homeostasis.

References

1. Rotthier A, Baets J, Timmerman V, Janssens K (2012) Mechanisms of disease in hereditary sensory and autonomic neuropathies. Nature reviews Neurology 8: 73-85.
2. Nave KA, Werner HB (2014) Myelination of the nervous system: mechanisms and functions. Annual review of cell and developmental biology 30: 503-533.
3. Nave KA (2010) Myelination and support of axonal integrity by glia. Nature 468: 244-252.
4. Woodhoo A, Sommer L (2008) Development of the Schwann cell lineage: from the neural crest to the myelinated nerve. Glia 56: 1481-1490.
5. Jessen KR, Mirsky R (2005) The origin and development of glial cells in peripheral nerves. Nature reviews Neuroscience 6: 671-682.
6. Jessen KR, Mirsky R (1997) Embryonic Schwann cell development: the biology of Schwann cell precursors and early Schwann cells. Journal of anatomy 191 (Pt 4): 501-505.
7. Corfas G, Velardez MO, Ko CP, Ratner N, Peles E (2004) Mechanisms and roles of axon-Schwann cell interactions. The Journal of neuroscience : the official journal of the Society for Neuroscience 24: 9250-9260.
8. Kuhlbrodt K, Herbarth B, Sock E, Hermans-Borgmeyer I, Wegner M (1998) Sox10, a novel transcriptional modulator in glial cells. The Journal of neuroscience : the official journal of the Society for Neuroscience 18: 237-250.
9. Bremer M, Frob F, Kichko T, Reeh P, Tamm ER, et al. (2011) Sox10 is required for Schwann-cell homeostasis and myelin maintenance in the adult peripheral nerve. Glia 59: 1022-1032.

10. Emery B (2013) Playing the field: Sox10 recruits different partners to drive central and peripheral myelination. PLoS genetics 9: e1003918.
11. Komiyama A, Suzuki K (1992) Age-related differences in proliferative responses of Schwann cells during Wallerian degeneration. Brain research 573: 267-275.
12. Birchmeier C, Nave KA (2008) Neuregulin-1, a key axonal signal that drives Schwann cell growth and differentiation. Glia 56: 1491-1497.
13. Gambarotta G, Fregnan F, Gnavi S, Perroteau I (2013) Neuregulin 1 role in Schwann cell regulation and potential applications to promote peripheral nerve regeneration. International review of neurobiology 108: 223-256.
14. Parkinson DB, Dong Z, Bunting H, Whitfield J, Meier C, et al. (2001) Transforming growth factor beta (TGFbeta) mediates Schwann cell death in vitro and in vivo: examination of c-Jun activation, interactions with survival signals, and the relationship of TGFbeta-mediated death to Schwann cell differentiation. The Journal of neuroscience : the official journal of the Society for Neuroscience 21: 8572-8585.
15. Feltri ML, Poitelon Y, Previtali SC (2015) How Schwann Cells Sort Axons: New Concepts. The Neuroscientist : a review journal bringing neurobiology, neurology and psychiatry.
16. Chan JR (2007) Myelination: all about Rac 'n' roll. The Journal of cell biology 177: 953-955.
17. Decker L, Desmarquet-Trin-Dinh C, Taillebourg E, Ghislain J, Vallat JM, et al. (2006) Peripheral myelin maintenance is a dynamic process requiring constant Krox20 expression. The Journal of neuroscience : the official journal of the Society for Neuroscience 26: 9771-9779.

18. Stassart RM, Fledrich R, Velanac V, Brinkmann BG, Schwab MH, et al. (2013) A role for Schwann cell-derived neuregulin-1 in remyelination. Nature neuroscience 16: 48-54.

19. Newbern J, Birchmeier C (2010) Nrg1/ErbB signaling networks in Schwann cell development and myelination. Seminars in cell & developmental biology 21: 922-928.

20. Garratt AN, Britsch S, Birchmeier C (2000) Neuregulin, a factor with many functions in the life of a schwann cell. BioEssays : news and reviews in molecular, cellular and developmental biology 22: 987-996.

21. Taveggia C, Zanazzi G, Petrylak A, Yano H, Rosenbluth J, et al. (2005) Neuregulin-1 type III determines the ensheathment fate of axons. Neuron 47: 681-694.

22. Brinkmann BG, Agarwal A, Sereda MW, Garratt AN, Muller T, et al. (2008) Neuregulin-1/ErbB signaling serves distinct functions in myelination of the peripheral and central nervous system. Neuron 59: 581-595.

23. Bakhti M, Aggarwal S, Simons M (2014) Myelin architecture: zippering membranes tightly together. Cellular and molecular life sciences : CMLS 71: 1265-1277.

24. Salzer JL, Brophy PJ, Peles E (2008) Molecular domains of myelinated axons in the peripheral nervous system. Glia 56: 1532-1540.

25. Kirschner DA, Ganser AL (1980) Compact myelin exists in the absence of basic protein in the shiverer mutant mouse. Nature 283: 207-210.

26. Zalc B, Goujet D, Colman D (2008) The origin of the myelination program in vertebrates. Current biology : CB 18: R511-512.

27. Miron VE, Kuhlmann T, Antel JP (2011) Cells of the oligodendroglial lineage, myelination, and remyelination. Biochimica et biophysica acta 1812: 184-193.

28. Scherer SS (1999) Nodes, paranodes, and incisures: from form to function. Annals of the New York Academy of Sciences 883: 131-142.

29. Schafer DP, Rasband MN (2006) Glial regulation of the axonal membrane at nodes of Ranvier. Current opinion in neurobiology 16: 508-514.

30. Maurel P, Einheber S, Galinska J, Thaker P, Lam I, et al. (2007) Nectin-like proteins mediate axon Schwann cell interactions along the internode and are essential for myelination. The Journal of cell biology 178: 861-874.

31. Faroni A, Mobasseri SA, Kingham PJ, Reid AJ (2014) Peripheral nerve regeneration: Experimental strategies and future perspectives. Advanced drug delivery reviews.

32. Martini R, Klein D, Groh J (2013) Similarities between inherited demyelinating neuropathies and Wallerian degeneration: an old repair program may cause myelin and axon perturbation under nonlesion conditions. The American journal of pathology 183: 655-660.

33. Glenn TD, Talbot WS (2013) Signals regulating myelination in peripheral nerves and the Schwann cell response to injury. Current opinion in neurobiology 23: 1041-1048.

34. Goldenberg MM (2012) Multiple sclerosis review. P & T : a peer-reviewed journal for formulary management 37: 175-184.

35. Tazir M, Hamadouche T, Nouioua S, Mathis S, Vallat JM (2014) Hereditary motor and sensory neuropathies or Charcot-Marie-Tooth diseases: an update. Journal of the neurological sciences 347: 14-22.

36. Juarez P, Palau F (2012) Neural and molecular features on Charcot-Marie-Tooth disease plasticity and therapy. Neural plasticity 2012: 171636.

37. Brennan KM, Bai Y, Shy ME (2015) Demyelinating CMT-what's known, what's new and what's in store? Neuroscience letters.

38. Tazir M, Bellatache M, Nouioua S, Vallat JM (2013) Autosomal recessive Charcot-Marie-Tooth disease: from genes to phenotypes. Journal of the peripheral nervous system : JPNS 18: 113-129.

39. Jerath NU, Shy ME (2015) Hereditary motor and sensory neuropathies: Understanding molecular pathogenesis could lead to future treatment strategies. Biochimica et biophysica acta 1852: 667-678.

40. Previtali SC, Quattrini A, Bolino A (2007) Charcot-Marie-Tooth type 4B demyelinating neuropathy: deciphering the role of MTMR phosphatases. Expert reviews in molecular medicine 9: 1-16.

41. El-Abassi R, England JD, Carter GT (2014) Charcot-Marie-Tooth disease: an overview of genotypes, phenotypes, and clinical management strategies. PM & R : the journal of injury, function, and rehabilitation 6: 342-355.

42. Nakhro K, Park JM, Hong YB, Park JH, Nam SH, et al. (2013) SET binding factor 1 (SBF1) mutation causes Charcot-Marie-Tooth disease type 4B3. Neurology 81: 165-173.

43. Bolis A, Zordan P, Coviello S, Bolino A (2007) Myotubularin-related (MTMR) phospholipid phosphatase proteins in the peripheral nervous system. Molecular neurobiology 35: 308-316.

44. Mruk DD, Cheng CY (2011) The myotubularin family of lipid phosphatases in disease and in spermatogenesis. The Biochemical journal 433: 253-262.

45. Bolino A, Muglia M, Conforti FL, LeGuern E, Salih MA, et al. (2000) Charcot-Marie-Tooth type 4B is caused by mutations in the gene encoding myotubularin-related protein-2. Nature genetics 25: 17-19.

46. Azzedine H, Bolino A, Taieb T, Birouk N, Di Duca M, et al. (2003) Mutations in MTMR13, a new pseudophosphatase homologue of MTMR2 and Sbf1, in two families with an autosomal recessive demyelinating form of Charcot-Marie-Tooth

disease associated with early-onset glaucoma. American Journal of Human Genetics 72: 1141-1153.

47. Senderek J, Bergmann C, Weber S, Ketelsen UP, Schorle H, et al. (2003) Mutation of the SBF2 gene, encoding a novel member of the myotubularin family, in Charcot-Marie-Tooth neuropathy type 4B2/11p15. Human Molecular Genetics 12: 349-356.

48. Laporte J, Bedez F, Bolino A, Mandel JL (2003) Myotubularins, a large disease-associated family of cooperating catalytically active and inactive phosphoinositides phosphatases. Human molecular genetics 12 Spec No 2: R285-292.

49. Di Paolo G, De Camilli P (2006) Phosphoinositides in cell regulation and membrane dynamics. Nature 443: 651-657.

50. Balla T (2013) Phosphoinositides: tiny lipids with giant impact on cell regulation. Physiological reviews 93: 1019-1137.

51. Hnia K, Vaccari I, Bolino A, Laporte J (2012) Myotubularin phosphoinositide phosphatases: cellular functions and disease pathophysiology. Trends in molecular medicine 18: 317-327.

52. Idevall-Hagren O, De Camilli P (2014) Detection and manipulation of phosphoinositides. Biochimica et biophysica acta.

53. Kutateladze TG (2010) Translation of the phosphoinositide code by PI effectors. Nature chemical biology 6: 507-513.

54. Martin TF (1998) Phosphoinositide lipids as signaling molecules: common themes for signal transduction, cytoskeletal regulation, and membrane trafficking. Annual review of cell and developmental biology 14: 231-264.

55. Frere SG, Chang-Ileto B, Di Paolo G (2012) Role of phosphoinositides at the neuronal synapse. Sub-cellular biochemistry 59: 131-175.

56. Nandurkar HH, Huysmans R (2002) The myotubularin family: novel phosphoinositide regulators. IUBMB life 53: 37-43.

57. Cullen PJ, Carlton JG (2012) Phosphoinositides in the Mammalian Endo-lysosomal Network. Sub-cellular biochemistry 59: 65-110.

58. Nicot AS, Laporte J (2008) Endosomal phosphoinositides and human diseases. Traffic 9: 1240-1249.

59. Kutateladze T, Overduin M (2001) Structural mechanism of endosome docking by the FYVE domain. Science 291: 1793-1796.

60. Schuh AL, Audhya A (2012) Phosphoinositide signaling during membrane transport in Saccharomyces cerevisiae. Sub-cellular biochemistry 59: 35-63.

61. Noda T, Matsunaga K, Taguchi-Atarashi N, Yoshimori T (2010) Regulation of membrane biogenesis in autophagy via PI3P dynamics. Seminars in cell & developmental biology 21: 671-676.

62. Backer JM (2008) The regulation and function of Class III PI3Ks: novel roles for Vps34. The Biochemical journal 410: 1-17.

63. Mizushima N (2007) Autophagy: process and function. Genes & development 21: 2861-2873.

64. Vanhaesebroeck B, Guillermet-Guibert J, Graupera M, Bilanges B (2010) The emerging mechanisms of isoform-specific PI3K signalling. Nature reviews Molecular cell biology 11: 329-341.

65. Funderburk SF, Wang QJ, Yue Z (2010) The Beclin 1-VPS34 complex--at the crossroads of autophagy and beyond. Trends in cell biology 20: 355-362.

66. Amoasii L, Hnia K, Laporte J (2012) Myotubularin phosphoinositide phosphatases in human diseases. Current topics in microbiology and immunology 362: 209-233.

67. Ng AA, Logan AM, Schmidt EJ, Robinson FL (2013) The CMT4B disease-causing phosphatases Mtmr2 and Mtmr13 localize to the Schwann cell cytoplasm and

endomembrane compartments, where they depend upon each other to achieve wild-type levels of protein expression. Human molecular genetics 22: 1493-1506.

68. Bolino A, Bolis A, Previtali SC, Dina G, Bussini S, et al. (2004) Disruption of Mtmr2 produces CMT4B1-like neuropathy with myelin outfolding and impaired spermatogenesis. The Journal of cell biology 167: 711-721.

69. Bolis A, Coviello S, Bussini S, Dina G, Pardini C, et al. (2005) Loss of Mtmr2 phosphatase in Schwann cells but not in motor neurons causes Charcot-Marie-Tooth type 4B1 neuropathy with myelin outfoldings. The Journal of neuroscience : the official journal of the Society for Neuroscience 25: 8567-8577.

70. Vaccari I, Dina G, Tronchere H, Kaufman E, Chicanne G, et al. (2011) Genetic interaction between MTMR2 and FIG4 phospholipid phosphatases involved in Charcot-Marie-Tooth neuropathies. PLoS genetics 7: e1002319.

71. Robinson FL, Dixon JE (2005) The phosphoinositide-3-phosphatase MTMR2 associates with MTMR13, a membrane-associated pseudophosphatase also mutated in type 4B Charcot-Marie-Tooth disease. The Journal of biological chemistry 280: 31699-31707.

72. Robinson FL, Niesman IR, Beiswenger KK, Dixon JE (2008) Loss of the inactive myotubularin-related phosphatase Mtmr13 leads to a Charcot-Marie-Tooth 4B2-like peripheral neuropathy in mice. Proceedings of the National Academy of Sciences of the United States of America 105: 4916-4921.

73. Devereaux K, Dall'Armi C, Alcazar-Roman A, Ogasawara Y, Zhou X, et al. (2013) Regulation of mammalian autophagy by class II and III PI 3-kinases through PI3P synthesis. PloS one 8: e76405.

74. Lenk GM, Meisler MH (2014) Mouse models of PI(3,5)P2 deficiency with impaired lysosome function. Methods in enzymology 534: 245-260.

75. Staiano L, De Leo MG, Persico M, De Matteis MA (2014) Mendelian disorders of PI metabolizing enzymes. Biochimica et biophysica acta.

76. Clague MJ, Urbe S, de Lartigue J (2009) Phosphoinositides and the endocytic pathway. Experimental cell research 315: 1627-1631.

77. McCrea HJ, De Camilli P (2009) Mutations in phosphoinositide metabolizing enzymes and human disease. Physiology 24: 8-16.

78. Skre H (1974) Genetic and clinical aspects of Charcot-Marie-Tooth's disease. Clin Genet 6: 98-118.

79. Scherer SS, Wrabetz L (2008) Molecular mechanisms of inherited demyelinating neuropathies. Glia 56: 1578-1589.

80. Patzko A, Shy ME (2011) Update on Charcot-Marie-Tooth disease. Current neurology and neuroscience reports 11: 78-88.

81. Pereira JA, Lebrun-Julien F, Suter U (2011) Molecular mechanisms regulating myelination in the peripheral nervous system. Trends in neurosciences 35: 123-134.

82. Previtali SC, Quattrini A, Bolino A (2007) Charcot-Marie-Tooth type 4B demyelinating neuropathy: deciphering the role of MTMR phosphatases. Expert Rev Mol Med 9: 1-16.

83. Bolino A, Muglia M, Conforti FL, LeGuern E, Salih MAM, et al. (2000) Charcot-Marie-Tooth type 4B is caused by mutations in the gene encoding myotubularin-related protein-2. Nature Genetics 25: 17-19.

84. Hnia K, Vaccari I, Bolino A, Laporte J (2012) Myotubularin phosphoinositide phosphatases: cellular functions and disease pathophysiology. Trends in Molecular Medicine 18: 317-327.

85. Leslie NR, Davies EM, Sheffield DA, Tibarewal P, Fedele CG, et al. (2012) The PTEN and Myotubularin Phosphoinositide 3-Phosphatases: Linking Lipid Signalling to Human Disease. Sub-cellular biochemistry 58: 281-336.

86. Zou J, Majerus PW, Wilson DB, Schrade A, Chang SC, et al. (2011) The role of myotubularin-related phosphatases in the control of autophagy and programmed cell death. Advances in enzyme regulation 52: 282-289.

87. Robinson FL, Dixon JE (2006) Myotubularin phosphatases: policing 3-phosphoinositides. Trends Cell Biol 16: 403-412.

88. Kim SA, Taylor GS, Torgersen KM, Dixon JE (2002) Myotubularin and MTMR2, phosphatidylinositol 3-phosphatases mutated in myotubular myopathy and type 4B Charcot-Marie-Tooth disease. Journal of Biological Chemistry 277: 4526-4531.

89. Berger P, Bonneick S, Willi S, Wymann M, Suter U (2002) Loss of phosphatase activity in myotubularin-related protein 2 is associated with Charcot-Marie-Tooth disease type 4B1. Human Molecular Genetics 11: 1569-1579.

90. Schaletzky J, Dove SK, Short B, Lorenzo O, Clague MJ, et al. (2003) Phosphatidylinositol-5-phosphate activation and conserved substrate specificity of the myotubularin phosphatidylinositol 3-phosphatases. Curr Biol 13: 504-509.

91. Falasca M, Maffucci T (2009) Rethinking phosphatidylinositol 3-monophosphate. Biochimica et biophysica acta 1793: 1795-1803.

92. Dove SK, Dong K, Kobayashi T, Williams FK, Michell RH (2009) Phosphatidylinositol 3,5-bisphosphate and Fab1p/PIKfyve underPPIn endo-lysosome function. Biochemical Journal 419: 1-13.

93. Ho CY, Alghamdi TA, Botelho RJ (2012) Phosphatidylinositol-3,5-bisphosphate: no longer the poor PIP2. Traffic 13: 1-8.

94. Robinson FL, Dixon JE (2005) The phosphoinositide-3-phosphatase MTMR2 associates with MTMR13, a membrane-associated pseudophosphatase also mutated in type 4B Charcot-Marie-Tooth disease. J Biol Chem 280: 31699-31707.

95. Berger P, Berger I, Schaffitzel C, Tersar K, Volkmer B, et al. (2006) Multi-level regulation of myotubularin-related protein-2 phosphatase activity by myotubularin-related protein-13/set-binding factor-2. Hum Mol Genet 15: 569-579.

96. Jean S, Cox S, Schmidt EJ, Robinson FL, Kiger AA (2012) Sbf/MTMR13 coordinates PI(3)P and Rab21 regulation in endocytic control of cellular remodeling. Molecular biology of the cell 23: 2723-2740.

97. Bolino A, Bolis A, Previtali SC, Dina G, Bussini S, et al. (2004) Disruption of Mtmr2 produces CMT4B1-like neuropathy with myelin outfolding and impaired spermatogenesis. J Cell Biol 167: 711-721.

98. Bonneick S, Boentert M, Berger P, Atanasoski S, Mantei N, et al. (2005) An animal model for Charcot-Marie-Tooth disease type 4B1. Hum Mol Genet 14: 3685-3695.

99. Tersar K, Boentert M, Berger P, Bonneick S, Wessig C, et al. (2007) Mtmr13/Sbf2-deficient mice: an animal model for CMT4B2. Hum Mol Genet 16: 2991-3001.

100. Bolis A, Coviello S, Bussini S, Dina G, Pardini C, et al. (2005) Loss of Mtmr2 phosphatase in Schwann cells but not in motor neurons causes Charcot-Marie-Tooth type 4B1 neuropathy with myelin outfoldings. J Neurosci 25: 8567-8577.

101. Bolis A, Coviello S, Visigalli I, Taveggia C, Bachi A, et al. (2009) Dlg1, Sec8, and Mtmr2 regulate membrane homeostasis in Schwann cell myelination. J Neurosci 29: 8858-8870.

102. Ohnishi A, Murai Y, Ikeda M, Fujita T, Furuya H, et al. (1989) Autosomal recessive motor and sensory neuropathy with excessive myelin outfolding. Muscle Nerve 12: 568-575.

103. Gabreels-Festen AA, Joosten EM, Gabreels FJ, Stegeman DF, Vos AJ, et al. (1990) Congenital demyelinating motor and sensory neuropathy with focally folded myelin sheaths. Brain 113: 1629-1643.

104. Michailov GV, Sereda MW, Brinkmann BG, Fischer TM, Haug B, et al. (2004) Axonal neuregulin-1 regulates myelin sheath thickness. Science 304: 700-703.

105. Flores AI, Narayanan SP, Morse EN, Shick HE, Yin X, et al. (2008) Constitutively active Akt induces enhanced myelination in the CNS. Journal of Neuroscience 28: 7174-7183.

106. Goebbels S, Oltrogge JH, Kemper R, Heilmann I, Bormuth I, et al. (2010) Elevated phosphatidylinositol 3,4,5-trisphosphate in glia triggers cell-autonomous membrane wrapping and myelination. Journal of Neuroscience 30: 8953-8964.

107. Sherman DL, Krols M, Wu LM, Grove M, Nave KA, et al. (2012) Arrest of myelination and reduced axon growth when Schwann cells lack mTOR. Journal of Neuroscience 32: 1817-1825.

108. Razidlo GL, Katafiasz D, Taylor GS (2011) Myotubularin regulates Akt-dependent survival signaling via phosphatidylinositol 3-phosphate. The Journal of biological chemistry 286: 20005-20019.

109. MacKeigan JP, Murphy LO, Blenis J (2005) Sensitized RNAi screen of human kinases and phosphatases identifies new regulators of apoptosis and chemoresistance. Nature Cell Biology 7: 591-600.

110. Chojnowski A, Ravise N, Bachelin C, Depienne C, Ruberg M, et al. (2007) Silencing of the Charcot-Marie-Tooth associated MTMR2 gene decreases

proliferation and enhances cell death in primary cultures of Schwann cells. Neurobiology of disease 26: 323-331.

111. Lee OK, Frese KK, James JS, Chadda D, Chen ZH, et al. (2003) Discs-Large and Strabismus are functionally linked to plasma membrane formation. Nature Cell Biology 5: 987-993.

112. Gorczyca D, Ashley J, Speese S, Gherbesi N, Thomas U, et al. (2007) Postsynaptic membrane addition depends on the Discs-Large-interacting t-SNARE Gtaxin. Journal of Neuroscience 27: 1033-1044.

113. Cotter L, Ozcelik M, Jacob C, Pereira JA, Locher V, et al. (2010) Dlg1-PTEN interaction regulates myelin thickness to prevent damaging peripheral nerve overmyelination. Science 328: 1415-1418.

114. Newbern JM, Li X, Shoemaker SE, Zhou J, Zhong J, et al. (2011) Specific functions for ERK/MAPK signaling during PNS development. Neuron 69: 91-105.

115. Ishii A, Fyffe-Maricich SL, Furusho M, Miller RH, Bansal R (2012) ERK1/ERK2 MAPK Signaling is Required to Increase Myelin Thickness Independent of Oligodendrocyte Differentiation and Initiation of Myelination. Journal of Neuroscience 32: 8855-8864.

116. Lee HW, Kim Y, Han K, Kim H, Kim E (2010) The phosphoinositide 3-phosphatase MTMR2 interacts with PSD-95 and maintains excitatory synapses by modulating endosomal traffic. Journal of Neuroscience 30: 5508-5518.

117. Gary JD, Wurmser AE, Bonangelino CJ, Weisman LS, Emr SD (1998) Fab1p is essential for PtdIns(3)P 5-kinase activity and the maintenance of vacuolar size and membrane homeostasis. J Cell Biol 143: 65-79.

118. Cooke FT, Dove SK, McEwen RK, Painter G, Holmes AB, et al. (1998) The stress-activated phosphatidylinositol 3-phosphate 5-kinase Fab1p is essential for vacuole function in S. cerevisiae. Curr Biol 8: 1219-1222.

119. Johnson EE, Overmeyer JH, Gunning WT, Maltese WA (2006) Gene silencing reveals a specific function of hVps34 phosphatidylinositol 3-kinase in late versus early endosomes. J Cell Sci 119: 1219-1232.

120. Chow CY, Zhang Y, Dowling JJ, Jin N, Adamska M, et al. (2007) Mutation of FIG4 causes neurodegeneration in the pale tremor mouse and patients with CMT4J. Nature 448: 68-72.

121. Dang H, Li Z, Skolnik EY, Fares H (2004) Disease-related Myotubularins Function in Endocytic Traffic in Caenorhabditis elegans. Mol Biol Cell 15: 189-196.

122. Velichkova M, Juan J, Kadandale P, Jean S, Ribeiro I, et al. Drosophila Mtm and class II PI3K coregulate a PI(3)P pool with cortical and endolysosomal functions. J Cell Biol 190: 407-425.

123. Parrish WR, Stefan CJ, Emr SD (2004) Essential Role for the Myotubularin-related Phosphatase Ymr1p and the Synaptojanin-like Phosphatases Sjl2p and Sjl3p in Regulation of PI(3)P in Yeast. Molecular Biology of the Cell 15: 3567-3579.

124. Arighi CN, Hartnell LM, Aguilar RC, Haft CR, Bonifacino JS (2004) Role of the mammalian retromer in sorting of the cation-independent mannose 6-phosphate receptor. Journal of Cell Biology 165: 123-133.

125. Krajewski KM, Lewis RA, Fuerst DR, Turansky C, Hinderer SR, et al. (2000) Neurological dysfunction and axonal degeneration in Charcot-Marie-Tooth disease type 1A. Brain 123: 1516-1527.

126. Goebbels S, Oltrogge JH, Wolfer S, Wieser GL, Nientiedt T, et al. (2012) Genetic disruption of Pten in a novel mouse model of tomaculous neuropathy. EMBO molecular medicine 4: 486-499.

127. Berger P, Tersar K, Ballmer-Hofer K, Suter U (2011) The CMT4B disease-causing proteins MTMR2 and MTMR13/SBF2 regulate AKT signalling. Journal of cellular and molecular medicine 15: 307-315.

128. Gillooly DJ, Morrow IC, Lindsay M, Gould R, Bryant NJ, et al. (2000) Localization of phosphatidylinositol 3-phosphate in yeast and mammalian cells. EMBO Journal 19: 4577-4588.

129. Ikonomov OC, Sbrissa D, Shisheva A (2001) Mammalian cell morphology and endocytic membrane homeostasis require enzymatically active phosphoinositide 5-kinase PIKfyve. J Biol Chem 276: 26141-26147.

130. Rutherford AC, Traer C, Wassmer T, Pattni K, Bujny MV, et al. (2006) The mammalian phosphatidylinositol 3-phosphate 5-kinase (PIKfyve) regulates endosome-to-TGN retrograde transport. Journal of Cell Science 119: 3944-3957.

131. Lorenzo O, Urbe S, Clague MJ (2006) Systematic analysis of myotubularins: heteromeric interactions, subcellular localisation and endosome related functions. J Cell Sci 119: 2953-2959.

132. Previtali SC, Zerega B, Sherman DL, Brophy PJ, Dina G, et al. (2003) Myotubularin-related 2 protein phosphatase and neurofilament light chain protein, both mutated in CMT neuropathies, interact in peripheral nerve. Hum Mol Genet 12: 1713-1723.

133. Goryunov D, Nightingale A, Bornfleth L, Leung C, Liem RK (2008) Multiple disease-linked myotubularin mutations cause NFL assembly defects in cultured cells and disrupt myotubularin dimerization. Journal of Neurochemistry 104: 1536-1552.

134. Franklin NE, Taylor GS, Vacratsis PO (2011) Endosomal targeting of the phosphoinositide 3-phosphatase MTMR2 is regulated by an N-terminal phosphorylation site. Journal of Biological Chemistry 286: 15841-15853.

135. Yoshimura S, Gerondopoulos A, Linford A, Rigden DJ, Barr FA (2010) Family-wide characterization of the DENN domain Rab GDP-GTP exchange factors. Journal of Cell Biology 191: 367-381.

136. Ratner N, Williams JP, Kordich JJ, Kim HA (2006) Schwann cell preparation from single mouse embryos: analyses of neurofibromin function in Schwann cells. Methods in enzymology 407: 22-33.

137. Schink KO, Raiborg C, Stenmark H (2013) Phosphatidylinositol 3-phosphate, a lipid that regulates membrane dynamics, protein sorting and cell signalling. BioEssays : news and reviews in molecular, cellular and developmental biology 35: 900-912.

138. Roberts R, Ktistakis NT (2013) Omegasomes: PI3P platforms that manufacture autophagosomes. Essays in biochemistry 55: 17-27.

139. Burd CG, Emr SD (1998) Phosphatidylinositol(3)-phosphate signaling mediated by specific binding to RING FYVE domains. Molecular cell 2: 157-162.

140. Gillooly DJ, Morrow IC, Lindsay M, Gould R, Bryant NJ, et al. (2000) Localization of phosphatidylinositol 3-phosphate in yeast and mammalian cells. The EMBO journal 19: 4577-4588.

141. Corvera S (2001) Phosphatidylinositol 3-kinase and the control of endosome dynamics: new players defined by structural motifs. Traffic 2: 859-866.

142. Maffucci T, Falasca M (2014) New insight into the intracellular roles of class II phosphoinositide 3-kinases. Biochemical Society transactions 42: 1378-1382.

143. Jerath NU, Shy ME (2014) Hereditary motor and sensory neuropathies: Understanding molecular pathogenesis could lead to future treatment strategies. Biochimica et biophysica acta.

144. Schu PV, Takegawa K, Fry MJ, Stack JH, Waterfield MD, et al. (1993) Phosphatidylinositol 3-kinase encoded by yeast VPS34 gene essential for protein sorting. Science 260: 88-91.

145. Zhou X, Wang L, Hasegawa H, Amin P, Han BX, et al. (2010) Deletion of PIK3C3/Vps34 in sensory neurons causes rapid neurodegeneration by disrupting

the endosomal but not the autophagic pathway. Proceedings of the National Academy of Sciences of the United States of America 107: 9424-9429.

146. Jaber N, Dou Z, Chen JS, Catanzaro J, Jiang YP, et al. (2012) Class III PI3K Vps34 plays an essential role in autophagy and in heart and liver function. Proceedings of the National Academy of Sciences of the United States of America 109: 2003-2008.

147. McLeod IX, Zhou X, Li QJ, Wang F, He YW (2011) The class III kinase Vps34 promotes T lymphocyte survival through regulating IL-7Ralpha surface expression. Journal of immunology 187: 5051-5061.

148. Willinger T, Flavell RA (2012) Canonical autophagy dependent on the class III phosphoinositide-3 kinase Vps34 is required for naive T-cell homeostasis. Proceedings of the National Academy of Sciences of the United States of America 109: 8670-8675.

149. Parekh VV, Wu L, Boyd KL, Williams JA, Gaddy JA, et al. (2013) Impaired autophagy, defective T cell homeostasis, and a wasting syndrome in mice with a T cell-specific deletion of Vps34. Journal of immunology 190: 5086-5101.

150. Bechtel W, Helmstadter M, Balica J, Hartleben B, Schell C, et al. (2013) The class III phosphatidylinositol 3-kinase PIK3C3/VPS34 regulates endocytosis and autophagosome-autolysosome formation in podocytes. Autophagy 9: 1097-1099.

151. Morishita H, Eguchi S, Kimura H, Sasaki J, Sakamaki Y, et al. (2013) Deletion of autophagy-related 5 (Atg5) and Pik3c3 genes in the lens causes cataract independent of programmed organelle degradation. The Journal of biological chemistry 288: 11436-11447.

152. Feltri ML, D'Antonio M, Previtali S, Fasolini M, Messing A, et al. (1999) P0-Cre transgenic mice for inactivation of adhesion molecules in Schwann cells. Annals of the New York Academy of Sciences 883: 116-123.

153. Beirowski B, Babetto E, Golden JP, Chen YJ, Yang K, et al. (2014) Metabolic regulator LKB1 is crucial for Schwann cell-mediated axon maintenance. Nature neuroscience 17: 1351-1361.

154. Grove M, Komiyama NH, Nave KA, Grant SG, Sherman DL, et al. (2007) FAK is required for axonal sorting by Schwann cells. The Journal of cell biology 176: 277-282.

155. Nodari A, Zambroni D, Quattrini A, Court FA, D'Urso A, et al. (2007) Beta1 integrin activates Rac1 in Schwann cells to generate radial lamellae during axonal sorting and myelination. The Journal of cell biology 177: 1063-1075.

156. Britsch S, Goerich DE, Riethmacher D, Peirano RI, Rossner M, et al. (2001) The transcription factor Sox10 is a key regulator of peripheral glial development. Genes & development 15: 66-78.

157. Svaren J, Meijer D (2008) The molecular machinery of myelin gene transcription in Schwann cells. Glia 56: 1541-1551.

158. Le N, Nagarajan R, Wang JY, Araki T, Schmidt RE, et al. (2005) Analysis of congenital hypomyelinating Egr2Lo/Lo nerves identifies Sox2 as an inhibitor of Schwann cell differentiation and myelination. Proceedings of the National Academy of Sciences of the United States of America 102: 2596-2601.

159. Topilko P, Schneider-Maunoury S, Levi G, Baron-Van Evercooren A, Chennoufi AB, et al. (1994) Krox-20 controls myelination in the peripheral nervous system. Nature 371: 796-799.

160. Jessen KR, Mirsky R (2008) Negative regulation of myelination: relevance for development, injury, and demyelinating disease. Glia 56: 1552-1565.

161. Klionsky DJ, Abdalla FC, Abeliovich H, Abraham RT, Acevedo-Arozena A, et al. (2012) Guidelines for the use and interpretation of assays for monitoring autophagy. Autophagy 8: 445-544.

162. Rusten TE, Stenmark H (2010) p62, an autophagy hero or culprit? Nature cell biology 12: 207-209.

163. Futter CE, Collinson LM, Backer JM, Hopkins CR (2001) Human VPS34 is required for internal vesicle formation within multivesicular endosomes. J Cell Biol 155: 1251-1264.

164. Siddhanta U, McIlroy J, Shah A, Zhang Y, Backer JM (1998) Distinct roles for the p110alpha and hVPS34 phosphatidylinositol 3'-kinases in vesicular trafficking, regulation of the actin cytoskeleton, and mitogenesis. J Cell Biol 143: 1647-1659.

165. Brown WJ, DeWald DB, Emr SD, Plutner H, Balch WE (1995) Role for phosphatidylinositol 3-kinase in the sorting and transport of newly synthesized lysosomal enzymes in mammalian cells. J Cell Biol 130: 781-796.

166. Patki V, Lawe DC, Corvera S, Virbasius JV, Chawla A (1998) A functional PtdIns(3)P-binding motif. Nature 394: 433-434.

167. Simonsen A, Lippe R, Christoforidis S, Gaullier JM, Brech A, et al. (1998) EEA1 links PI(3)K function to Rab5 regulation of endosome fusion. Nature 394: 494-498.

168. Raiborg C, Schink KO, Stenmark H (2013) Class III phosphatidylinositol 3-kinase and its catalytic product PtdIns3P in regulation of endocytic membrane traffic. The FEBS journal.

169. Cao C, Backer JM, Laporte J, Bedrick EJ, Wandinger-Ness A (2008) Sequential actions of myotubularin lipid phosphatases regulate endosomal PI(3)P and growth factor receptor trafficking. Molecular biology of the cell 19: 3334-3346.

170. Jang SY, Shin YK, Park SY, Park JY, Rha SH, et al. (2015) Autophagy is involved in the reduction of myelinating Schwann cell cytoplasm during myelin maturation of the peripheral nerve. PloS one 10: e0116624.

171. Norris FA, Majerus PW (1994) Hydrolysis of phosphatidylinositol 3,4-bisphosphate by inositol polyphosphate 4-phosphatase isolated by affinity elution chromatography. The Journal of biological chemistry 269: 8716-8720.

172. Feltri ML, D'Antonio M, Quattrini A, Numerato R, Arona M, et al. (1999) A novel P0 glycoprotein transgene activates expression of lacZ in myelin-forming Schwann cells. The European journal of neuroscience 11: 1577-1586.

173. Ng AA, Logan AM, Schmidt EJ, Robinson FL (2013) The CMT4B disease-causing phosphatases Mtmr2 and Mtmr13 localize to the Schwann cell cytoplasm and endomembrane compartments, where they depend upon each other to achieve wild-type levels of protein expression. Human Molecular Genetics.

174. Harada K, Truong AB, Cai T, Khavari PA (2005) The class II phosphoinositide 3-kinase C2beta is not essential for epidermal differentiation. Mol Cell Biol 25: 11122-11130.

175. Robinson FL, Dixon JE (2006) Myotubularin phosphatases: policing 3-phosphoinositides. Trends in cell biology 16: 403-412.

176. Hughes RA (2002) Peripheral neuropathy. BMJ 324: 466-469.

177. Laporte J, Hu LJ, Kretz C, Mandel JL, Kioschis P, et al. (1996) A gene mutated in X-linked myotubular myopathy defines a new putative tyrosine phosphatase family conserved in yeast. Nature genetics 13: 175-182.

178. Balla T (2005) Inositol-lipid binding motifs: signal integrators through protein-lipid and protein-protein interactions. J Cell Sci 118: 2093-2104.

179. Simonsen A, Wurmser AE, Emr SD, Stenmark H (2001) The role of phosphoinositides in membrane transport. Current opinion in cell biology 13: 485-492.

180. Ronan B, Flamand O, Vescovi L, Dureuil C, Durand L, et al. (2014) A highly potent and selective Vps34 inhibitor alters vesicle trafficking and autophagy. Nature chemical biology 10: 1013-1019.

181. Engelman JA, Luo J, Cantley LC (2006) The evolution of phosphatidylinositol 3-kinases as regulators of growth and metabolism. Nature reviews Genetics 7: 606-619.

182. Falasca M, Maffucci T (2007) Role of class II phosphoinositide 3-kinase in cell signalling. Biochemical Society transactions 35: 211-214.

183. Martyn C, Li J (2013) Fig4 deficiency: a newly emerged lysosomal storage disorder? Progress in neurobiology 101-102: 35-45.

184. Dowdle WE, Nyfeler B, Nagel J, Elling RA, Liu S, et al. (2014) Selective VPS34 inhibitor blocks autophagy and uncovers a role for NCOA4 in ferritin degradation and iron homeostasis in vivo. Nature cell biology 16: 1069-1079.